NAVAL POSTGRADUATE SCHOOL

MONTEREY, CALIFORNIA

THESIS

AIR-OCEAN CHARACTERISTICS DURING THE IMPACT OF TYPHOONS ON THE OCEAN IN THE PACIFIC (ITOP) PROGRAM

by

Amy D. Heck

September 2011

Thesis Advisor:	Patrick. A. Harr
Second Reader:	John L. Dumas

Approved for public release; distribution is unlimited

THIS PAGE INTENTIONALLY LEFT BLANK

REPORT DOCUMENTATION PAGE			Form Approved OMB No. 0704-0188
Public reporting burden for this collection of information is estimated to average 1 hour per response, including the time for reviewing instruction, searching existing data sources, gathering and maintaining the data needed, and completing and reviewing the collection of information. Send comments regarding this burden estimate or any other aspect of this collection of information, including suggestions for reducing this burden, to Washington headquarters Services, Directorate for Information Operations and Reports, 1215 Jefferson Davis Highway, Suite 1204, Arlington, VA 22202-4302, and to the Office of Management and Budget, Paperwork Reduction Project (0704-0188) Washington DC 20503.			
1. AGENCY USE ONLY *(Leave blank)*	**2. REPORT DATE** September 2011	**3. REPORT TYPE AND DATES COVERED** Master's Thesis	
4. TITLE AND SUBTITLE Air-Ocean Characteristics During the Impact of Typhoons on the Ocean in the Pacific (ITOP) Program		**5. FUNDING NUMBERS**	
6. AUTHOR(S) Amy D. Heck			
7. PERFORMING ORGANIZATION NAME(S) AND ADDRESS(ES) Naval Postgraduate School Monterey, CA 93943-5000		**8. PERFORMING ORGANIZATION REPORT NUMBER**	
9. SPONSORING /MONITORING AGENCY NAME(S) AND ADDRESS(ES) N/A		**10. SPONSORING/MONITORING AGENCY REPORT NUMBER**	
11. SUPPLEMENTARY NOTES The views expressed in this thesis are those of the author and do not reflect the official policy or position of the Department of Defense or the U.S. Government. IRB Protocol number N/A			
12a. DISTRIBUTION / AVAILABILITY STATEMENT Approved for public release; distribution is unlimited		**12b. DISTRIBUTION CODE** A	

13. ABSTRACT (maximum 200 words)

Interactions between a tropical cyclone (TC) and the underlying ocean environment can have significant impacts on physical mechanisms during the formation and intensification of the storm. During the summer of 2010, the Impact of Typhoons on the Ocean in the Pacific (ITOP) program was conducted to examine interactions between the ocean and TCs using a variety of experimental approaches. Specific observational assets included an array of moored buoys, two WC-130J aircraft, and a U.S. research vessel (RV Revelle). Airborne-deployed sensors included dropwindsondes, airborne expendable bathythermographs (AXBTs), Lagrangian floats, and drifters.

In this thesis, AXBT observations were used to examine basic characteristics of the ocean environment during TCs that occurred during ITOP. Observations were compared to the Naval Research Laboratory East Asian Seas Nowcast Forecast System (NRL EASNS). For high ocean heat content (OHC), the model analyzed OHC was too low and for low OHC, the model analyses were too high. The largest analyzed and observed differences were found to occur in regions of TC-induced ocean changes. The significance of this comparison is the contribution to understanding the relationship between OHC and TC structure, with specific focus on the representation in the operational NRL EASNFS.

14. SUBJECT TERMS Tropical Cyclone, Air-Ocean Interaction, Ocean Heat Content, Typhoon			**15. NUMBER OF PAGES** 117
			16. PRICE CODE
17. SECURITY CLASSIFICATION OF REPORT Unclassified	**18. SECURITY CLASSIFICATION OF THIS PAGE** Unclassified	**19. SECURITY CLASSIFICATION OF ABSTRACT** Unclassified	**20. LIMITATION OF ABSTRACT** UU

NSN 7540-01-280-5500 Standard Form 298 (Rev. 2-89)
Prescribed by ANSI Std. 239-18

THIS PAGE INTENTIONALLY LEFT BLANK

Approved for public release; distribution is unlimited

AIR-OCEAN CHARACTERISTICS DURING THE IMPACT OF TYPHOONS ON THE OCEAN IN THE PACIFIC (ITOP) PROGRAM

Amy D. Heck
Lieutenant Commander, United States Navy
B.S., United States Naval Academy, 2000

Submitted in partial fulfillment of the
requirements for the degree of

**MASTER OF SCIENCE IN
METEOROLOGY AND PHYSICAL OCEANOGRAPHY**

from the

**NAVAL POSTGRADUATE SCHOOL
September 2011**

Author: Amy D. Heck

Approved by: Dr. Patrick A. Harr
Thesis Advisor

CDR John L. Dumas
Second Reader

Dr. Wendel Nuss
Chair, Department of Meteorology

THIS PAGE INTENTIONALLY LEFT BLANK

ABSTRACT

Interactions between a tropical cyclone (TC) and the underlying ocean environment can have significant impacts on physical mechanisms during the formation and intensification of the storm. During the summer of 2010, the Impact of Typhoons on the Ocean in the Pacific (ITOP) program was conducted to examine interactions between the ocean and TCs using a variety of experimental approaches. Specific observational assets included an array of moored buoys, two WC-130J aircraft, and a U.S. research vessel (RV Revelle). Airborne-deployed sensors included dropwindsondes, airborne expendable bathythermographs (AXBTs), Lagrangian floats, and drifters.

In this thesis, AXBT observations were used to examine basic characteristics of the ocean environment during TCs that occurred during ITOP. Observations were compared to the Naval Research Laboratory East Asian Seas Nowcast Forecast System (NRL EASNS). For high ocean heat content (OHC), the model analyzed OHC was too low and for low OHC, the model analyses were too high. The largest analyzed and observed differences were found to occur in regions of TC-induced ocean changes. The significance of this comparison is the contribution to understanding the relationship between OHC and TC structure, with specific focus on the representation in the operational NRL EASNFS.

THIS PAGE INTENTIONALLY LEFT BLANK

TABLE OF CONTENTS

LIST OF FIGURES

THIS PAGE INTENTIONALLY LEFT BLANK

LIST OF TABLES

THIS PAGE INTENTIONALLY LEFT BLANK

LIST OF ACRONYMS AND ABBREVIATIONS

AXBT	Airborne Expendable Bathythermograph
AVHRR	Advanced Very High Resolution Radar
BOND	Battlespace ON Demand
EASNFS	East Asian Seas Nowcast/Forecast System
ENSO	El Niño—Southern Oscillation
IR	Infra Red Satellite
ITOP	Impact of Typhoons on the Ocean in the Pacific
JTWC	Joint Typhoon Warning Center
MLD	Mixed Layer Depth
MTSAT	Meteorological Satellite
MW	Microwave Satellite
NOAA	National Oceanic and Atmospheric Administration
NOGAPS	Navy Operational Global Atmospheric Prediction System
NRL SSC	Naval Research Laboratory at Stennis Space Center, MS
OHC	Ocean Heat Content (based on 26^{o}C Isotherm)
OHC24	Ocean Heat Content (based on 24^{o}C Dew Point Temperature)
SSMI	Special Sensor Microwave Imager
SST	Sea Surface Temperature
STY	Super Typhoon
T100	Average Temperature of the top 100 meters of the Ocean
TC	Tropical Cyclone
TD	Tropical Depression
TS	Tropical Storm
TUTT	Tropical Upper Tropospheric Trough
TY	Typhoon
UCAR	University Corporation for Atmospheric Research
UTC	Coordinated Universal Time
WESTPAC	Western Pacific Ocean
WV	Water Vapor Satellite
Z26	Depth of the 26^{o}C Isotherm

THIS PAGE INTENTIONALLY LEFT BLANK

ACKNOWLEDGMENTS

I would like to thank my thesis advisor, Professor Patrick Harr, for all his assistance, patience, guidance, and his unique gift for inducing calm into a stressful process. I would also like to thank CDR J. Dumas for his support and assistance as not only a second reader, but as a great Program Officer and mentor. I would also like to thank LCDR Tom Seigenthaller and his wife, Michelle, for helping me by sharing some MATLAB computer workspace at a critical juncture in the production cycle, and Mr. Bob Creasy for his MATLAB expertise. Thank you to LCDR Pablo Breuer and his wife, Matthea, for all your encouragement.

Professionally, I would also like to extend my appreciation and gratitude to CDR P. Travis for her mentorship and encouragement that got me "across the finish line." Thank you to CAPT R. Kiser and CAPT J. Pettigrew for the opportunity to come to FNMOC to finish this thesis.

Personally, I would like to thank Ms. Lorianne Liptak for her support, encouragement, and being the best friend a person could ask for. "Money might make you wealthy, but friends make you rich." – Anonymous. Thank you to Mom and Dad Heck and to Mr. Loren "Dad" Liptak, who has been known to say, "You always end up where you are supposed to be." I have been blessed with many people to help me on this journey since coming back to Monterey, so I must be here for a reason. I hope that in the future I will be able to pay back all those who have been there for me during this challenging time by paying it forward. This thesis is dedicated in memory of my beloved Grandmother, Mrs. Mary Pluta, "Žiť živ naplno." I know she would be very proud. Thanks be to God for the wisdom, faith, and perseverance that He has been bestowed upon me during this project, and throughout my life: "I can do everything through him who give me strength" (Philippians 4:13).

THIS PAGE INTENTIONALLY LEFT BLANK

I. INTRODUCTION

A. MOTIVATION

The most familiar historical example of a tropical cyclone (TC) impacting United States naval forces is ADM Halsey's fleet impact and the heavy losses resulting from Typhoon Cobra in the Philippine Sea 1944. Three destroyers and 790 sailors were lost (Melton 2007). The presence of fleet assets in that region was operationally crucial, and thus outweighed the risk posed by potential losses or damage incurred during a tropical cyclone. It is easy to dismiss this cautionary tale of the dangers of operating in a region with tropical cyclones as antiquated. While one may think that this type of scenario would have been made obsolete by advances in technology, satellite imagery, and weather modeling over 65 years, it has not. In the spring of 2010, ships in the operationally crucial 5th Fleet Area of Responsibility were impacted by two tropical cyclones (TC Bandu and TC Phet) that developed in the usually inactive Northern Indian Ocean and the Gulf of Aden. Both of these systems were inaccurately forecast by all available numerical models and, as a result, had forecast tracks with high uncertainty. This uncertainty in turn caused significant logistical and operational maneuvers for all the ships operating in the area. Missions were impacted or delayed, and ships were diverted many miles out of the area due to the uncertainty. In addition, once the likelihood emerged that one storm would have significant humanitarian impacts in Pakistan, ships were then diverted again to deliver aid.

The two western North Pacific tropical storms of 2010 examined in this study were also extremely hazardous to coastal populations. Typhoon (TY) Megi caused major destruction in the Philippines and extensive damage to the south of Hong Kong, China. Over 150,000 people were evacuated from coastal provinces in China as well as all shipping traffic in vicinity of the port of Hong Kong (CNN 2010). In the northern Philippines, "about $30 million worth of infrastructure and crops were damaged and nearly 5,000 houses were damaged or destroyed by Megi's winds." The Associated Press

listed the death toll from Megi at 28. In total, Megi did damage more than 500 homes and forced evacuations of more than 300,000 (The Washington Post 2010). The second system, TY Malakas, had a 440 km outer storm edge that brought damaging winds and heavy rainfall to the Japanese islands of Honshu, Iwo To, and Chi Chi Jima (NASA 2010b).

The TCs of 2010 described above highlight many aspects of our modern naval operations, and how we can still be vulnerable to damage and loss imposed by a tropical cyclone or be called upon as a natural disaster first responder requiring our fleet assets to endure enhanced weather risks to transit to impacted regions. We are not immune to the risk to operations conducted in regions where tropical cyclones occur, and it is critically important that knowledge of their development and structural characteristics be advanced. Enhanced information obtained from studying typhoons in the Pacific such as the interactions between a tropical cyclone and the underlying ocean environment is important and can be applied to enhance, expand, and refine knowledge of tropical cyclone development in other areas.

Several studies such as those by Shay (1999), Cione and Uhlhorn (2003), Lin and Wu (2005), and Kepert (2001) underscore the need to expand the understanding of the ocean variations in impacting TC characteristics, and incorporate that understanding into improved modeling techniques. This thesis will further the understanding of the important role of the oceanic structure influence on TCs by examining data obtained from a scientific field experiment named Impacts of Typhoon on the Ocean in the Pacific (ITOP). Aircraft-deployed Airborne Expendable Bathy-Thermograph (AXBT) in-situ observation data will be examined, along with numerical model output of ocean characteristics in the vicinity of typhoons.

B. RESEARCH QUESTIONS

A primary question of tropical cyclone analysis is how changes in the underlying ocean conditions impact the formation, intensification, and structure characteristics of a passing TC. The long-term objective of ITOP was to define these impacts and variations

in structural characteristics of western North Pacific (WPAC) TCs based on ocean characteristics such as sea-surface temperature (SST), ocean heat content (OHC), and depth of the mixed layer. This thesis determines their impact with respect to TC conditions, such as wind speed, and storm location and progression as they are impacted by changes in OHC. In this thesis, the primary objective is then to compare in-situ measurements of ocean conditions near tropical cyclones with the analysis of the Naval Research Laboratory (NRL) East Asia Seas Nowcast/Forecast System (EASNFS) and examine any systematic differences. Specific questions address the rate at which changes in TC development are observed and how changes in TC characteristics vary with respect to the large-scale storm and ocean environment. For example, it is important to determine whether the intense mixing across the thermocline reflects any indications in tropical cyclone development or structural organization for strengthening or weakening of a system. A first step needed to achieve these objectives is to document current capabilities with regard to the depiction of ocean characteristics by operational products in the vicinity of a tropical cyclone. In this case, the operational product is the NRL EASNFS model output. It is expected that the results will show higher values of OHC will correlate with more favorable TC development conditions, and lower values of OHC produced in areas of cold ocean eddy activity or produced by the cold wake of the churning storm will correlate to a less favorable TC development environment.

C. WESTERN NORTH PACIFIC TROPICAL CYCLONES

The Western Pacific Ocean is a region where there is a high concentration of U.S. Naval activity. It is important that TC impacts to operations carried out in this region are mitigated by the best forecasting techniques possible. Tropical cyclones are classified by wind speed using the Joint Typhoon Warning Center (JTWC) wind threshold definitions for Tropical Depressions (TD), Tropical Storms, and Typhoons. Tropical depressions have winds less than 55 km per hour (29 kts), Tropical Storms have wind speeds of than 56 to 102 km per hour (30 to 55 kts), Typhoons have wind speeds of 103 to 211 km per hour (56 to 114 kts), Super Typhoons have wind speeds of 212 km per hour (115 kts) and above. Climatology available for this region shows 25 tropical cyclones occur here on

average each year, and it is the busiest region for tropical cyclone activity in the world. Of the average number of 25 tropical cyclones, 18 typically further develop into tropical storms. Of those 18, seven develop into typhoons and five develop into super typhoons. Although 2010 had slightly overall less tropical cyclone activity than normal, this region remains a significant basin of tropical cyclone activity with some of the largest and most intense TC systems in the world. TCs are warm core in nature, meaning that their development depends upon latent heat release involved in these types of low-pressure storm systems. The warm core nature of TCs is the major difference between TCs and mid-latitude low-pressure systems. Some TCs can cover more than 600 miles in diameter, bringing a wide swath of intense destruction along their track. Most storms form east of the Philippines, and move across the Pacific towards the Philippines, Japan, and China; a few TCs form in the South China Sea. The season extends from April through December. However, tropical cyclones are more common in off-season months in this area than anywhere else. The peak of the season is July through September, when nearly 70% of all typhoons develop. There is a noticeable seasonal shift in TC tracks in this region. From July through September, TCs move north of the Philippines and recurve, while early and last-season typhoons move on a more westerly track through the Philippines before re-curving. The months of September and October, when the ITOP experiment observed three typhoons, the climatological average is 1.5 tropical storms, and 4.1 typhoons. (Bowditch 2002).

D. IMPACT OF TYPHOONS ON THE OCEAN IN THE PACIFIC (ITOP) PROGRAM

During the summer of 2010, the ITOP program was conducted over the western North Pacific to examine interactions between the ocean and TCs. Specific goals of ITOP included: (i) examination of the formation and dissipation of the ocean cold wake formed by a TC; (ii) observations of air-sea fluxes in a TC environment; (iii) The impact of ocean eddies on TC and the influence of the TC on the ocean eddy; (iv) examination of the surface ocean wave field under a TC; and (v) the relationships among environmental factors and TC formation.

The ITOP program (Figure 1) was designed to use a variety of experimental approaches to examine the TC and the ocean. Specific observational assets included an array of moored buoys, two WC-130J aircraft (Figure 2), an ASTRA business-class jet, and a U.S. research vessel (RV Revelle). Airborne-deployed sensors included dropwindsondes, AXBTs, Lagrangian floats, and drifters.

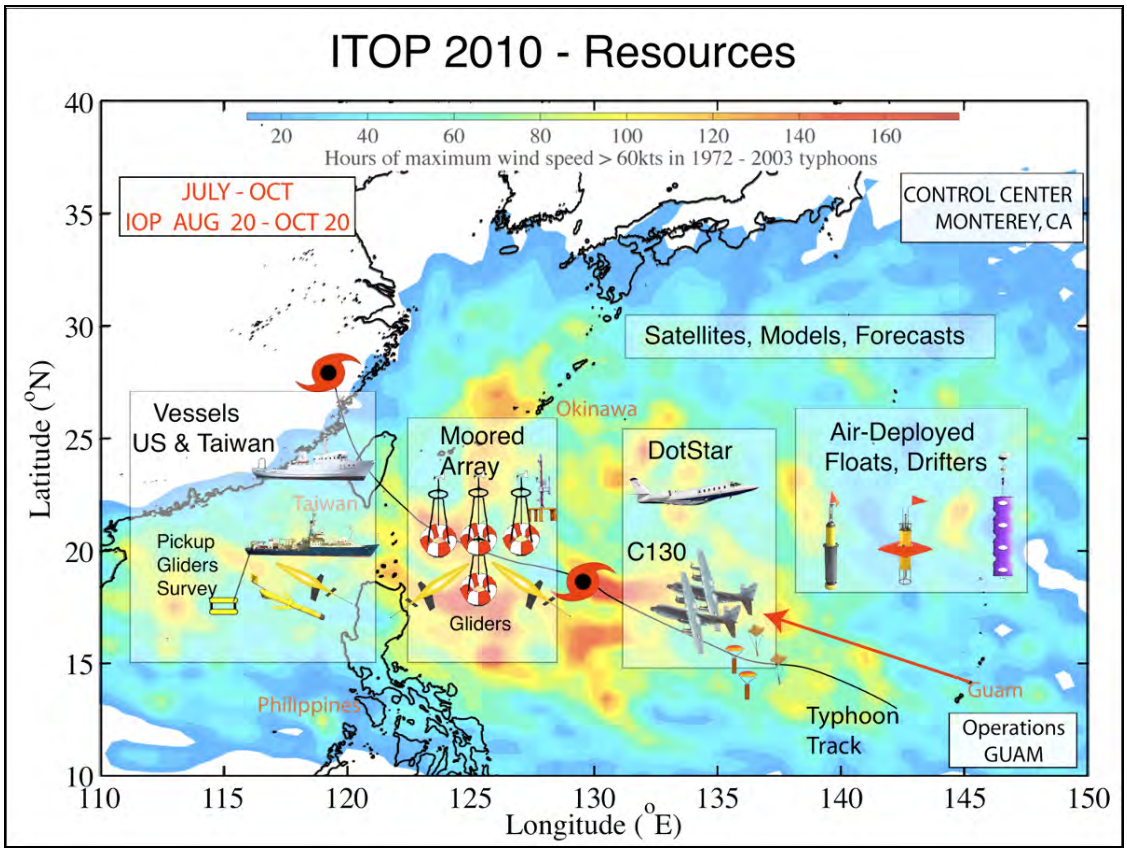

Figure 1. Schematic of observation assets used during ITOP 2010.

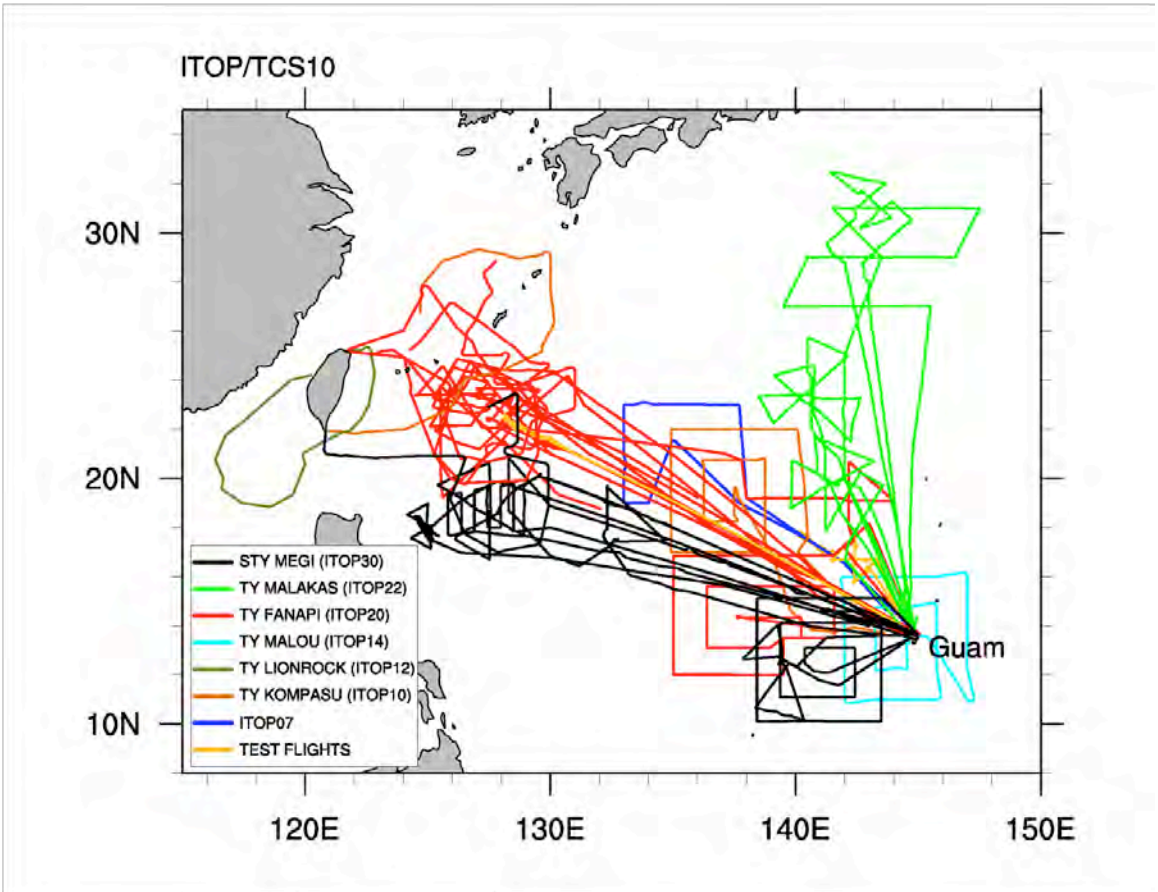

Figure 2. ITOP Flight tracks of the WC-130J aircraft during ITOP.

During ITOP, three typhoons formed and were examined using the variety of observational assets defined above. In addition to the collection of in situ observations, several numerical model products were developed and used to guide operations and the deployment of instruments. The combination of observations and numerical products provides a unique capability to identify the ability of numerical products to represent upper ocean thermal structure in the vicinity of typhoons.

Of particular interest in this study are observations based on WC-130J deployed drifting buoys and AXBT data. The representative accuracy of aircraft data was defined through comparison with ship-based profiles that were conducted at the time of aircraft overpasses.

Similar data were collected and analyzed for this region for the 2008 TC season during ITOP-08 (DePalma 2011). Based on this previous work, it is expected that data collected during ITOP will identify characteristic responses in a tropical cyclone, due to impacts by the ocean and will expand knowledge based on the 2008 data (Elsberry and Harr 2008). It is anticipated that improvements to forecast models will be realized by these comparisons and increase the value of model forecasts as significant contributions to the progression of a tropical cyclone life cycle.

E. 2010 PACIFIC SYNOPTIC OVERVIEW

During the summer of 2010, the large-scale environment of the western North Pacific was quite anomalous with a very weak monsoon trough. The entire ocean basin was therefore characteristic of La Niña conditions. Because of the weak monsoon trough and predominance of trade-wind easterlies, La Niña conditions are generally unfavorable for TC development. Consequently, in 2010, there were 19 tropical cyclones in total, with 14 reaching tropical storm strength. Of those 14, eight further developed into typhoons, and one into a super typhoon (STY) (U.S. Naval Maritime Forecast Center, 2010). During the ITOP period three typhoons formed: Typhoon (TY) Malakas, TY Megi, and TY Fanapi. TY Malakas and TY Megi were selected for this thesis because both had ITOP data sets that included multi-day flights over their respective storms at varying over-flight times throughout the day. During TY Malakas, a sequence of four aircraft missions was conducted and a sequence of five missions was conducted in TY Megi. Both TY Megi and TY Malakas formed in the western Pacific Ocean in September and October of 2010.

1. Western Pacific Conditions During 2010

The El-Niño Southern Oscillation (ENSO) cycle had El Niño conditions from approximately June of 2009 through April of 2010. The ENSO then transitioned to a brief neutral condition that extended through May and June of 2010 until a shift to La Niña conditions that persisted from August of 2010 to April of 2011 (NOAA 2011). In the central equatorial and eastern Pacific, slightly cooler than average SSTs existed (Figures

3, 4, 5, 6). In the Philippine Sea, SSTs were generally above 30°C, which corresponded to a 0.3–1.2°C anomaly for that region in those months of 2010. A small area along northern Japan experienced SST anomalies at 2.5°C above normal (Figures 5, 6). SSTs of 27°C and above are considered a favorable factor for tropical cyclone development. During this period, Ocean Heat Content (OHC) for this time was greater than the threshold favored for tropical cyclone development throughout the Philippine Sea (60 KJ cm^{-2} and above, which will be referenced threshold later in this thesis as well). Higher values of OHC will correlate with more favorable TC development conditions, and lower values of OHC produced in areas of cold ocean eddy activity of produced by the cold wake of the churning storm will correlate to a less favorable TC development environment (Lin et al. 2008; Minelli et al. 2008).

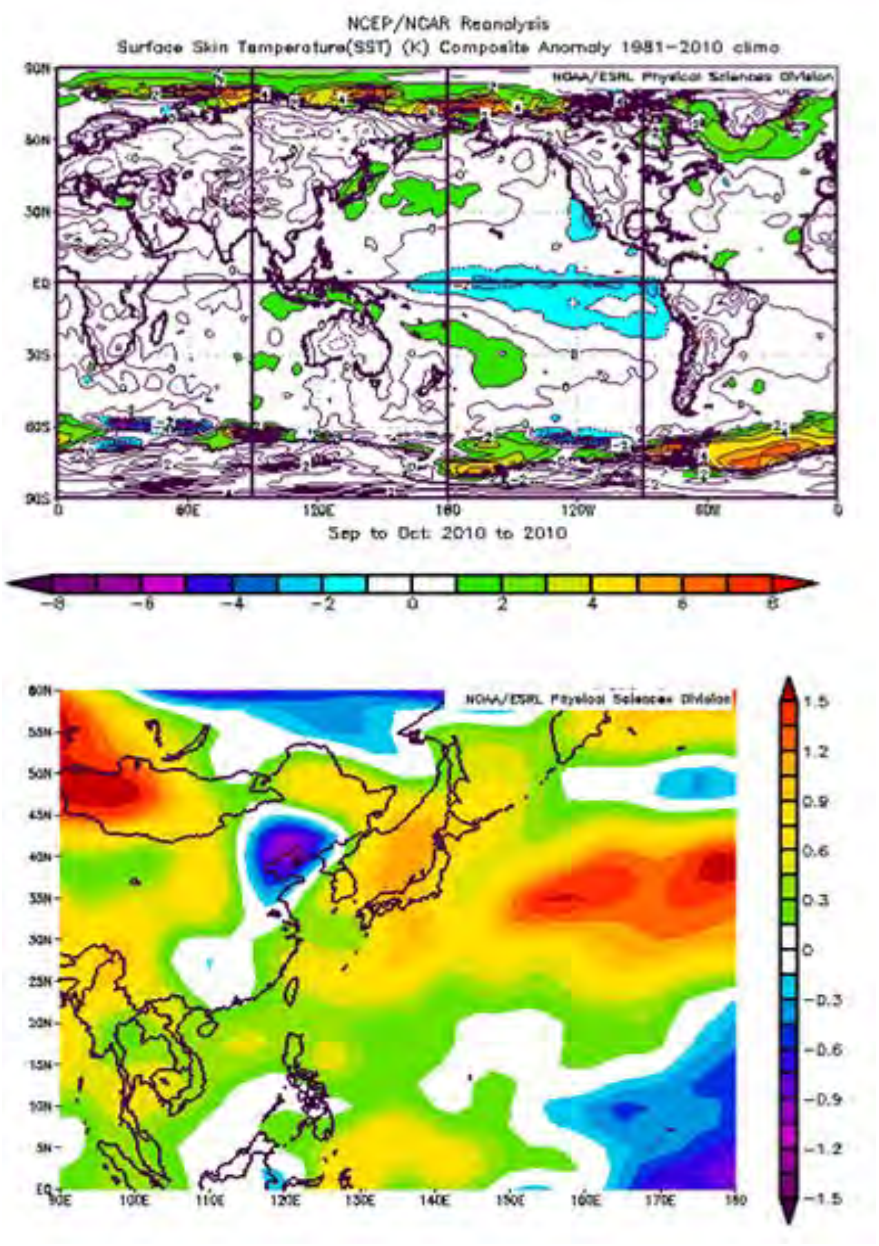

Figure 3. Analyzed global (top) and Philippine Sea (bottom) SST anomaly (°C) pattern during September through October 2010.

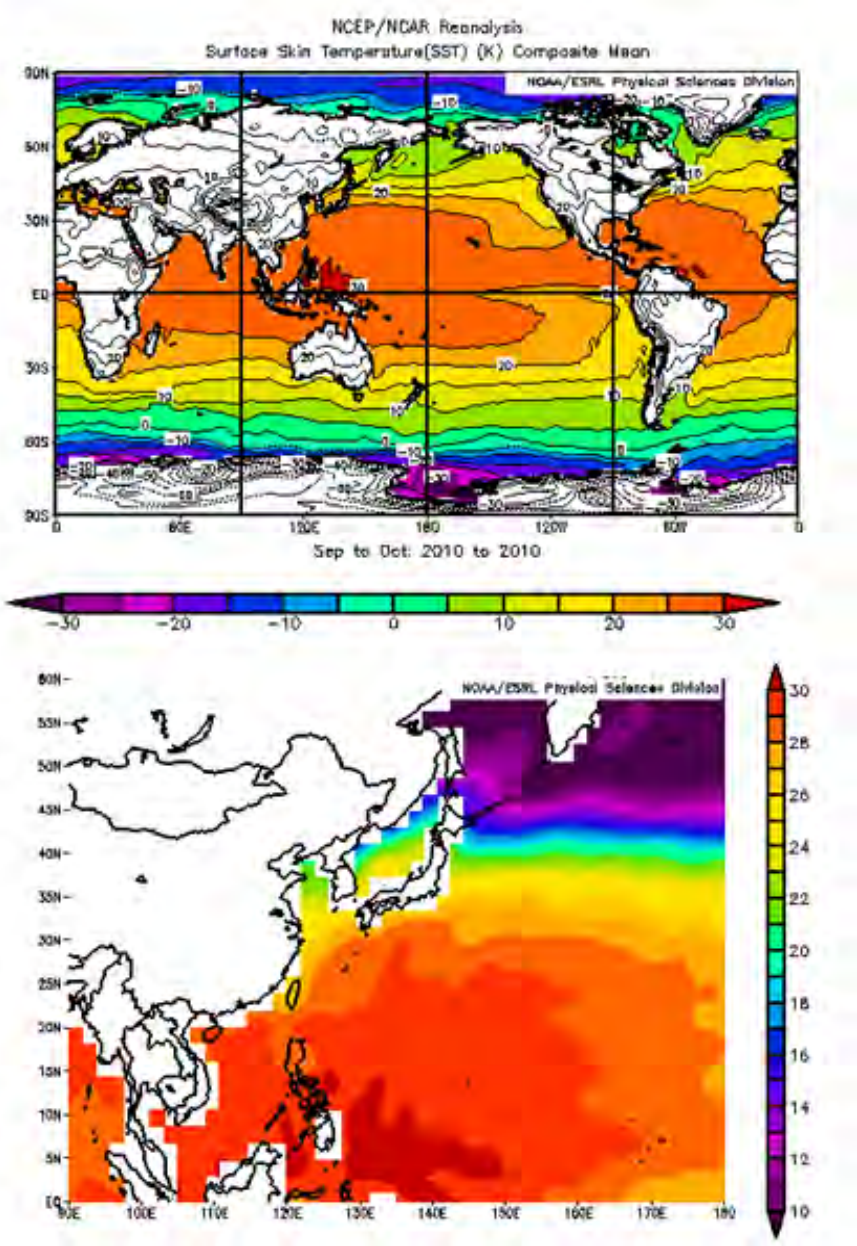

Figure 4. Analyzed global (top) and Philippine Sea (bottom) mean SST (°C) during September through October 2010.

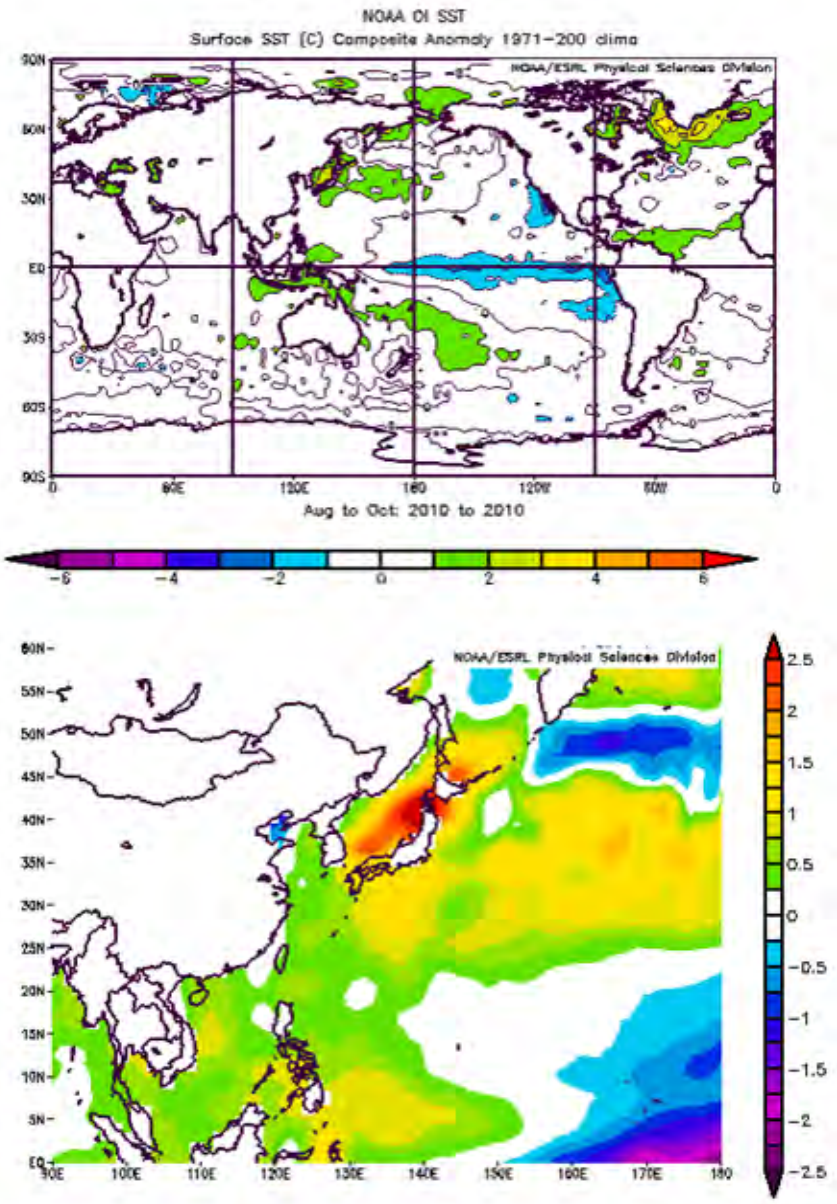

Figure 5. Analyzed global (top) and Philippine Sea (bottom) SST anomalies (°C) over the regions during August through October 2010.

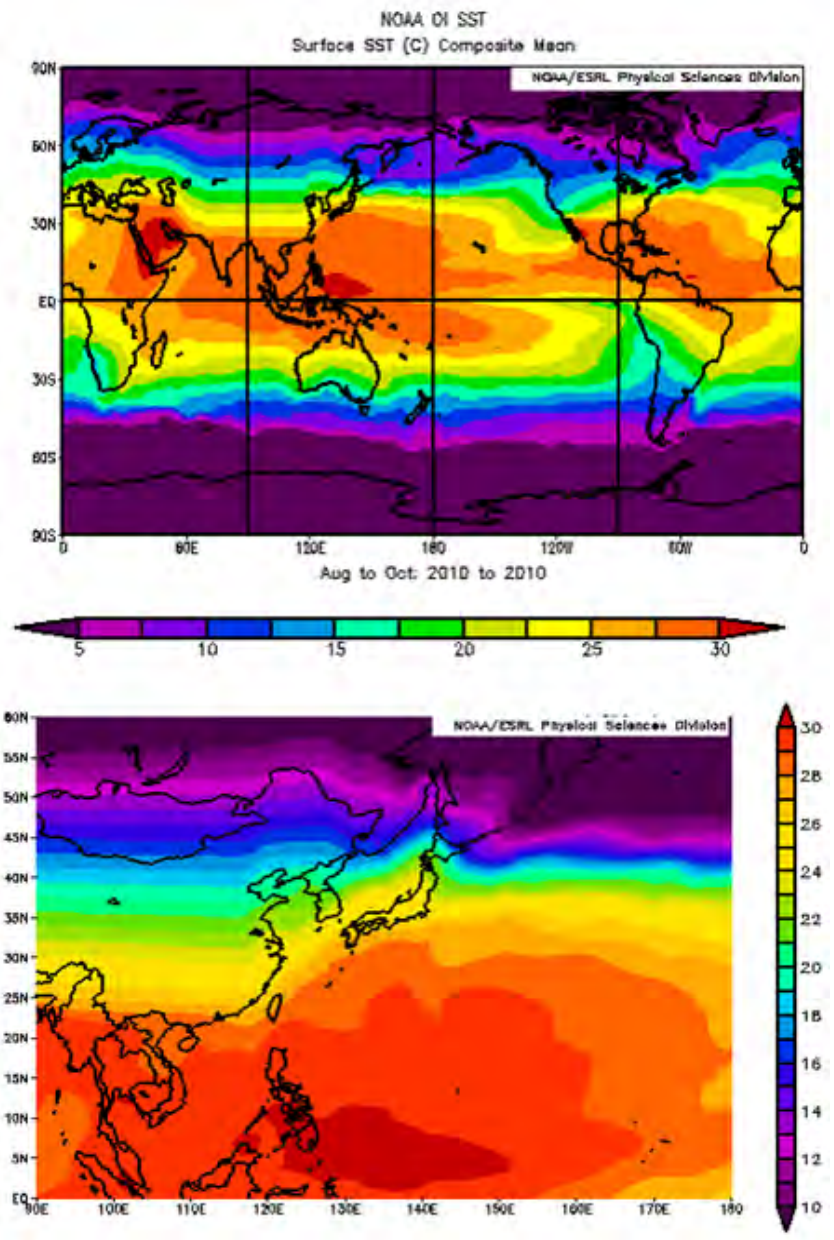

Figure 6. Analyzed global (top) and Philippine Sea (bottom) mean SST (°C) composite from August to October of 2010.

During September and October of 2010, a large region of low-level anomalous easterly winds covered the central Pacific and extended into the western Pacific and Philippine Sea (Figures 7, 8). These low-level wind anomalies characterized the weak monsoon trough that was present over the Philippine Sea in the fall of 2010 and were also an indicator of developing La Niña conditions.

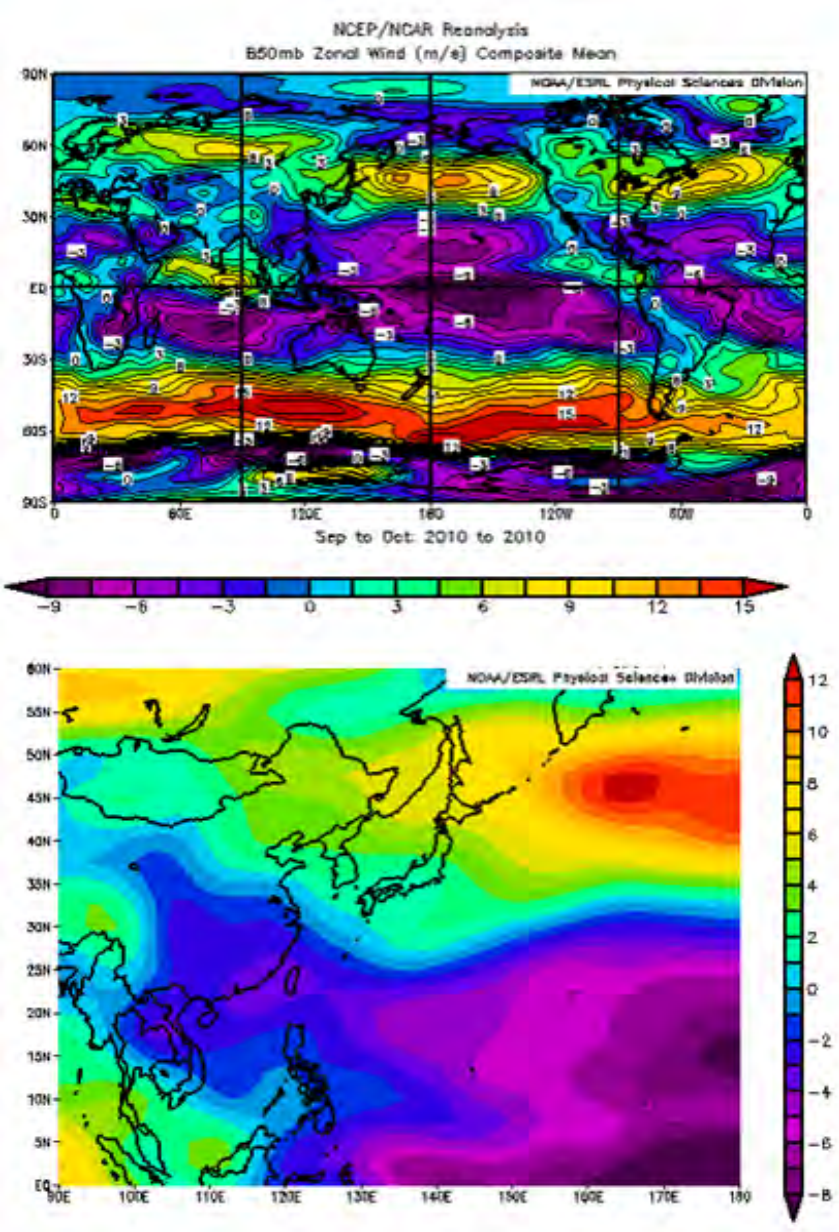

Figure 7. Analyzed global (top) and Philippine Sea (bottom) zonal wind mean (m s^{-1}) at 850 hPa over the regions during September through October 2010.

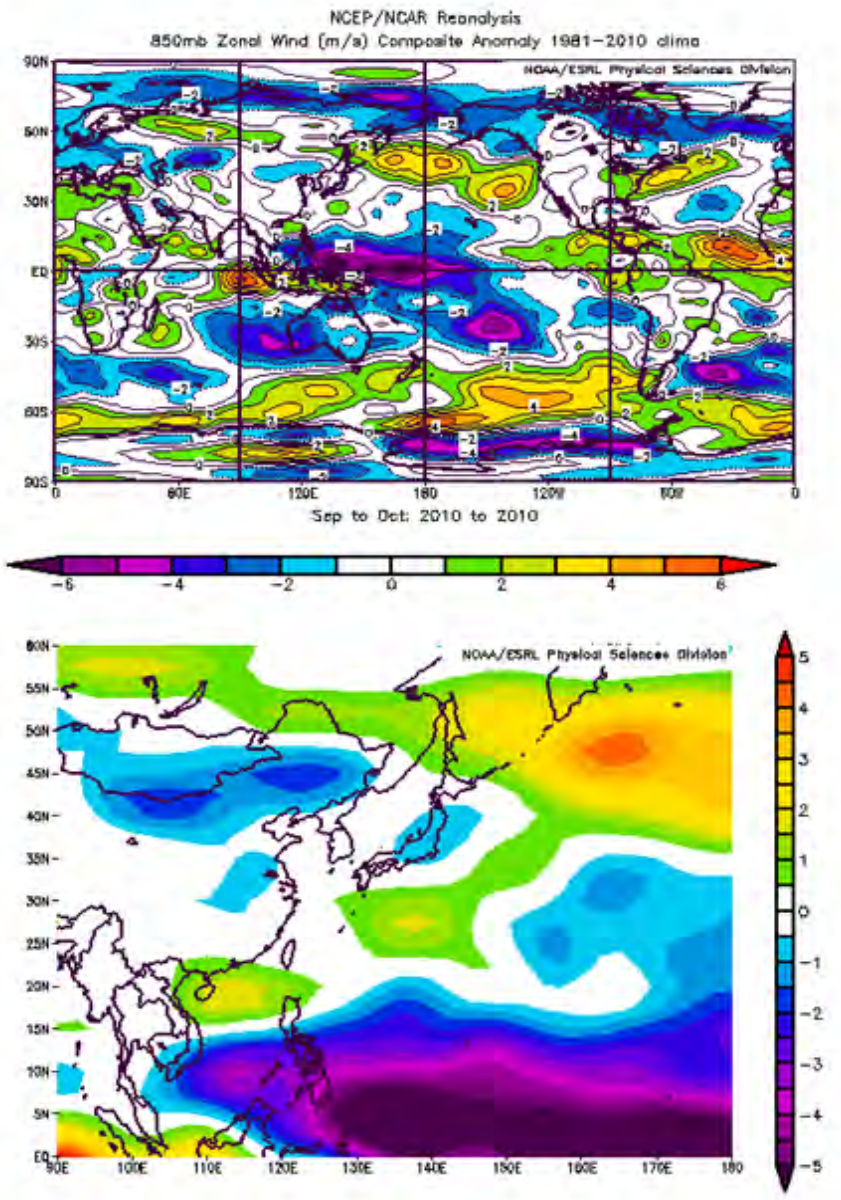

Figure 8. Analyzed global (top) and Philippine Sea (bottom) zonal wind anomaly (m s^{-1}) at 850 hPa over the regions during September through October 2010.

Typically, during La Niña conditions, tropical cyclone formations occur farther west and north than during El Niño conditions (Figure 9). During the timeframe of the ITOP experiment, tropical cyclone development and tracks occurred over the northern portion of the western North Pacific (Figure 10), which was typical of the La Niña conditions.

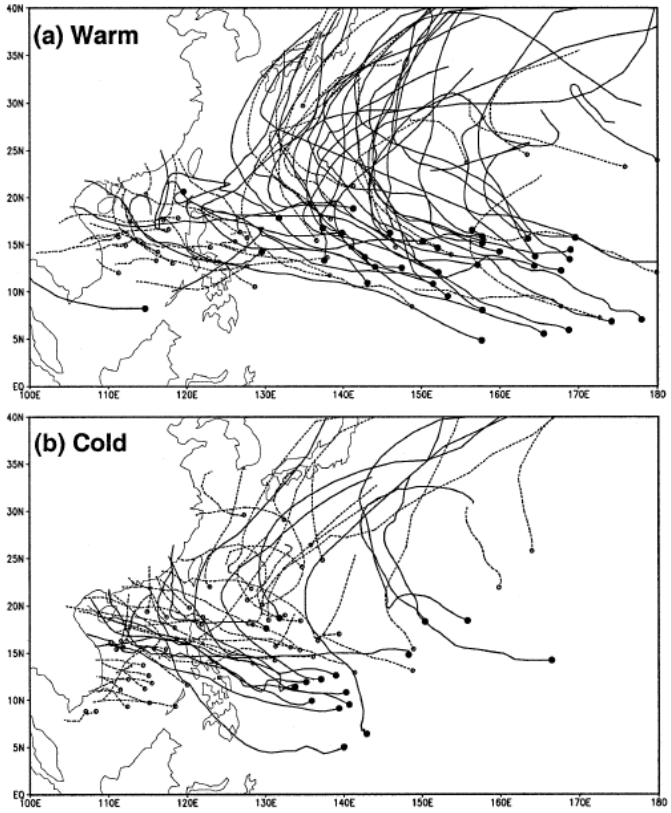

Figure 9. (a) El Niño and (b) La Niña TC formation locations are denoted by dots with associated tracks annotated by extending lines for the six warmest (El Niño) and coldest (La Niña) years between 1965–1999 (Wang and Chan 2002).

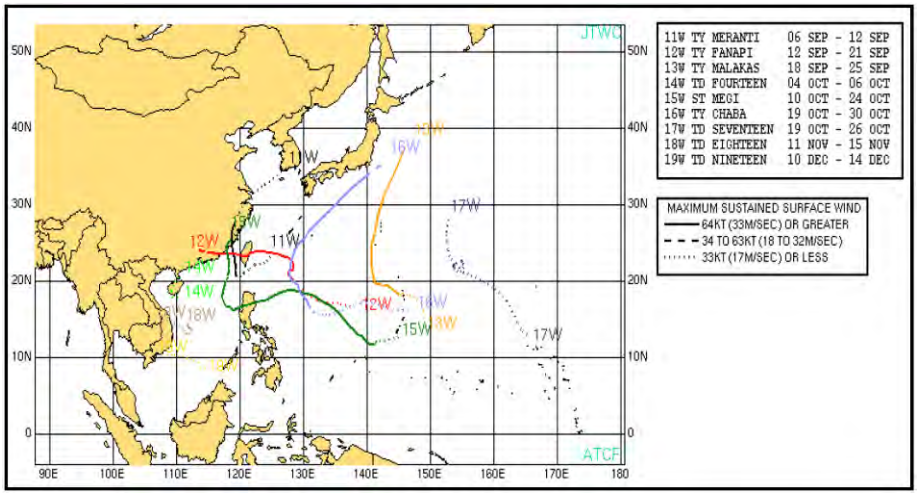

Figure 10. JTWC 2010 Pacific storm tracks.

2. Tropical Cyclones

a. TY Malakas

The storm was identified as Tropical Depression 13 (TD13) on 20 September by JTWC (Figure 11). Typhoon Malakas then formed on 21 September in the vicinity of 18°N 145°W. The synoptic environment at the time of initial development included warm sea surface temperatures and low vertical wind shear, which are favorable for development of a TC. TY Malakas reached a peak intensity of 100 knots on 24 September and existed for a total duration of five days. Three days of ITOP flights were conducted during the lifespan of this storm (Figures 12–16).

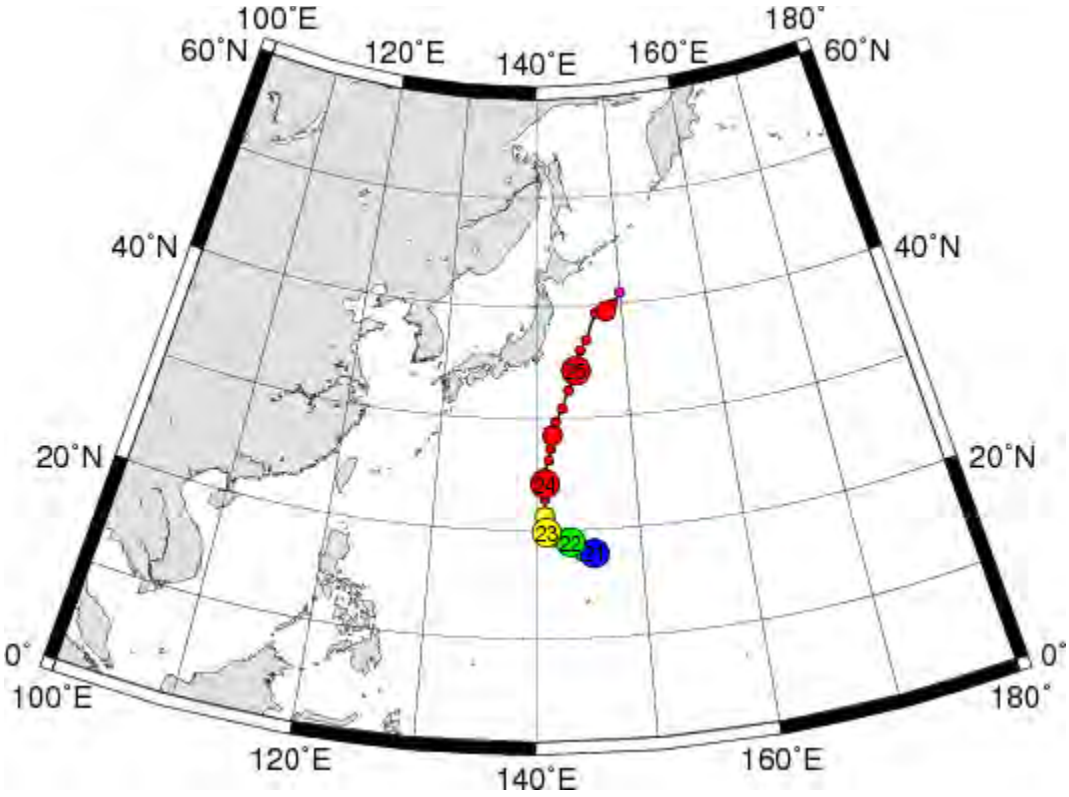

Figure 11. The analyzed track of TY Malakas with date of position indicated by number and intensity change indicated by color (From: KITAMOTO Asanobu 2011).

By 22 September (Figure 12), the low-level center of circulation was partially exposed due to the northerly vertical wind shear, which prevented additional intensification. By 23 September (Figure 13), better organization was noted as the distribution of high cloud tops increased and deep convection became organized along outer bands. Cloud top temperatures colder than −53.7°C throughout a large area within Tropical Storm Malakas were observed (Figure 13).

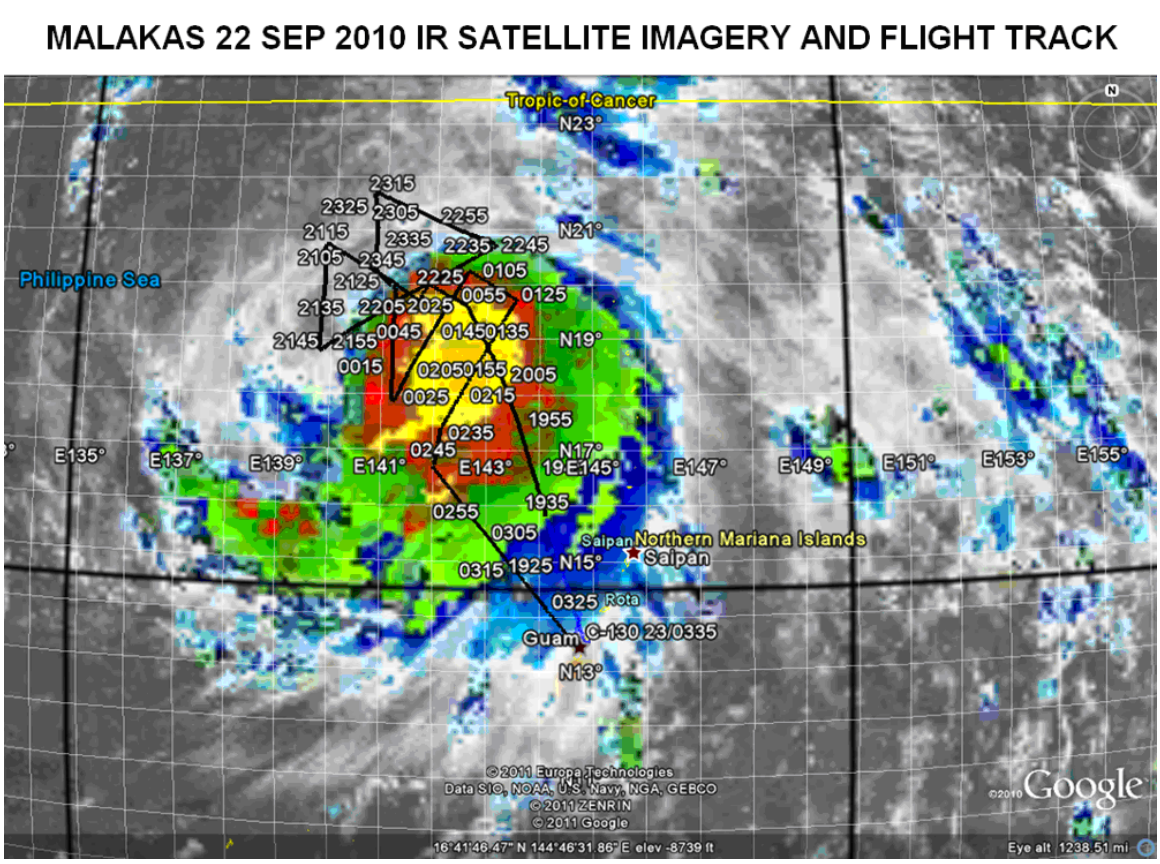

Figure 12. The annotated flight track of the WC130J on 22 September in TY Malakas overlaid on the geostationary infrared (IR MTSAT) satellite imagery.

The cells in the northern quadrant of the storm were also stronger and more organized than those in the southern quadrant. Strong convection on either side of the storm eye was defined in radar imagery of the typhoon. A well-defined eye structure was observed from 23 to 24 September (Figures 13 and 14). Maximum cloud top heights extend to approximately 16 km in the northern quadrant, and about 15 kilometers in the southern quadrant of the storm (Figures 13 and 14).

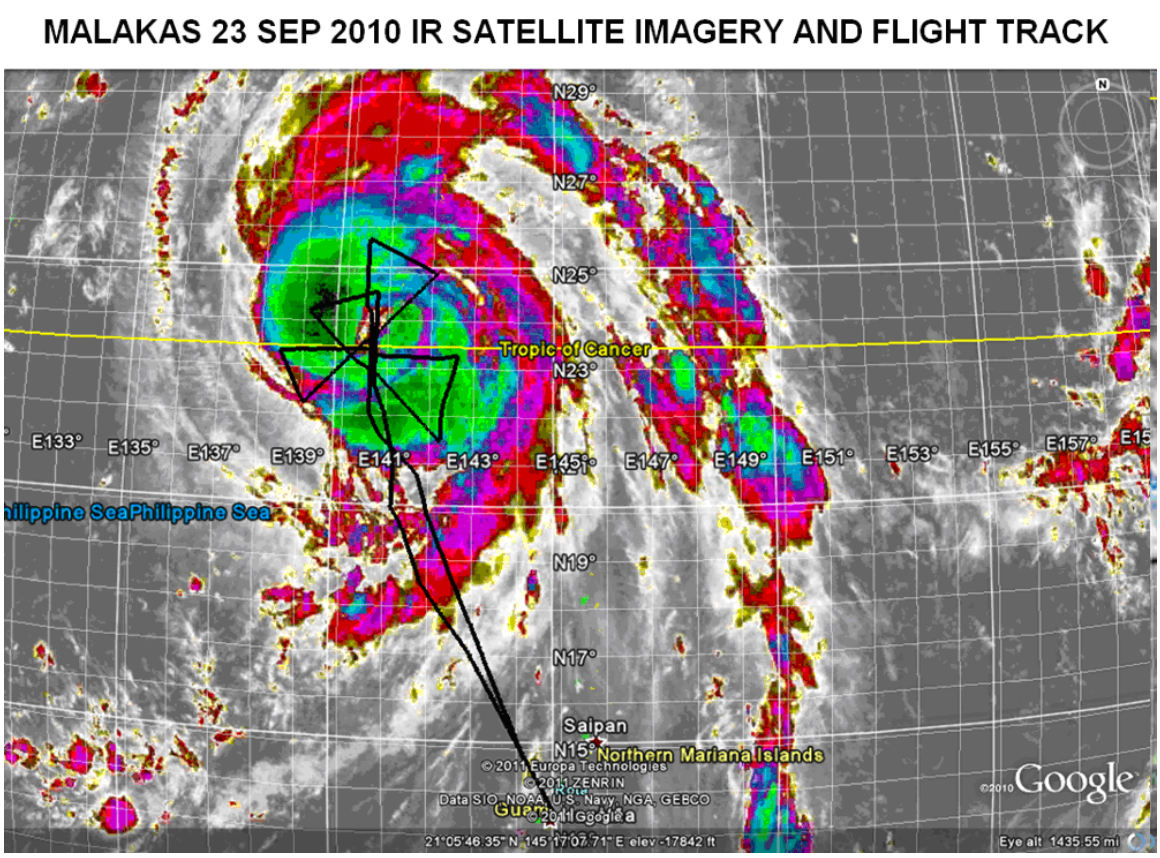

Figure 13. The annotated flight track of the WC-130J on 23 September in TY Malakas overlaid on IR satellite imagery.

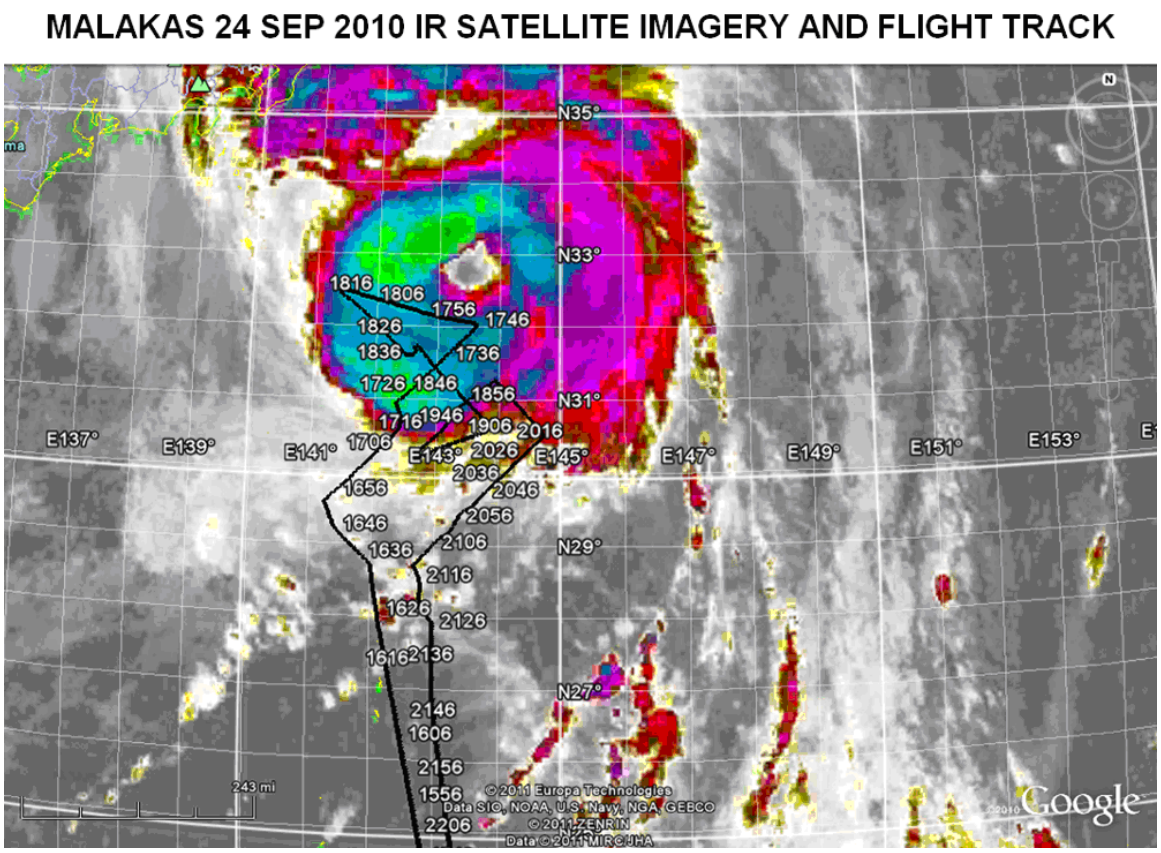

Figure 14. The annotated flight track of the WC-130J in TY Malakas on 24 September overlaid on IR satellite imagery.

At peak intensity, TY Malakas had a translation speed of 23 knots and generated seas of 31 feet. The eye of the storm was detected to be 50 nautical miles (n mi) wide and the overall span was measured from satellite data to be over 150 n mi at peak intensity. The track of Malakas passed over the Japanese islands of Iwo To and Chi Chi Jima, then paralleled the coast of Japan. The storm was weakened by strong vertical westerly wind shear as it headed to the north over the subtropical western North Pacific Ocean. Two final flights (Figure 15) were conducted to observe the cold wake that developed following TY Malakas on 28 and 29 September (Figure 15) (NASA 2010a). Minimum central pressure recorded was 945 hPa on 24 to 25 September (Figure 16).

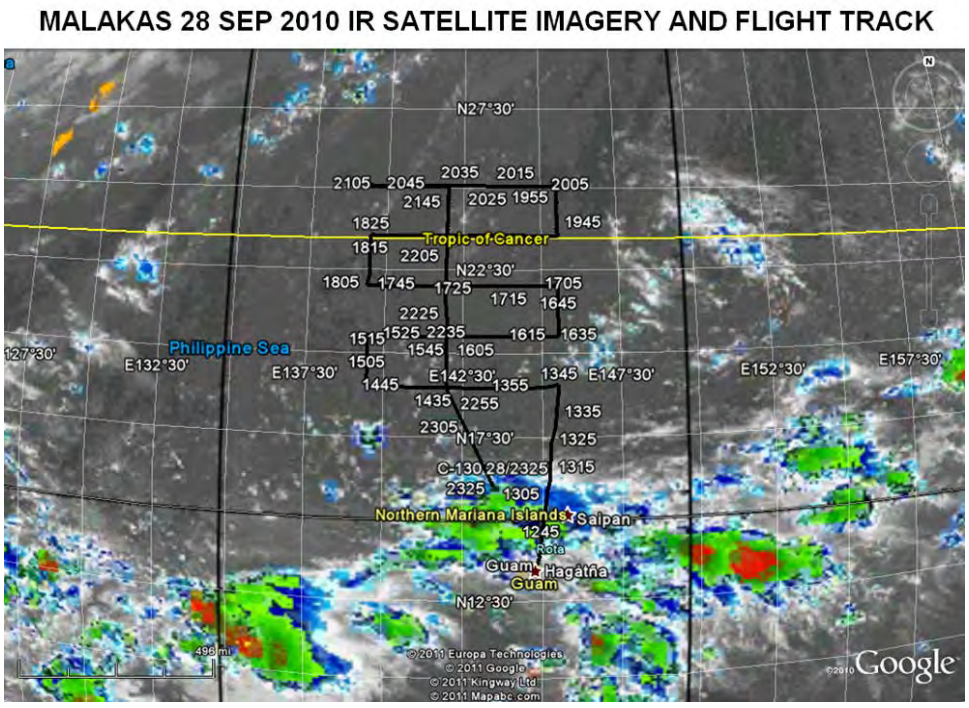

Figure 15. The annotated flight track of the WC-130J in TY Malakas on 28 September overlaid IR satellite imagery

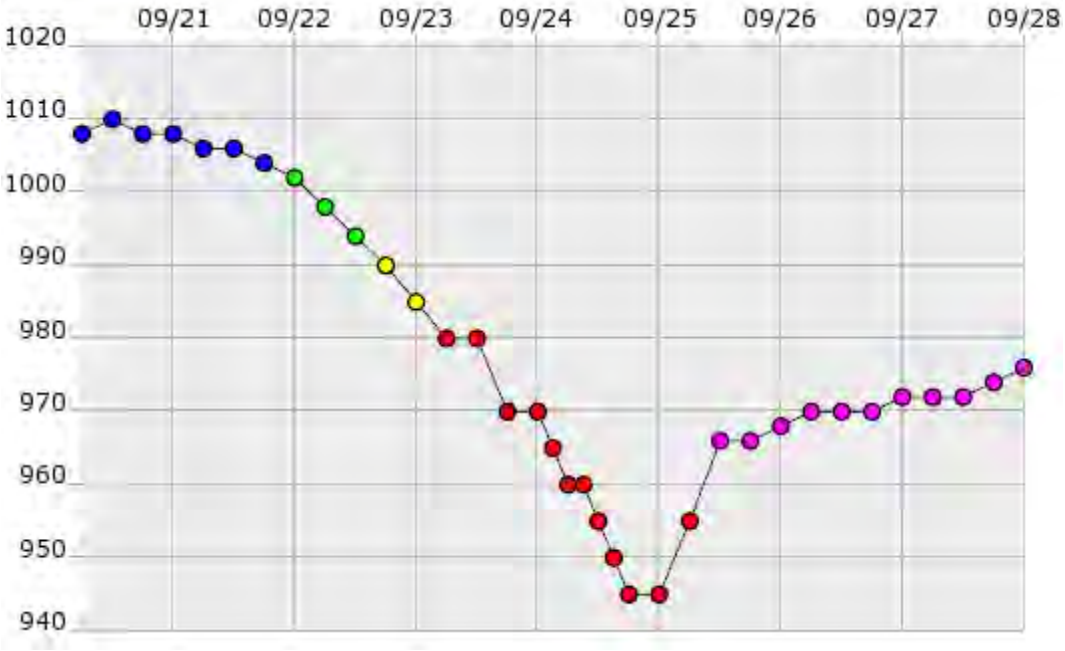

Figure 16. The central pressure (hPa) of TY Malakas (From: KITAMOTO Asanobu 2011)

b. TY Megi

Megi initially formed as a TD over the western Pacific Ocean on 13 October 2010 with a broad area of instability and convective activity (Figure 17). Typhoon Megi then formed on 14 October in the vicinity of 10°N 140°E TY Megi had a lifespan of nine days and reached a peak intensity of Super Typhoon on 17 October. Five days of ITOP flights were conducted in TY Megi (Figures 17–23). Because of the broad circulation and disorganized convective patterns, the flight plan for the 12 October mission was to cover a uniformly spaced and broad area of the region of convective activity (Figure 17).

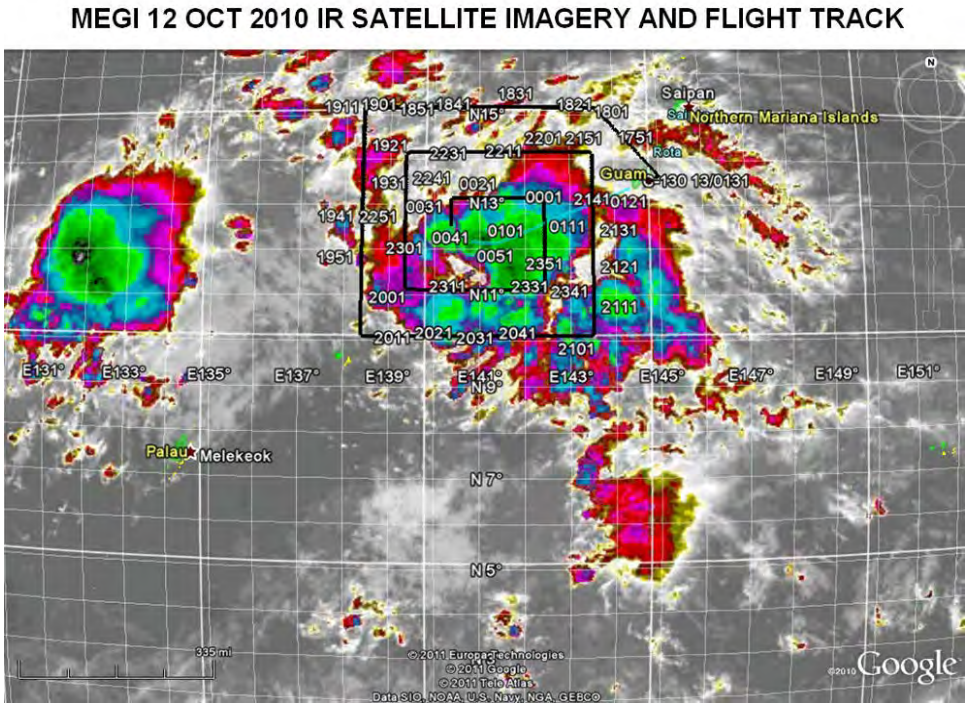

Figure 17. The annotated flight track of the WC-130J in TY Megi on 12 October overlaid on IR satellite imagery.

Megi quickly strengthened (Figure 18) to a named storm under favorable TC development conditions that included low vertical wind shear, sea surface temperatures above 28° C, a poleward outflow channel, and upper-level divergence. Environmental

conditions remained favorable for TY Megi throughout the observation period (Figure 19). The observation strategy on 15 October (Figure 20) was to fly ahead of the storm and lay out a grid of ocean instruments that would measure the air-sea interactions as Megi passed over the array (Figure 21) 24-h later. Then, on 17 October (Figure 22), a second flight measured the changes in the structure of TY Megi that were realized after passing the region where the ocean instruments were placed (Figure 23).

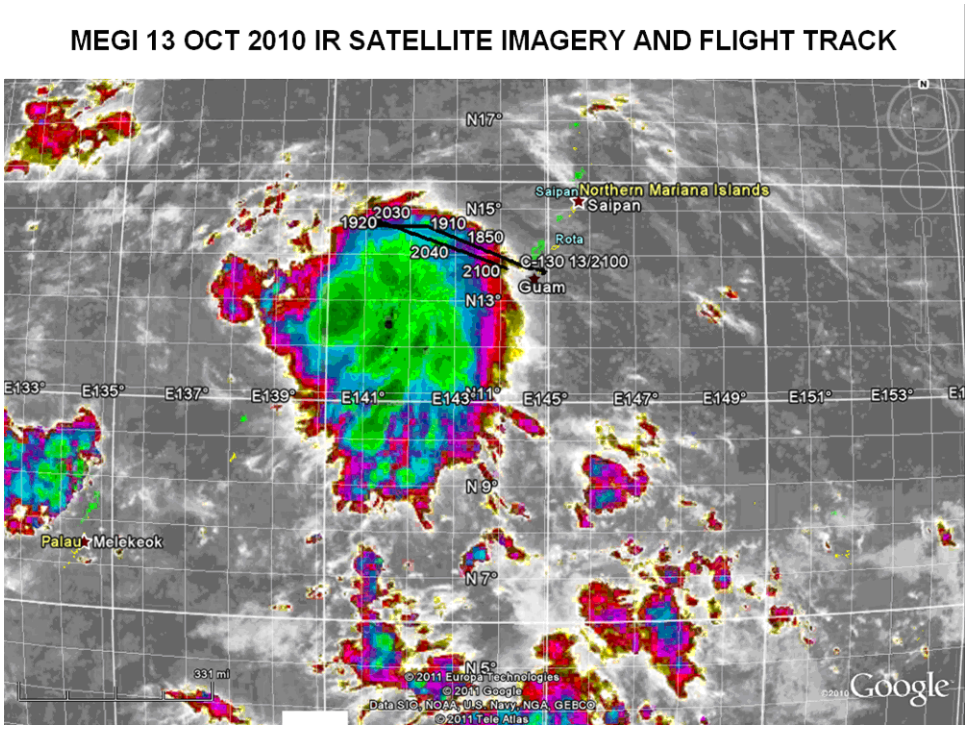

Figure 18. The annotated flight track of the WC-130J in TY Megi on 13 October overlaid on IR satellite imagery.

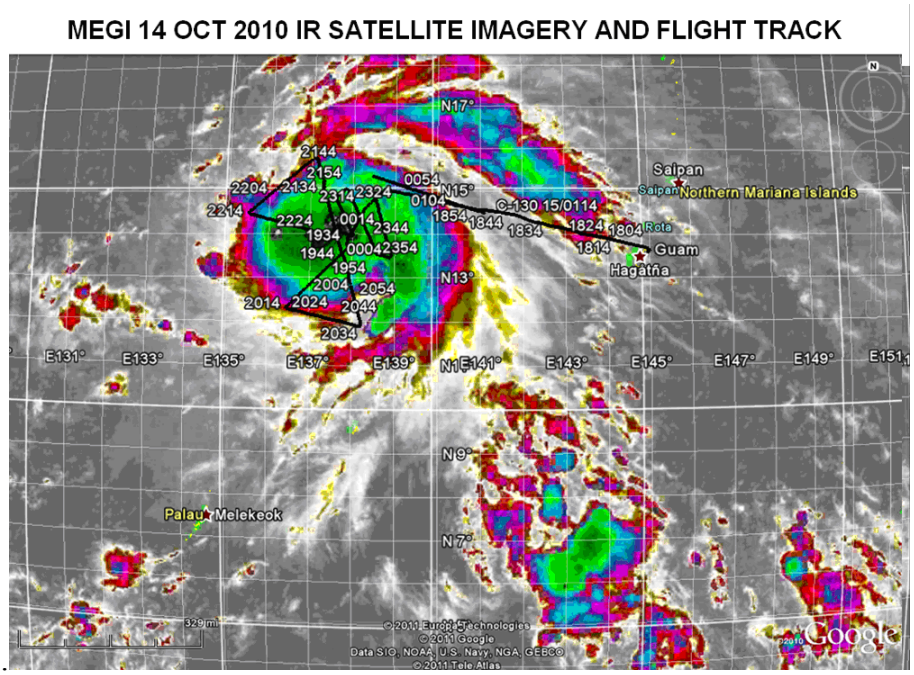

Figure 19. The annotated flight track of the WC-130J in TY Megi on 14 October overlaid on IR satellite imagery.

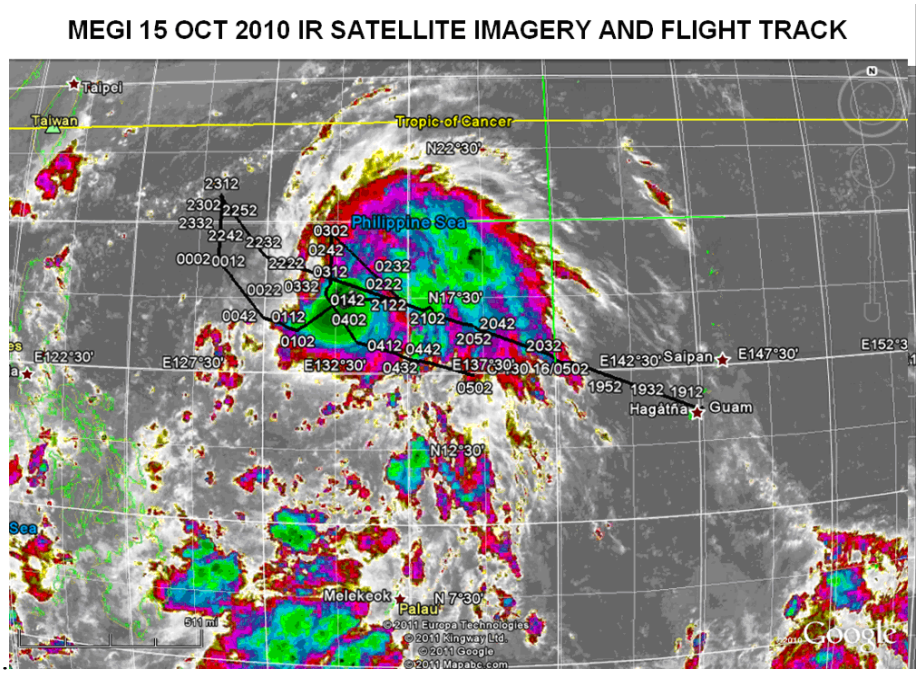

Figure 20. The annotated flight track of the WC-130J in TY Megi on 15 October overlaid on IR satellite imagery.

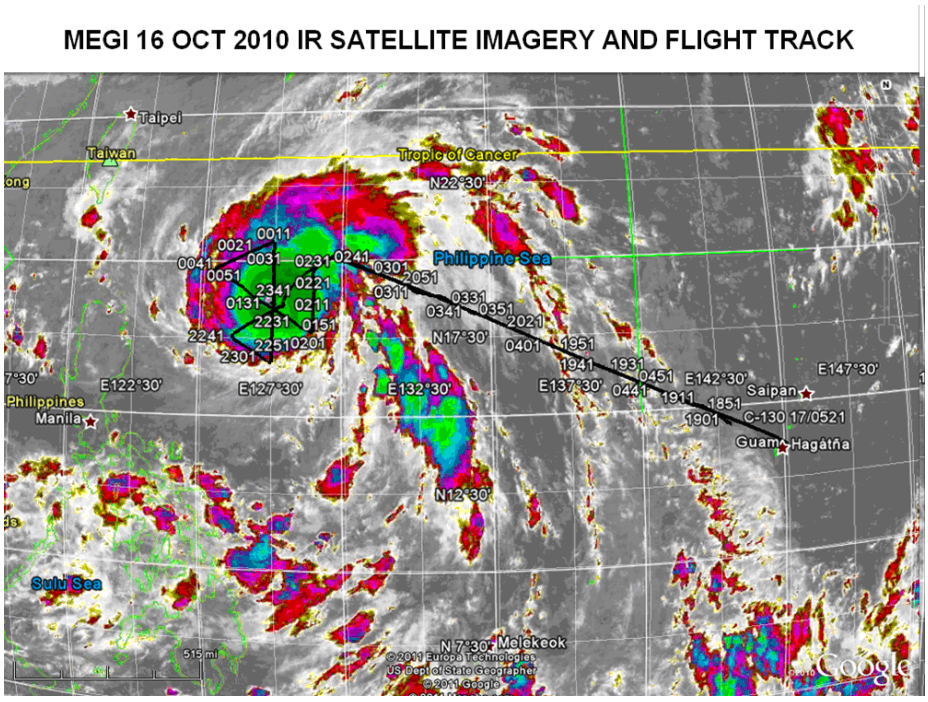

Figure 21. The annotated flight track of the WC-130J in TY Megi on 16 October overlaid on IR satellite imagery.

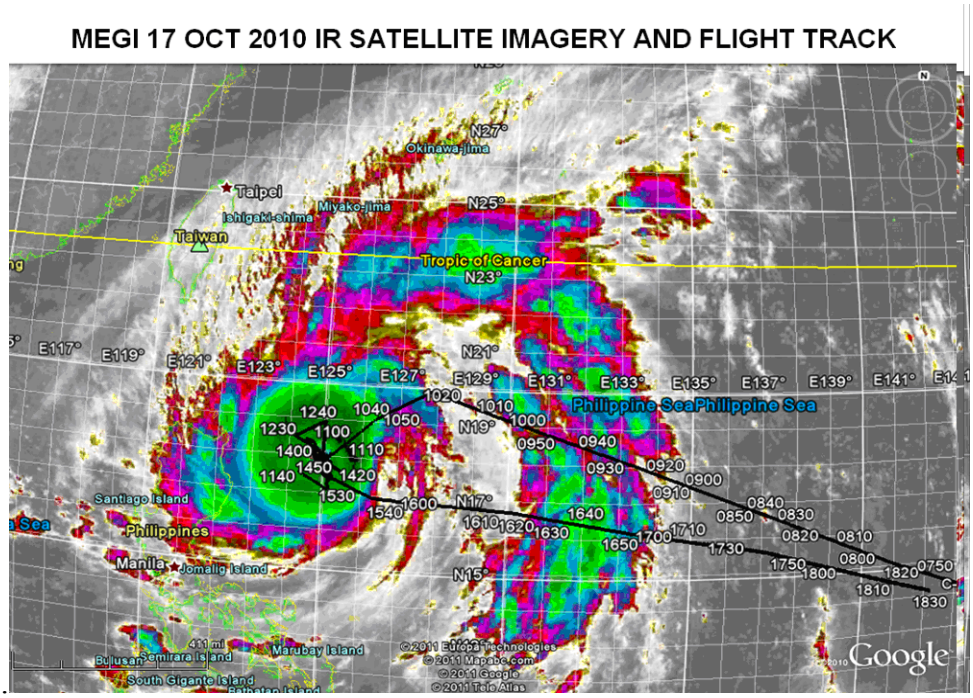

Figure 22. The annotated flight track of the WC-130J in TY Megi on 17 October overlaid on IR satellite imagery.

The final flight associated with TY Megi occurred on 18 October and focused on the formation of the cold wake produced by the TC (Figure 23). From 16 to 18 October, TY Megi remained a strong, well-organized system. The peak intensity of 159 kt with gusts of 175 kt (super typhoon) and a lowest central pressure of 888 hPa occurred on 18 October (Figures 24−25). The eye of Megi was measured at 74 km (40 n mi) in diameter on 20 October, when the maximum winds decreased to 90 kt after landfall over the Philippines. By 21 October, the winds had strengthened to 100 kt after the storm moved over the South China Sea. Heaviest rainfall of about 2 inches per hour from TRMM rainfall analysis was located in the thunderstorm bands on the eastern portion of Megi's eyewall. The storm then moved into an area with increased shear, causing weakened convection in the storm as it continued to travel north at 7 kts (Figure 24). Over the South China Sea, Megi re-strengthened somewhat before making landfall along the Chinese coast on 23 October. The storm dropped heavy precipitation along a curving path between the Philippines and China. Rainfall amounts of up to 24 inches in numerous regions were observed. The least rainfall associated with TY Megi was 3 inches.

The extensive swath of the storm translated to significant destructive impacts for areas that were not directly along the storm path as well. East of Taiwan, areas of torrential rains led to deadly landslides. Floods and landslides had killed as many as 31 people in that island nation according to the Associated Press as of 24 October. United Daily News reported that the heavy rains in Taiwan might have resulted from interactions between Megi and monsoon weather patterns northeast of the storm. After landfall, Megi dissipated quickly due to a merge with a stationary frontal boundary (NASA 2010b).

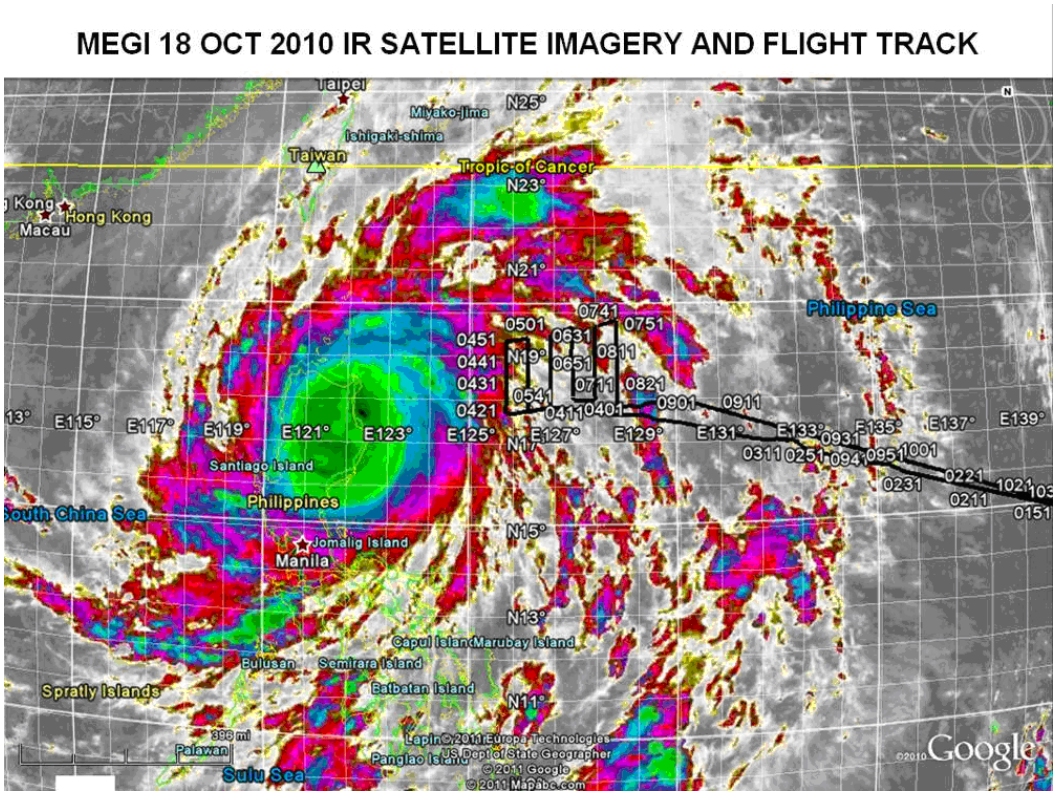

Figure 23. The annotated flight track of the WC-130J in TY Megi on 18 October overlaid on IR satellite imagery.

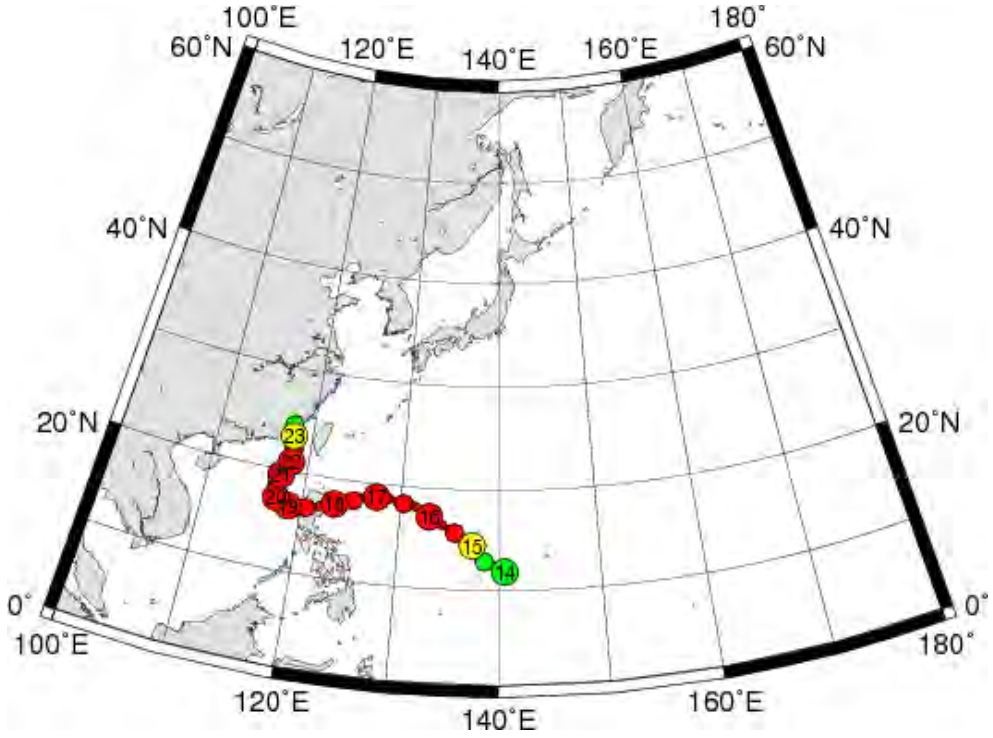

Figure 24. The analyzed track of TY Megi. Color changes represent changes of intensity. (From: KITAMOTO Asanobu 2011)

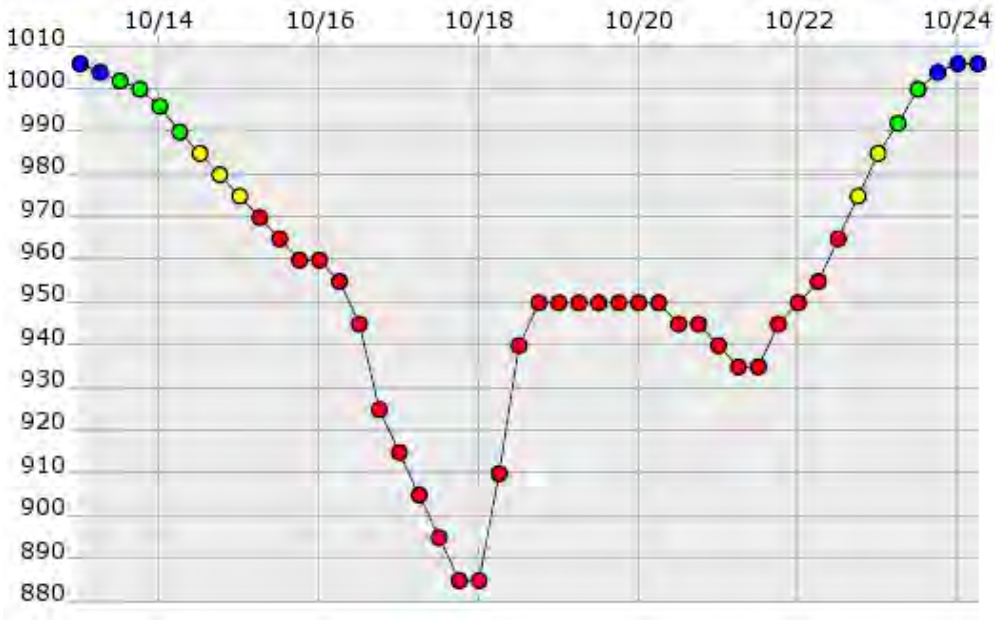

Figure 25. The central pressure (hPa) of TY Megi. (From: KITAMOTO Asanobu 2011)

II. DATA AND METHODOLOGY

A. DATA SOURCES

1. In-Situ Observations

The in-situ observations collected during the ITOP experiment included AXBTs deployed from WC-130J aircraft and bathythermograph soundings collected from surface ships. The primary observational data set examined in this thesis consists of aircraft-based observations of mature TCs during the ITOP field campaign. These observations were obtained with AXBTs, which provide in situ observations sea-surface temperature and temperature with ocean depth. For this study, AXBT data were processed to a vertical resolution of 1 m. The processing involved analysis of the temperature profile to ensure that the recording of data on the aircraft captured the splash of the AXBT on the ocean surface. For those profiles that were missing the entry point into the ocean, the raw files were reanalyzed to capture the surface temperature and the initial few meters under the surface. Flight path diagrams are included in Appendix A, Figures 31–39. Sample processed AXBTs are provided in Appendix B, Figure 40.

By examining ocean mixed layer characteristics from in situ measurements and numerical models with an accurate ocean initialization scheme, improved estimates of the impact of the OHC in TC conditions will be quantified for use in operations. Two important factors are identified in this study. One is the increased understanding of the role of ocean variability in TC characteristics. This is an important contribution to improve forecasts of TC intensity and wind structures. The second is the use of in-situ measurements to evaluate operational models. Since models are dependent on input data that define structure in the ocean (including currents) and atmosphere, it is important to properly analyze data acquired from aircraft since the community cannot rely solely on fortuitous encounters with moored ocean buoys (Mainelli et al. 2008). Because in situ data are rarely available, the primary capability for future improvements in TC-ocean

forecast of interaction will be dependent on numerical models. Therefore, this study concentrates on providing a benchmark measurement of the model-defined ocean structure in relation to measurements taken during ITOP.

This study will further the understanding of the important role of oceanic structure influence on TCs by comparing the aircraft AXBT data with available satellite and numerical model data. Several studies such as those by Shay (1999), Cione and Uhlhorn (2003), Lin and Wu (2005), and Kepert (2001) underscore the need to expand the understanding of the ocean variations in impacting TC characteristics and incorporate that into improved modeling techniques.

2. Remotely-Sensed Observations

The aircraft flight paths were examined in conjunction with available satellite imagery to identify the structural characteristics of the TC at the flight time. Satellite images were obtained at the time closest to the flight center time. Satellite data corresponding to flight times for both storms were obtained from the NRL MTSAT page, utilizing infrared (IR), visible, 37GHz (vertical and horizontal), 85GHz, and 91GHz products. Images were paired and correlated for flight times using Google Earth to create a geo-referenced overlay to be compared qualitatively with the OHC data collected by the aircraft AXBTs.

3. NRL EASNFS Model Data

The NRL EASNFS model is based on the Naval Coastal Ocean Model and covers geographical areas including the Philippine Sea, Sea of Japan, and the China Sea with resolution levels from 6 to 9 km. The NRL EASNFS receives model inputs from U. S. Navy's Operational Global Atmospheric Prediction System (NOGAPS) for surface wind and sea level pressure inputs. It receives observation data in the forms of Advanced Very High Resolution Radar (AVHRR) sea surface temperatures, satellite altimetry, and sea surface height anomaly. Parameters that were analyzed included wind characteristics at various levels, air and ocean temperatures, ocean mixed-layer depth, and OHC. The NRL

EASNFS analyses of OHC were obtained near the center time of each flight in TY Malakas and TY Megi. The OHC data are interpolated to the position of each AXBT for comparison with the AXBT-derived OHC value. These data were compared to similar sets collected in the 2008 season that compared observed AXBT data with model forecasted values for corresponding TC events (DePalma 2011) to further characterize the wind speeds at various atmospheric levels, OHC, and overall TC structure.

B. ANALYSIS METHODS

AXBT files were processed using MATLAB and Excel. Satellite imagery and flight track .kml files were correlated using Google Earth. When processing the AXBT data for each flight, computations were made for the depth of the 26° C isotherm (Z26) and OHC. Plots were generated for each file's temperature versus depth profile to examine the depth and contour of the thermocline associate with each AXBT location. Mixed Layer Depth (MLD) is defined as the depth to the edge of the uniformity layer of the properties temperature and salinity, bottom of the layer that is being mixed at the surface due to various processes. The OHC was calculated for the column of water that is greater than 26° C. The T100 is the average temperature of the ocean layer extending to a depth of 100 meters down from the surface. The calculation used for OHC is based on hurricane heat potential as defined by Leipper and Volgenau (1972) and OHC as defined by Price (2009):

$$OHC(x,y) = \rho_0 C_p \int_{Z_{26}}^{0} \left(T_i(x,y,z) - 26 dz \right).$$

where ρ_0 is sea water density of 1025 kg m^{-3}, Cp is heat capacity of 4.0 x 10^3 Jkg $°C^{-1}$, Z_{26} represents the lower limit of integration to the depth of the 26°C isotherm, and T is temperature. Calculations for OHC for each AXBT are listed in Tables 3–11 of Appendix B.

These calculations of in-situ data for OHC and the temperature distributions of ocean characteristics are important to the comparison of remotely sensed data in order to capture accurate model verification and to describe factors that may aid the understanding

of how the ocean environment interacts with an active tropical cyclone. SST has always been an important trait for assessing potential for TC development, but the assumption that the SST field is uniform with depth providing an even base of potential energy is not the most realistic characterization given the churning effect of strong TCs and the cold wake effect. Comparing OHC observed values with satellite and model data is the focus to identify areas where modeling performed well or any trends relating the OHC values with the development progression of the individual storms.

C. PROCESSED DATA SUMMARY

1. 2010 Individual Typhoons

The data from both storms were analyzed to include flight log details such as the flight pattern conducted for each day's mission and the number of AXBTs launched during the course of the flight. Sample processed AXBT profiles are contained in Figure 40, Appendix B.

a. TY Megi

Flight data summary for TY Megi included a variety of flight path patterns and over 135 ABXTs deployed (Table 1). Flight pattern and AXBT drop locations are illustrated for TY Megi in Figures 31–36 located in Appendix A. The majority of the flights were conducted in the overnight hours with the exception of the flight on 17 October, which took place during daylight hours.

TY Megi Flight Patterns

Flight	Mission Start (hhmm)	Mission End (hhmm)	Radial Legs	AXBTs	Pattern
12 2010	1921	0052	10	27	Square Spiral
13 2010	0009	0452	3	22	Butterfly
14 2010	1919	0030	6	26	Modified butterfly with racetrack
15 2010	0102	0505	3	12	Alpha
16 2010	2136	0224	3	28	Butterfly
17 2010	1032	1445	7	21	Modified butterfly with racetrack

Table 1. The flight pattern summary for TY Megi.

b. TY Malakas

The data collection during this storm included flights over three days and over 60 AXBTs deployed (Table 2). The flight plans for TY Malakas showing AXBT drop locations are illustrated in Figures 37–39 located in Appendix A.

TY Malakas Flight Patterns

Flight	Mission Start (hhmm)	Mission End (hhmm)	Radial Legs	AXBTs	Pattern
21 2010	0126	0352	2	13	Alpha
22 2010	2004	0232	5	23	Modified butterfly with racetrack
23 2010	1545	2243	5	29	Butterfly

Table 2. The flight pattern summary for TY Malakas.

2. NRL EASNFS

The model data for the period examined during ITOP showed a La Niña pattern with primarily easterly wind flow and a tradewind regime rather than a more typical monsoon pattern. This corresponds to expected conditions associated with the La Niña pattern in this region that began in June of 2010. The basin-wide equatorial upper ocean (0–300 m) heat content is greatest prior to and during the early stages of a Pacific warm (El Niño) episode and least prior to and during the early stages of a cold (La Niña) episode. The NRL EASNFS model incorporates real world observations from satellites (remotely sensed observations), ship, buoy, and surface observations (in-situ

observations), as well as climatological data to produce its forecasts. This model utilizes environmental variable data provided from the Navy Operational Global Atmospheric Prediction System (NOGAPS) and satellite altimetry observations obtained from the Advanced Very High Resolution Radiometer (AVHRR) to produce model ocean profiles for the region analysis (Lin et al. 2008).

III. ANALYSIS OF OCEAN AND ATMOSPHERE CONDITIONS

A. AIRCRAFT OHC OBSERVATIONS COMPARED TO MODEL OHC

The NRL EASNFS model-derived OHC was interpolated to the location of each AXBT that was deployed in TY Malakas and TY Megi. Comparisons between the AXBT OHC values and the NRL model data were made to identify any systematic variation between observed OHC and model-derived OHC. The results indicate a negative association between model analyzed OHC value and AXBT observed OHC (Figure 26). Individual day AXBT OHC values and the NRL model data comparisons for both storms are included in Figures 41–49, Appendix D. For all flight times in both storms, higher observed OHC were found to correspond to a negative difference between the model and observed value (i.e., the model analyzed OHC was larger than the observed OHC). The association remained independent of the ocean state over which the storms were moving. One possible explanation for this association is that the model does not register changes in OHC that were caused by the storm. Therefore, reduced OHC values due to the passage of the storm were not properly analyzed in the NRL EASFNS. This is expected as the AXBT observations were not assimilated by the model. The rate of change in ocean properties is a much slower rate than atmospheric changes. The less dynamic ocean environment within the model therefore does not keep pace with the actual ocean changes resulting from the churning of the storm, which results in a longer time for the model to register the TC-induced OHC changes. The tables in Appendix C and the graphs in Appendix D clearly identify the negative association between observed OHC values and the difference between observed and model OHC values.

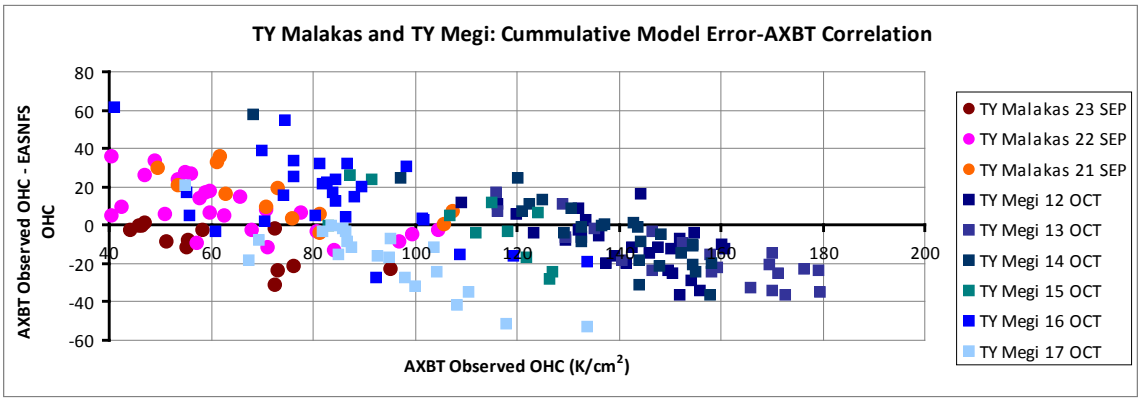

Figure 26. Differences between observed and model analyzed OHC versus the observed OHC. Various shades of blue squares denote data from TY Megi, and shades of red circles denote data from TY Malakas.

Although the goal of ITOP was to measure the relative impacts of the ocean on TC intensity, the intensity of a TC is also sensitive to other factors such as vertical wind shear. Therefore, it is of interest to compare the changes in OHC, vertical wind shear, and storm intensity for each storm. Over the region of TY Megi, OHC values remained above 60 KJ cm^{-2} (Figure 27) from 11 to 17 October as the storm gained strength. During the long period of development of TY Megi between 1200 UTC 11 October and 0000 UTC 14 October, the wind shear was above 10 knots. However, the OHC was the highest it would be during the entire lifespan of TY Megi. Therefore, the extremely large OHC allowed the developing convection to overcome the negative effects of the strong vertical wind shear. By 16 October, the OHC was decreasing slightly, but the vertical wind shear became extremely low as TY Megi reached peak intensity at 1200 UTC on 17 October (Figure 27). The comparisons between the AXBT observations and NRL EASFNS for 12 October are listed in Table 3 in Appendix C. All other day calculation tables are provided in Appendix C, Tables 4–11.

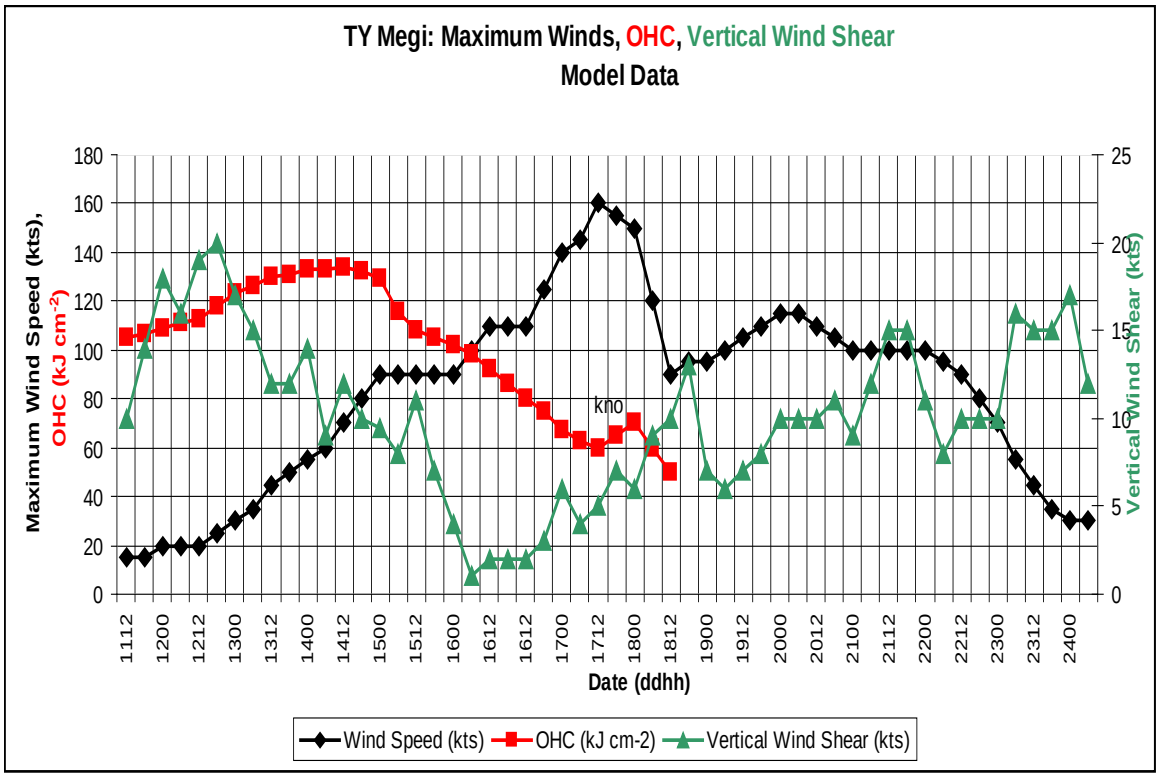

Figure 27. TY Megi maximum wind speed (kt), OHC (KJ cm^{-2}), vertical wind shear (kt) during the lifetime of TY Megi.

During the development of TY Malakas between 1200 UTC 19 September through 1200 UTC 22 September (Figure 28). OHC values remained above 70 KJ cm^{-2} while wind shear was moderate. Once TY Malakas wind speeds intensified above 70 kts, the OHC values decreased dramatically as TY Malakas moved poleward through the eddy zone that separates the high OHC water of the tropical western North Pacific to the subtropical regions (Figure 29 and Figures 50–58 located in Appendix E). However, the vertical wind shear also decreased dramatically, which allowed the storm to reach maximum intensity of 90 kts by 0000 UTC 24 September. The overall storm intensity decreased upon encountering the mid-latitude westerlies and the associated high values of vertical wind shear (above 35 kts) (Figure 28).

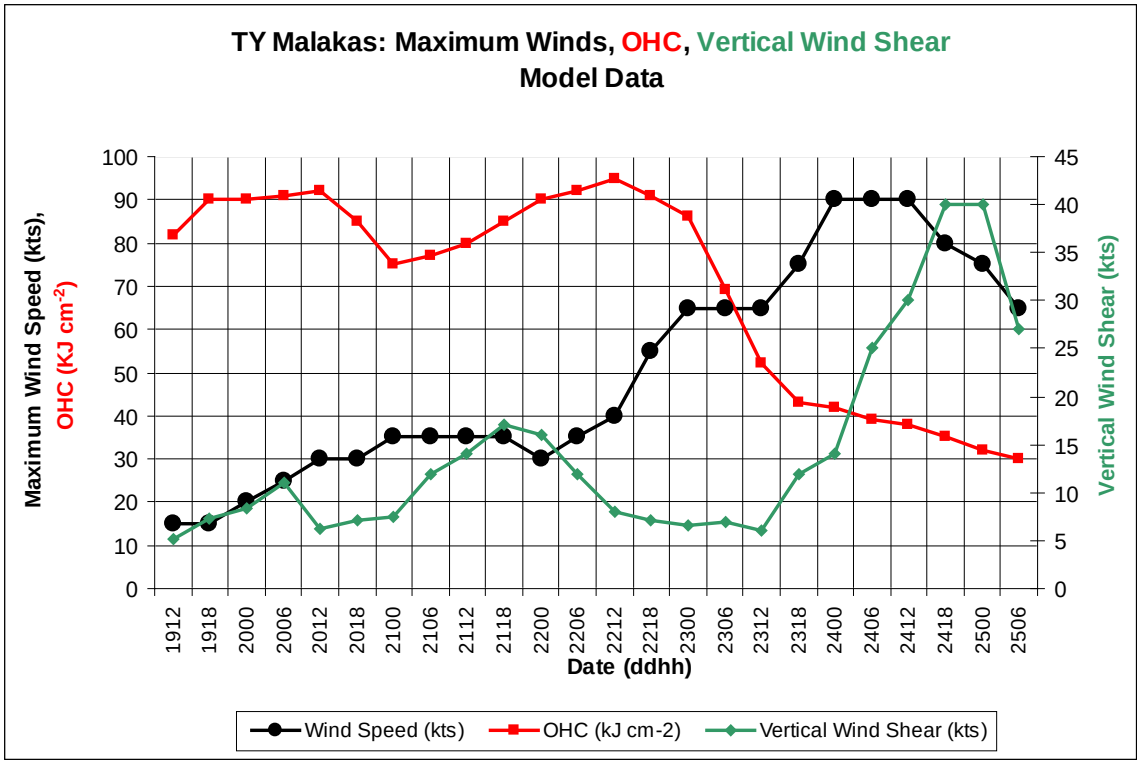

Figure 28. TY Malakas maximum wind speed (kt), OHC (KJ cm^{-2}), vertical wind shear (kt) during the lifetime of TY Malakas.

B. AIRCRAFT AND NRL EASNFS

The difference between aircraft observed OHC and NRL EASNFS model-derived OHC were also calculated for each day of flight data. The OHC data tables for TY Megi and TY Malakas are included in Tables 4–11 of Appendix C. The track of TY Megi remained in a region of very high observed and analyzed OHC compared to that of TY Malakas. TY Megi did not encounter any cold eddies or pockets of reduced observed and analyzed OHC. However, TY Malakas encountered observed and analyzed OHC values that were just above the threshold for favorable TC development for the majority of its life cycle (60 KJ cm^{-2}) (Appendix D, Figures 41–49). TY Megi encountered high observed and analyzed OHC of over 150 KJ cm^{-2} on 14 October and again on 17 October,

which provided a favorable environment for the TC to develop. Figure 29 is a sample of the data comparison conducted, the additional data analysis plots for both TY Megi and TY Malakas are located in Appendix E (Figures 50–58).

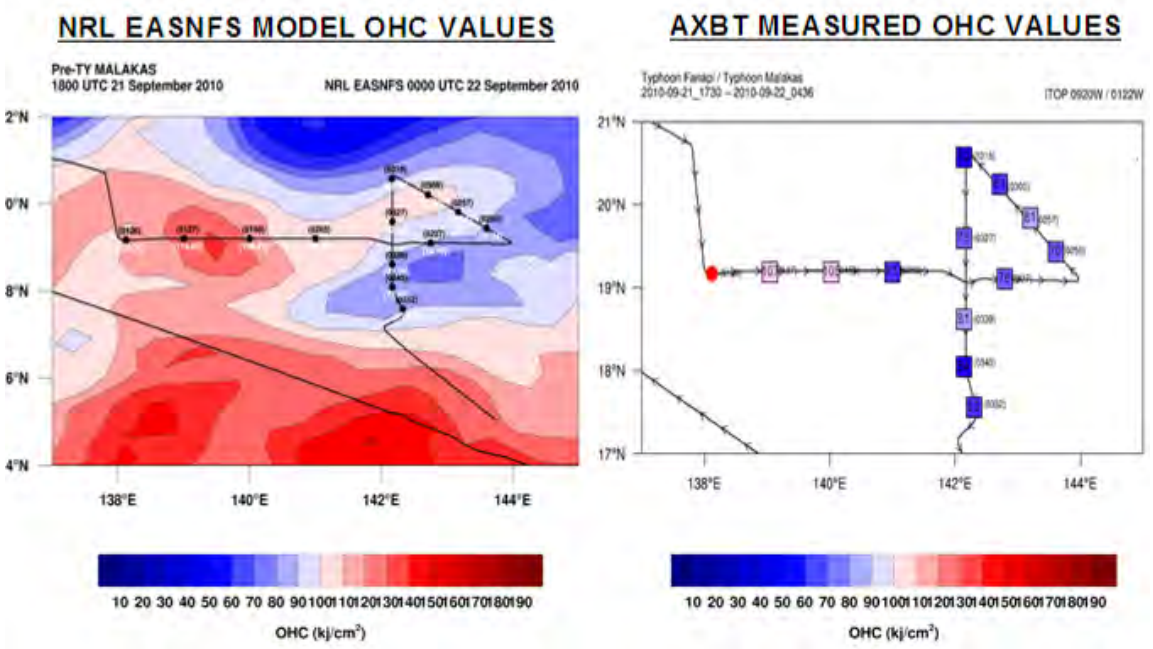

Figure 29. Analyzed OHC at 1800 UTC 21 September from the NRL EASNFS (left) with the WC-130J flight defined by the black line. Black circles identify the location of AXBT deployments. (Right) the flight track of the WC-130J with shaded squares at the locations of the AXBT deployments. The number in each square defines the observed OHC value that is also shaded according to the color bar below the figure.

A uniform, large region of colder SST and lower analyzed OHC values correlates well with observed AXBT data for TY Malakas on 22 September. A single observation in the west leg corner of 104 KJ cm^{-2} correlates with an analyzed warm eddy region to the west of the track (Appendix D, Figure 47). On 23 September, a uniform, large region of colder SST and lower analyzed OHC values correlates well with observed AXBT data. The model depicts a cold core area to the southeast of the track pattern that matches up well with a low observed OHC value of 70 KJ cm^{-2} (Appendix D, Figures 48 and 49). This persistent region of lower observed and analyzed OHC values and cooler SST was

generates by a cool ocean eddy situated to the northern side of the track of TY Malakas. These environmental conditions were not favorable for continued intensification of TY Malakas. This less than favorable environment of OHC distribution also correlates with the satellite imagery to depict a lack of symmetry for TC strength and organization. The eastern side of the storm contained less convective banding in association with the lower OHC-increased convective activity on the west side of the storm co-located with the higher observed OHC.

TY Megi experienced a broad region of warm SST and high OHC values on 12 October (Appendix F, Figure 62). The model analysis defines a significant area of high OHC values throughout the region of the developing cloud cluster. Throughout the area, the observed AXBT values match the model-analyzed high OHC values. The highest observed value is 160 KJ cm^{-2}, which is co-located with the model-defined area of highest OHC. Overall, the model-observation differences were low for this day in comparison to other days during which a more variable OHC field existed in the near vicinity of the typhoon. On 14 October (Appendix F, Figure 63), the model-analyzed OHC continued to define a significant region of high OHC values to the northwest of the developing circulation. The observed AXBT values also indicate a region of significantly high OHC values in the same area as defined in the model analysis (Appendix F, Figure 63). Model analyses in the region of TY Megi on 15 October (Appendix F, Figure 64) defined a region of high OHC values. While the majority of the observed OHC observations also define very high values of OHC, there are two points of observed low OHC values in the center-north part of the butterfly flight pattern that are not defined in the model data. These two observations do not correlate with an observed cool eddy in the area, and may be a result of local mixing, possibly resulting from upwelling generated by the storm.

A region of cooler SST and low OHC values was analyzed to the north of Megi by the NRL EASNFS on 16 October (Appendix F, Figure 65) as TY Megi passed just south of the southern eddy zone over the Philippine Sea. A region of high OHC near 150 KJ cm^{-2} was analyzed over south of the storm and oriented west-east along approximately

19° N. Over this region, the observed AXBT observations of OHC have a maximum of approximately 125 KJ cm^{-2}, which is much lower than the model analyzed OHC values. The lowest observed OHC observations are located poleward of 19° N and are similar to the model OHC field. Because the boundary between the high OHC water of the Philippine Sea and the southern eddy zone along 19^{o} N is well defined in both model analyses and observations, it is concluded that the model is capable of representing such a synoptic-scale boundary. However, the AXBT observations were all lower than the model analyzed OHC over the region of high OHC to the south of 19^{o} N.

On 17 October (Appendix F, Figure 66), TY Megi had reached peak intensity. The general character of a zonally-oriented boundary between the high OHC water of the Philippine Sea and the southern eddy zone to the north was still evident. However, the model analyzed the development of a region of low (e.g., 60 KJ cm^{-2}) OHC to the northeast of the storm center. The first flight leg to the center of Megi was oriented along this region of low OHC (Appendix F, Figure 67). The observed AXBT OHC also define the region of low OHC to the northeast of the storm center The observed OHC and the model-analyzed OHC are very similar over this region of low OHC. Therefore, it is suggested that the model may have been analyzing the presence of the cold wake of the storm at this time. Although the wake of TY Malakas did not seem to be well represented in the model analyses, the wake of Megi appears to be contained in the NRL EASNFS analysis. This may be due to the fact that TY Megi was a very intense and well-developed storm such that the definition of the storm in the initial conditions provided to the NRL EASNFS via the NOGAPS wind field was sufficient to generate the wake conditions accurately.

In summary, the comparison of model-analyzed OHC and observed OHC derived from AXBT data from both storms over all days identifies a consistent negative association between model-observed difference and observed OHC. This initial examination suggests that the primary differences were caused by features related to local modifcations to the ocean conditions by the TC circulation. However, when TY Megi was an extremely intense cyclone, the initiation of the cold wake was well represented in

the NRL EASNFS. It is suggested that this intense storm may have been well represented in the initial conditions (provided by NOGAPS) to a much better degree than the weaker TY Malakas. Another possible explanation was that TY Megi was moving along the boundary between the high OHC water of the Philippine Sea and the southern eddy zone, and the TC circulation was able to organize the eddy zone features, which were well represented in the NRL EASNFS, into the initial formation of the wake.

Aircraft AXBT data and NRL EASFNS data were compared with satellite imagery for correlating data observation times. A sample of the imagery used for TY Malakas is below (Figure 30). All other satellite images are included in Appendix F, Figures 59–67.

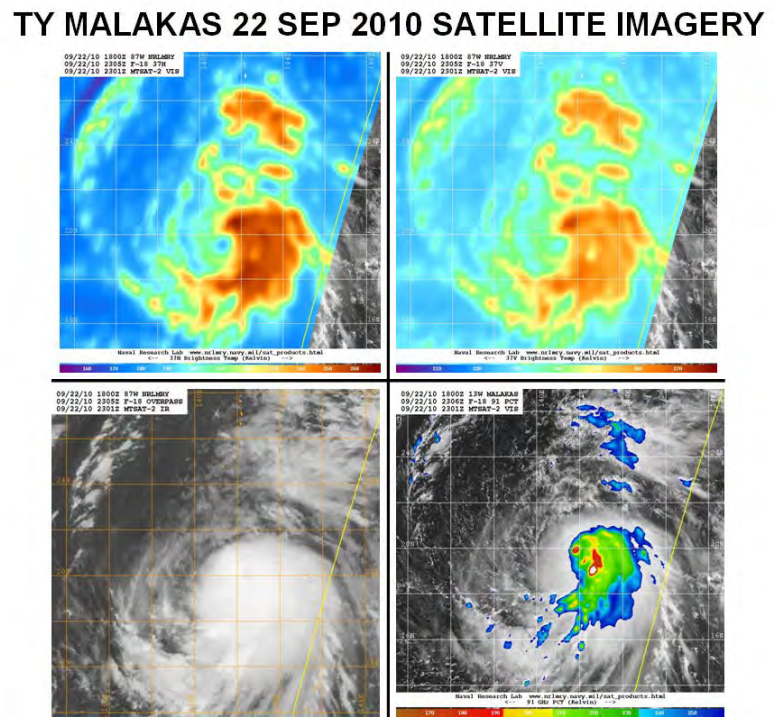

Figure 30. The 37GHz V, 37GHz H, 85GHz and 91GHz TY Malakas IR satellite imagery for 22 September 2010.

IV. CONCLUSION

A. SUMMARY

The interactions between TCs, and warm or cold eddies in the ocean have significant impacts on storm intensity and ocean conditions. In this study, comparisons between observed ocean conditions (i.e., OHC) and model-analyzed conditions were investigated in the vicinity of two typhoons over the western North Pacific. A definitive negative association between OHC and observation-model differences were observed. As observed OHC increased, the difference between model and observation became more negative. The association remained the same whether the storm was moving over a warm or cold ocean eddy region. One possible explanation for this observed behavior is that the less dynamic ocean environment within the model does not register the rapid actual ocean changes that result from the storm passage.

The largest model-observation differences were observed in regions of warm eddies that were over-analyzed by the model as the conditions were not as warm as predicted, or areas of cold wake produced by the storm that were not captured or forecasted by the model. Upon examining ocean characteristics with regard to typhoon conditions, the dependence on wind speed, air temperature and storm location (with regard to SST) demonstrated the anticipated relationship between high OHC and increased possibility for TC development. In the case of TY Malakas, the intense mixing across the thermocline reflects indications in tropical cyclone development or structural organization that relate to the strengthening or weakening of the TC. Thermocline depths were deeper on the west side of the storm, and reflect the lack of a symmetric organization as was observed in the satellite analysis.

Finally, the NRL EASNFS was able to analyze the initiation of the cold wake during TY Megi. It is suggested that the NOGAPS wind fields used to initialize the NRL EASNFS may have depicted the very intense TY Megi more accurately than TY Malakas, in which the NRL EASNFS did not accurately represent the initiation of the cold wake.

B. RECOMMENDATIONS FOR FURTHER STUDY

The contribution expected from this research effort would aid in the understanding of atmosphere and ocean characteristics that are important to define the TC wind distribution and potential areas for favorable TC development. This has significant impacts on definition of the ocean wave field that influences maritime activity. Further understanding of WPAC TC characteristics would benefit forecast procedures and improve accuracy such that future TC forecast model tendencies could be defined. This will lead to an overall improvement in the forecast process and increased advanced warning for U. S. Navy activities. Another aspect of data that could be analyzed would be the comparison of AXBT data sets to correlating ship bathythermograph observations for these two typhoons or other systems in the ITOPS study.

Battlespace ON Demand (BOND) is the U.S. Navy's Meteorology and Oceanography operational concept to inform decision makers on key environmental conditions. The base tier (Tier Zero) of the BOND pyramid encompasses the data collection process through all available methods, such as the in-situ AXBT observations and remotely sensed satellite data utilized in the ITOP study. Tier Zero builds the base for Tier One, which involves the processing of the collected data, and its incorporation into numerical modeling. This thesis compared "Tier One" information from the NRL EASFS model data to "Tier Zero" observations from AXBT data. The next level in the pyramid describes creating a performance surface, or dynamic visual representation of the environmental data, called Tier Two. These three base layers all support the top tier, which represents the decision to be made by the warfighter. Based on previous work, we expected to find that ocean heat content and ocean characteristic response to a tropical

cyclone does have a significant contribution to the progression of a tropical cyclone life cycle, and improvements in capturing this data and better incorporation into modeling capability would increase the value added to future modeling designs. Improved modeling design or increased accuracy resulting from it would directly benefit the warfighter in capitalizing on our ability to maximize our knowledge of the environment, improve forecasting ability, which translates directly to enhanced information available to the decision making BOND tier.

It is recommended that identification of the subtle ocean condition changes due to a TC be used to develop a performance surface to identify future TC intensity changes. Ocean temperature signature relating to ocean heat content may be a first indicator for tendency of tropical cyclone development that can be visually presented in a performance surface to visually aid warfighters in decision making.

THIS PAGE INTENTIONALLY LEFT BLANK

APPENDIX A. FLIGHT TRACK PATHS AND AXBT DROP LOCATIONS

A. TY MEGI

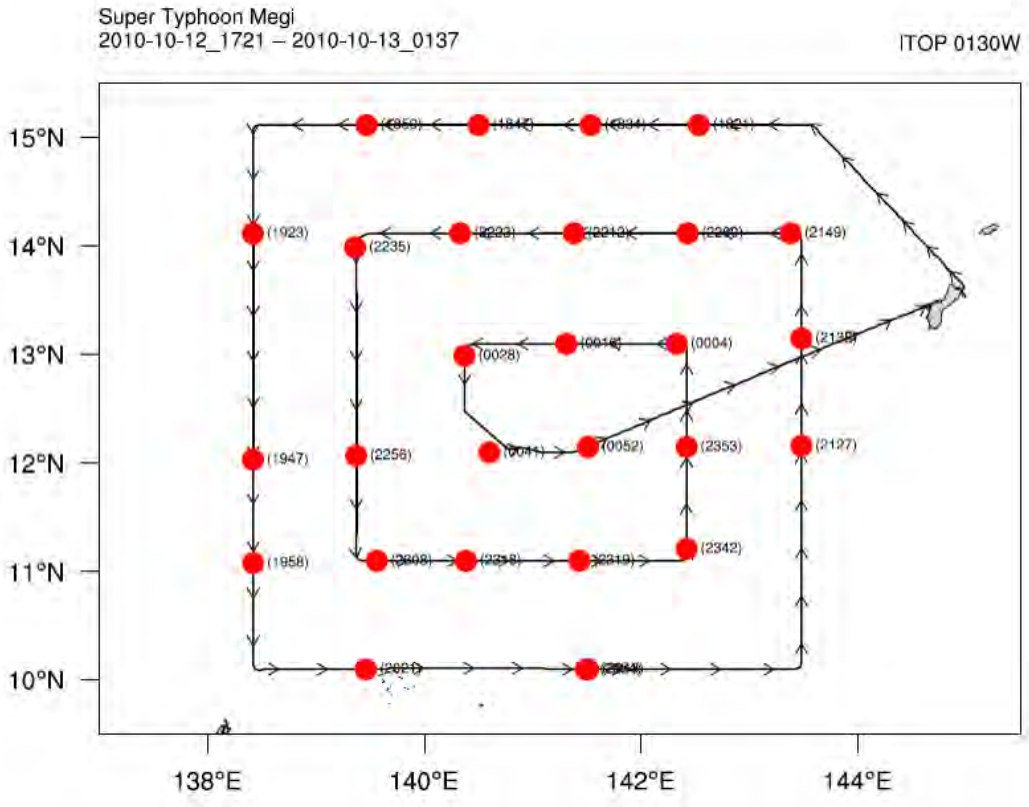

Figure 31. The square spiral flight pattern flown in TY Megi on 12 October. The red circles define the locations of the AXBTs and the time (hhmm) of each AXBT is provided next to each red circle.

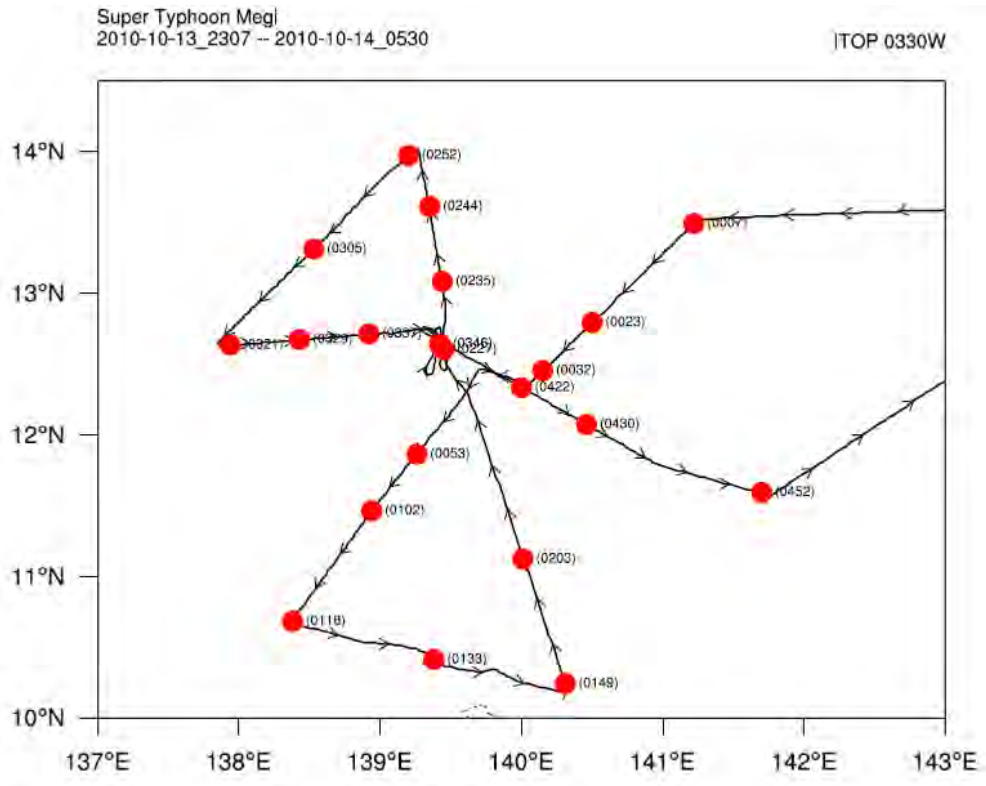

Figure 32. The butterfly flight pattern flown in TY Megi on 13 October. The red circles define the locations of the AXBTs and the time (hhmm) of each AXBT is provided next to each red circle.

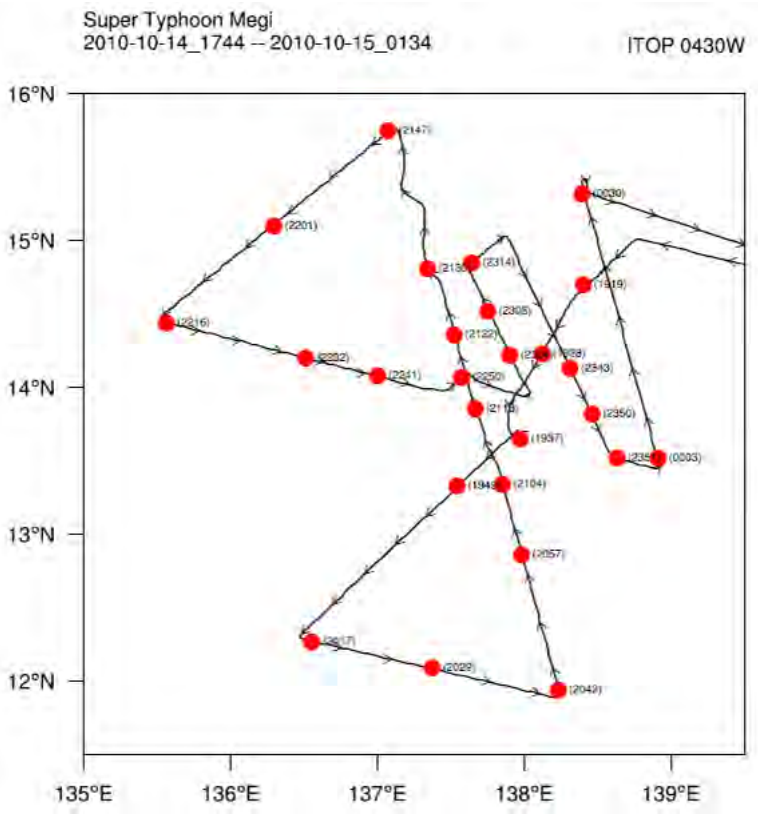

Figure 33. The butterfly flight pattern modified with a racetrack pattern flown in TY Megi on 14 October. The red circles define the locations of the AXBTs and the time (hhmm) of each AXBT is provided next to each red circle.

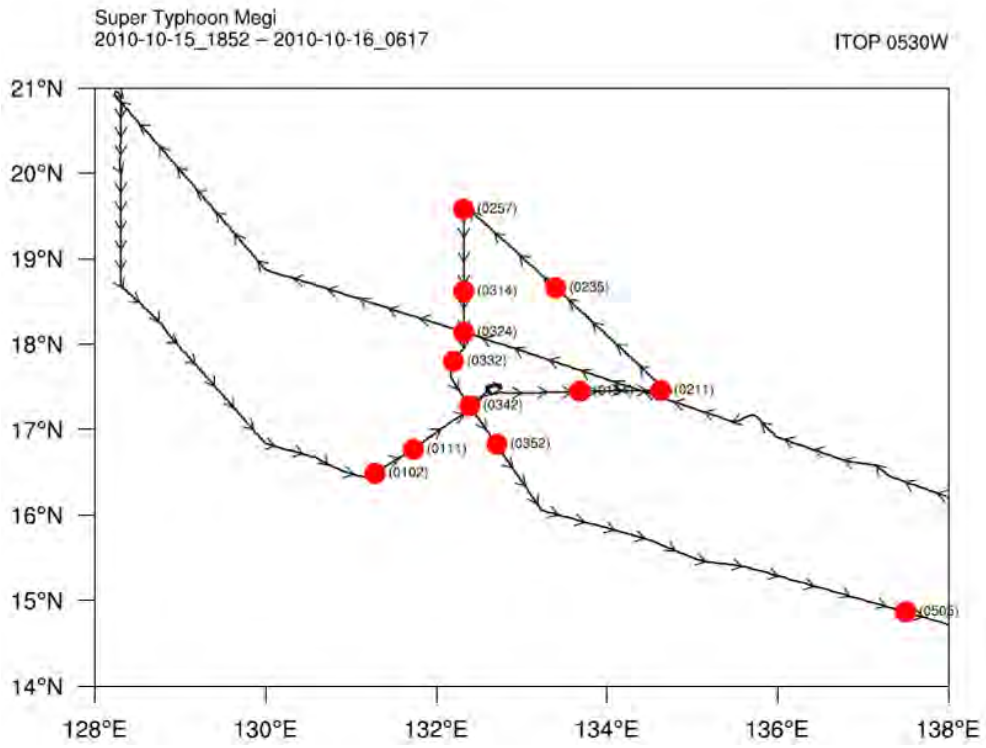

Figure 34. The modified alpha flight pattern flown in TY Megi on 15 October. The red circles define the locations of the AXBTs and the time (hhmm) of each AXBT is provided next to each red circle.

.

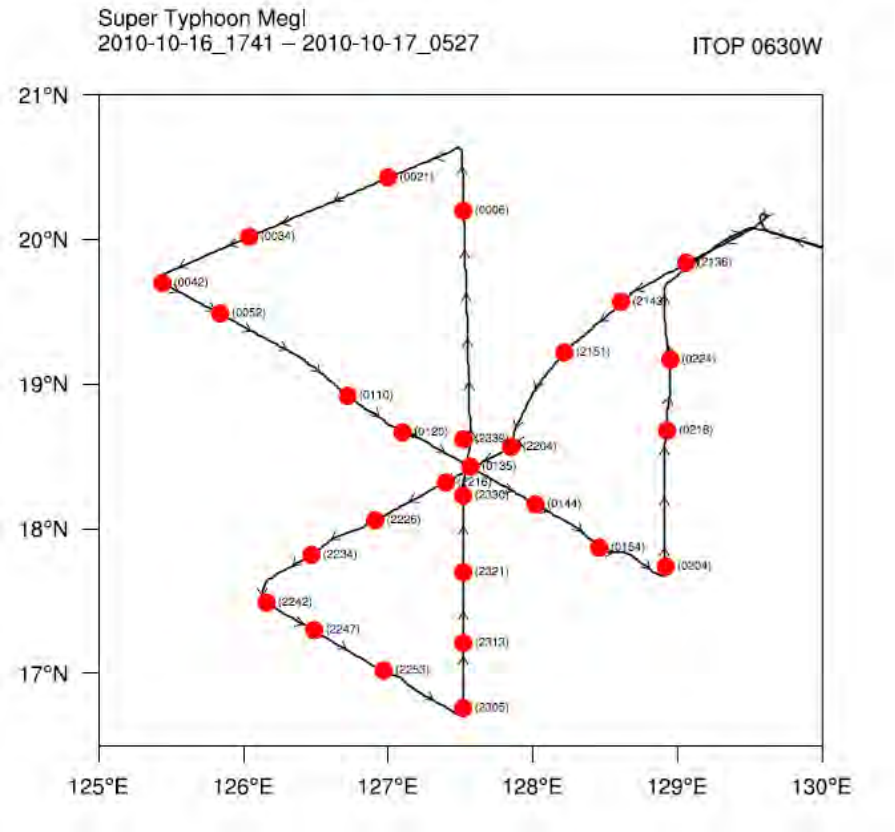

Figure 35. The butterfly flight pattern flown in TY Megi on 16 October. The red circles define the locations of the AXBTs and the time (hhmm) of each AXBT is provided next to each red circle.

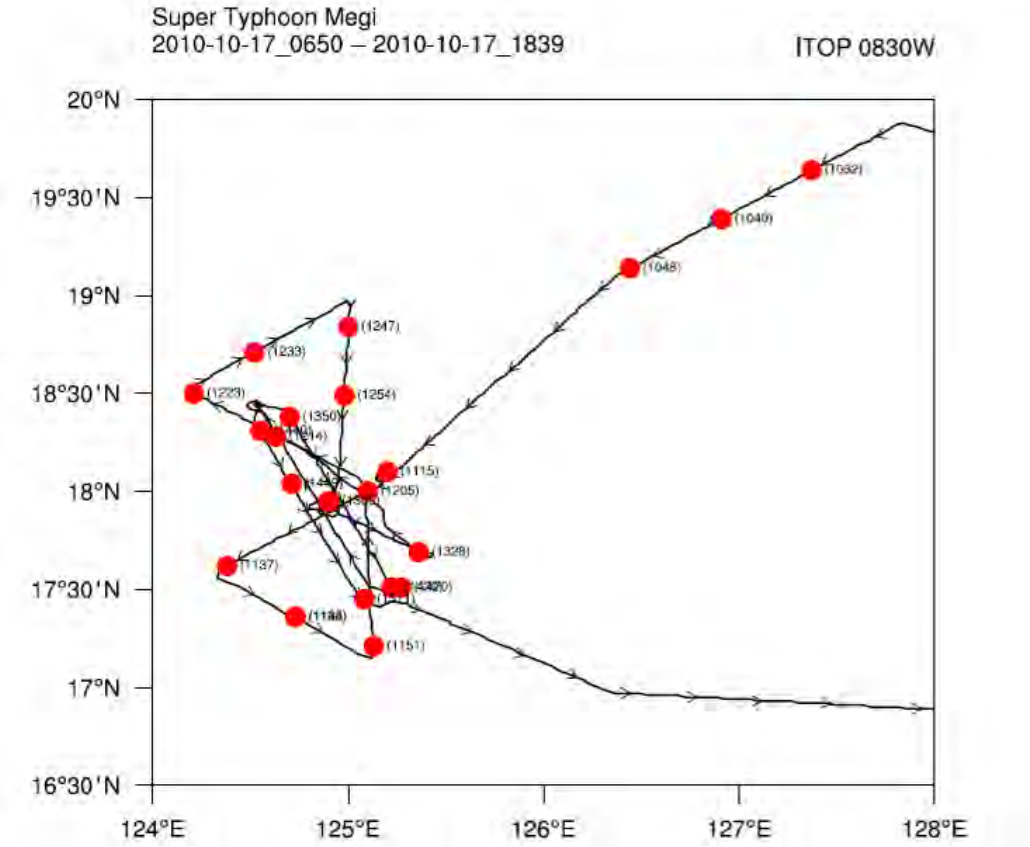

Figure 36. The butterfly pattern modified with a racetrack flight pattern flown in TY Megi on 17 October. The red circles define the locations of the AXBTs and the time (hhmm) of each AXBT is provided next to each red circle.

B. TY MALAKAS

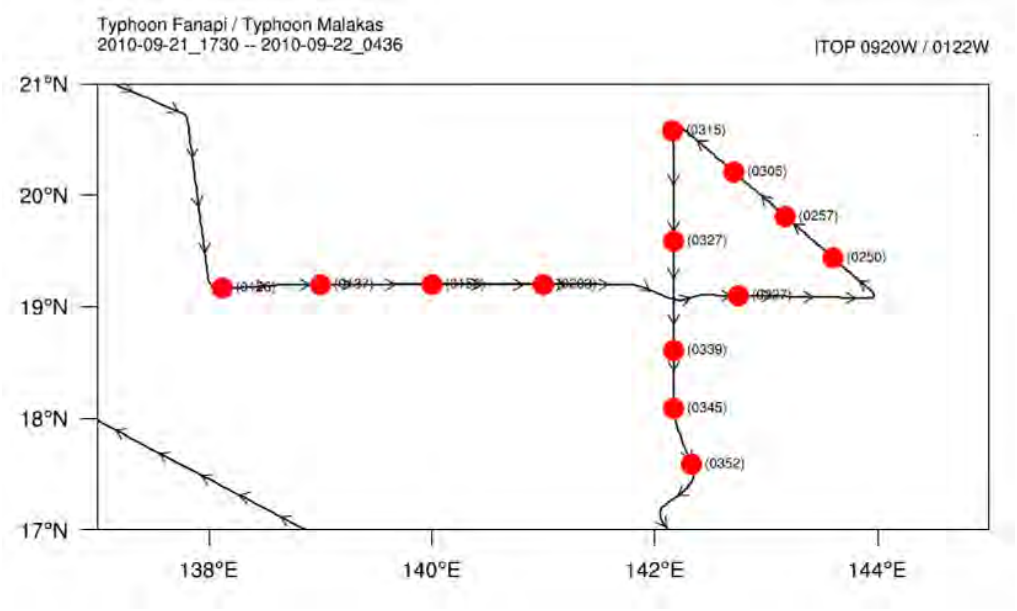

Figure 37. The alpha flight pattern flown in TY Malakas on 21 September. The red circles define the locations of the AXBTs and the time (hhmm) of each AXBT is provided next to each red circle.

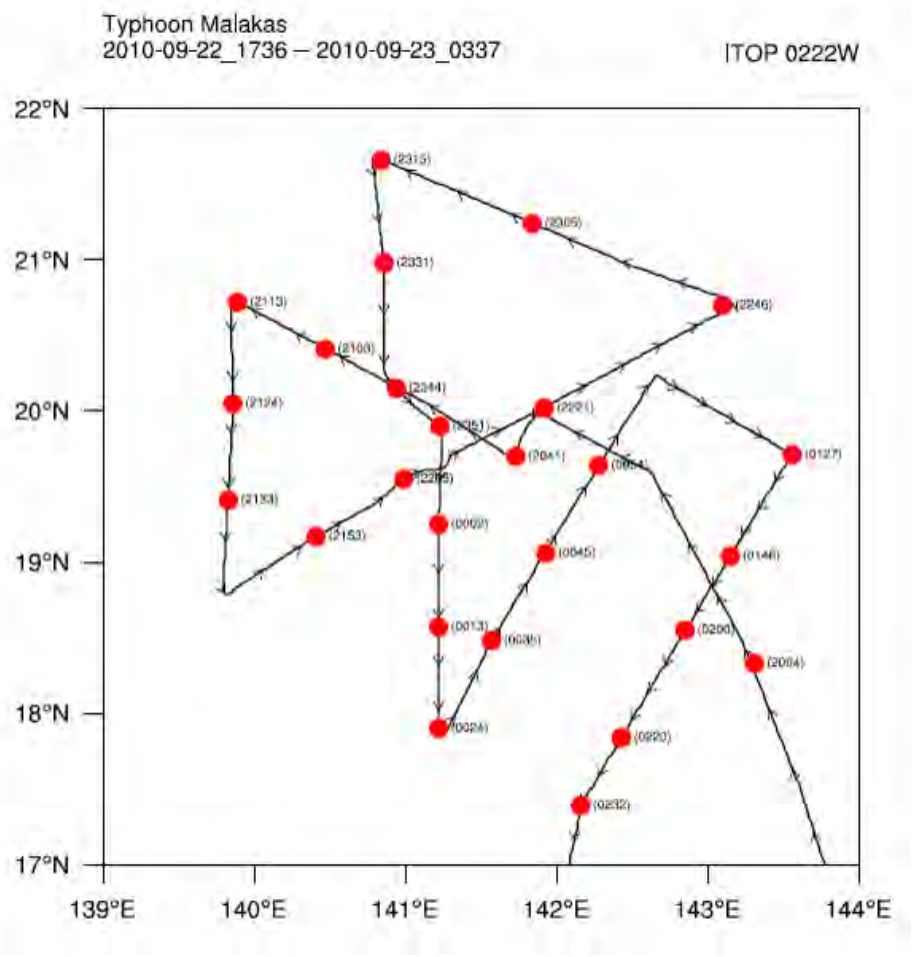

Figure 38. The butterfly pattern modified with a racetrack pattern that was flown in TY Malakas on 22 September. The red circles define the locations of the AXBTs and the time (hhmm) of each AXBT is provided next to each red circle.

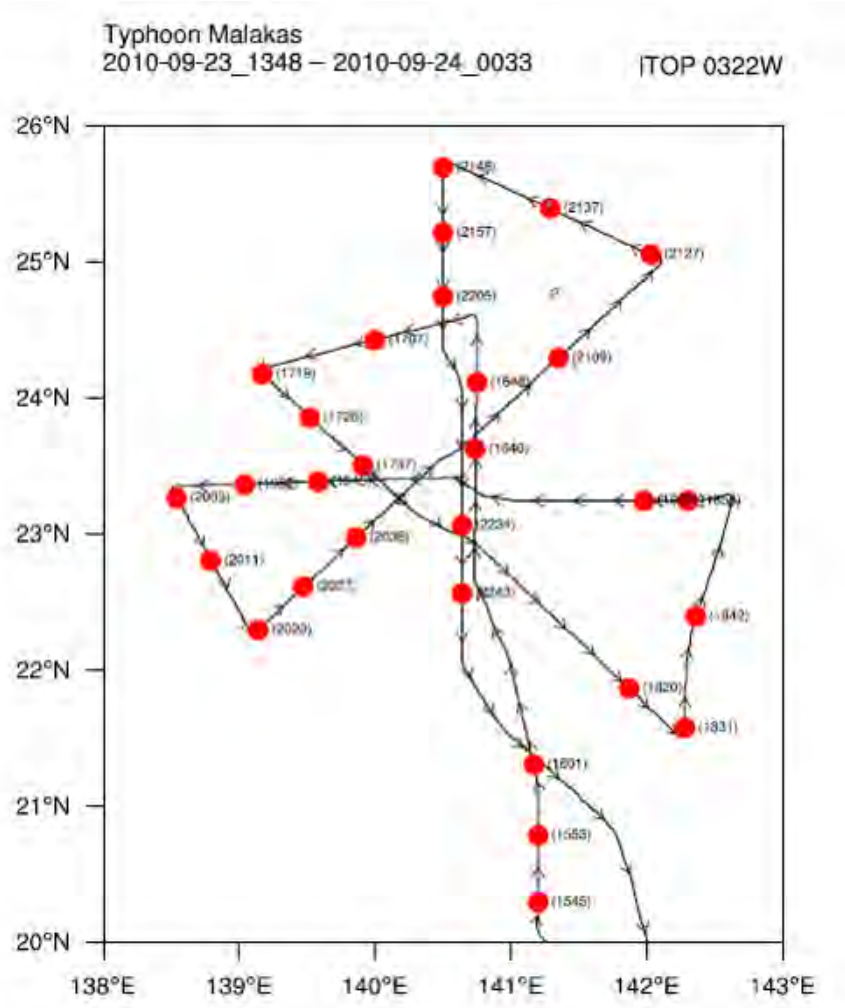

Figure 39. The butterfly flight pattern flown in TY Malakas on 23 September. The red circles define the locations of the AXBTs and the time (hhmm) of each AXBT is provided next to each red circle.

THIS PAGE INTENTIONALLY LEFT BLANK

APPENDIX B. SAMPLE PROCESSED AXBT DATA

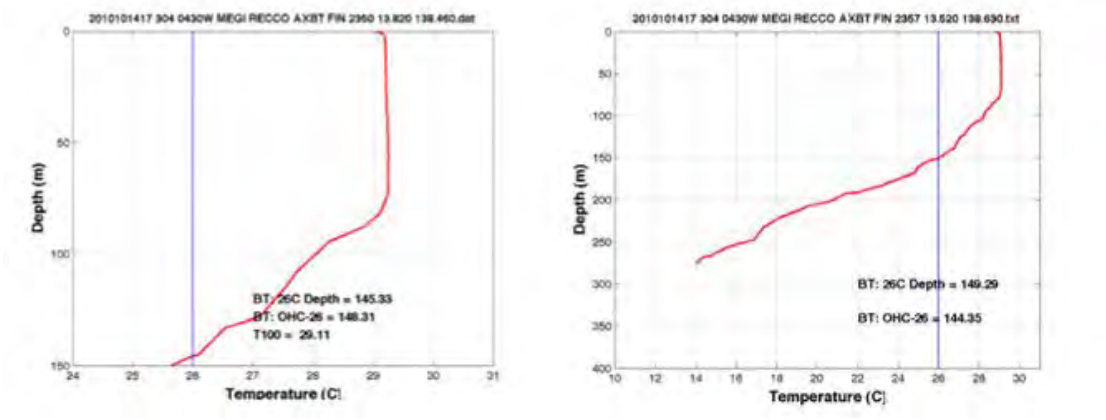

Figure 40. An example AXBT profile deployed in TY Megi. (left) Enlarged view of the 150m of the top of the total profile. (right) Profile processed down to full depth of sounding.

THIS PAGE INTENTIONALLY LEFT BLANK

APPENDIX C. MODEL—AXBT OHC ERROR CALCULATION TABLES

A. TY MEGI

TY Megi AXBT Data					
DATE:			**12-OCT-10**		
AXBT Time (hhmm)	**Latitude (degrees)**	**Longitude (degrees)**	**AXBT OHC (KJ/cm^2)**	**EASNFS OHC (KJ/cm^2)**	**Difference (Model-Observed)**
1821	15.117	142.533	137.66	117.76	-19.9
1834	15.117	141.533	109.27	121	11.73
1847	15.117	140.5	136.11	130.13	-5.98
1859	15.117	139.467	152.68	142.53	-10.15
1923	14.117	138.417	154.91	150.36	-4.55
1947	12.033	138.417	150.47	138.17	-12.3
1958	11.08	138.42	146.21	131.36	-14.85
2021	10.1	139.46	150.66	125	-25.66
2043	10.1	141.51	141.69	121.45	-20.24
2054	10.1	141.49	156.11	121.45	-34.66
2127	12.16	143.48	129.55	121.85	-7.7
2138	13.15	143.48	120.04	125.78	5.74
2149	14.12	143.38	151.98	114.94	-37.04
2200	14.12	142.43	123.5	119.43	-4.07
2212	14.12	141.38	116.22	127.07	10.85
2223	14.12	140.33	132.28	140.65	8.37
2235	13.99	139.36	144.53	160.58	16.05
2256	12.07	139.37	160.21	149.93	-10.28
2308	11.1	139.56	147.89	136.15	-11.74
2318	11.1	140.38	142.64	130.69	-11.95
2319	11.1	141.43	132.22	129.29	-2.93
2342	11.21	142.42	154.29	124.95	-29.34
2353	12.15	142.42	149.83	125.89	-23.94
0004	13.1	142.33	139.28	122.6	-16.68
0016	13.1	141.31	132.79	126.34	-6.45
0028	12.99	140.37	160.84	148.22	-12.62
0041	12.1	140.6	152.01	144.92	-7.09
0052	12.15	141.51	133.54	135.97	2.43

TY Megi AXBT Data					
DATE:			**12-OCT-10**		
AXBT Time (hhmm)	**Latitude (degrees)**	**Longitude (degrees)**	**AXBT OHC (KJ/cm^2)**	**EASNFS OHC (KJ/cm^2)**	**Difference (Model-Observed)**
				RMSE	**11.06239964**
				BIAS	**-9.819642857**

Table 3. The AXBT data deployed in TY Megi on 12 October comparison with NRL EASNFS model analyzed OHC interpolated to the AXBT location.

TY Megi AXBT Data					
DATE:			**13-OCT-10**		
AXBT Time (hhmm)	**Latitude (degrees)**	**Longitude (degrees)**	**AXBT OHC (KJ/cm^2)**	**EASNFS OHC (KJ/cm^2)**	**Difference (Model-Observed)**
0007	13.4	141.22	129.54	122.92	-6.62
0023	12.79	140.5	166.06	132.93	-33.13
0032	12.45	140.15	170.08	135.7	-34.38
0053	11.86	139.26	129.14	140	10.86
0102	11.46	138.94	172.66	136.23	-36.43
0118	10.68	138.38	158.29	133.56	-24.73
0133	10.41	139.38	140.62	122.33	-18.29
0149	10.24	140.31	146.53	122.58	-23.95
0203	11.12	140.01	135.43	133.72	-1.71
0227	12.6	139.45	179.53	144.11	-35.42
0235	13.08	139.44	169.58	148.93	-20.65
0244	13.61	139.35	179.2	155.7	-23.5
0252	13.97	139.2	170.22	155.66	-14.56
0305	13.31	138.53	176.33	153.31	-23.02
0321	12.63	137.94	157.94	142.01	-15.93
0329	12.67	138.43	146.69	143.47	-3.22
0337	12.71	138.92	171.28	145.55	-25.73
0346	12.64	139.42	152.51	143.31	-9.2
0422	12.33	140	159.31	137.17	-22.14
0430	12.07	140.46	116.13	133.12	16.99
0452	11.5	141.7	116.42	123.7	7.28
				RMSE	**7.301168529**
				BIAS	**-16.07047619**

Table 4. The AXBT data deployed in TY Megi on 13 October comparison with NRL EASNFS model analyzed OHC interpolated to the AXBT location.

TY Megi AXBT Data					
DATE:			**14-OCT-10**		
AXBT Time (hhmm)	**Latitude (degrees)**	**Longitude (degrees)**	**AXBT OHC (KJ/cm^2)**	**EASNFS OHC (KJ/cm^2)**	**Difference (Model-Observed)**
2357	13.52	138.63	144.35	135.54	-8.81
2350	13.82	138.46	148.31	143.21	-5.1
2343	14.13	138.31	154.6	144.19	-10.41
2314	14.85	137.64	129.25	124.87	-4.38
2308	14.5	137.75	121.1	127.74	6.64
2304	14.2	137.9	143.9	142.37	-1.53
2250	14.07	137.57	152.23	137.32	-14.91
2241	14.08	137	144.22	125.7	-18.52
2232	14.2	136.51	148.05	126.58	-21.47
2216	14.44	135.56	132.9	131.92	-0.98
2201	15.1	136.293	130.7	139.31	8.61
2147	15.75	137.07	97.27	121.32	24.05
2130	14.81	137.34	132.75	123.63	-9.12
2122	14.36	137.52	68.27	125.57	57.3
2113	13.8550	137.664	154.58	143.84	-10.74
2104	13.34	137.85	136.8	136.02	-0.78
2057	12.86	137.98	158.14	121.55	-36.59
2042	11.94	138.23	144.25	113	-31.25
2029	12.09	137.37	137.36	137.71	0.35
2017	12.267	136.55	124.99	137.68	12.69
1949	13.33	137.54	158.24	137.77	-20.47
1937	13.65	137.97	154.53	133.88	-20.65
1928	14.23	138.12	143.03	143.99	0.96
1919	14.7	138.4	120.33	144.93	24.6
0030	15.32	138.39	122.63	133.45	10.82
0003	13.52	138.91	155.27	130.52	-24.75
				RMSE	**19.76573625**
				BIAS	**-3.632307692**

Table 5. The AXBT data deployed in TY Megi on 14 October comparison with NRL EASNFS model analyzed OHC interpolated to the AXBT location.

TY Megi AXBT Data					
DATE:	**15-OCT-10**				
AXBT Time (hhmm)	**Latitude (degrees)**	**Longitude (degrees)**	**AXBT OHC (KJ/cm^2)**	**EASNFS OHC (KJ/cm^2)**	**Difference (Model-Observed)**
0535	14.13	140.03	127.38	--	--
0505	14.87	137.5	106.34	--	--
0352	16.83	132.71	122.09	105.21	-16.88
0342	17.28	132.39	118.34	115.13	-3.21
0332	17.8	132.2	91.59	115.11	23.52
0324	18.14	132.32	112.06	107.95	-4.11
0314	18.62	132.32	87.27	112.71	25.44
0257	19.58	132.32	83.23	82.83	-0.4
0235	18.66	133.4	107	111.95	4.95
0211	17.46	134.63	126.55	97.93	-28.62
0154	17.45	133.68	126.97	102.13	-24.84
0111	16.77	131.73	124.39	130.88	6.49
0102	16.49	131.28	115.09	126.94	11.85
				RMSE	**16.9379877**
				BIAS	**-0.528181818**

Table 6. The AXBT data deployed in TY Megi on 15 October comparison with NRL EASNFS model analyzed OHC interpolated to the AXBT location.

TY Megi AXBT Data					
DATE:	**16-OCT-10**				
AXBT Time (hhmm)	**Latitude (degrees)**	**Longitude (degrees)**	**AXBT OHC (KJ/cm^2)**	**EASNFS OHC (KJ/cm^2)**	**Difference (Model-Observed)**
2339	18.62	127.52	88.34	103.02	14.68
2330	18.23	127.52	83.96	100.37	16.41
2321	17.7	127.52	86.82	118.29	31.47
2313	17.21	127.52	98.41	128.77	30.36
2305	16.76	127.52	74.53	129.2	54.67
2253	17.02	126.97	81.44	113.03	31.59
2247	17.3	126.49	76.2	101.55	25.35
2242	17.49	126.16	76.44	109.54	33.1
2234	17.82	126.47	82.01	103.02	21.01
2226	18.06	126.91	89.51	109.31	19.8
2216	18.32	127.4	84.47	96.46	11.99

TY Megi AXBT Data					
DATE:	**16-OCT-10**				
AXBT Time (hhmm)	**Latitude (degrees)**	**Longitude (degrees)**	**AXBT OHC (KJ/cm^2)**	**EASNFS OHC (KJ/cm^2)**	**Difference (Model-Observed)**
2204	18.567	127.85	74.2	89.56	15.36
2151	19.22	128.22	92.35	64.85	-27.5
2144	19.57	128.61	61.1	57.64	-3.46
2136	19.84	129.06	55.94	60.41	4.47
0224	19.17	128.95	55.19	71.84	16.65
0218	18.68	128.93	41.27	102.29	61.02
0204	17.74	128.92	119.39	103.2	-16.19
0154	17.87	128.46	101.82	104.49	2.67
0144	18.17	128.02	84.67	107.92	23.25
0135	18.43	127.57	86.49	90.79	4.3
0120	18.667	127.1	82.93	105.1	22.17
0110	18.92	126.72	70.13	108.79	38.66
0052	19.49	125.84	133.86	114.47	-19.39
0042	19.7	125.44	101.65	104.87	3.22
0034	20.02	126.04	108.99	93.66	-15.33
0021	20.43	127	80.58	85.12	4.54
0006	20.2	127.52	70.78	72.66	1.88
				RMSE	**25.05975936**
				BIAS	**14.52678571**

Table 7. The AXBT data deployed in TY Megi on 16 October comparison with NRL EASNFS model analyzed OHC interpolated to the AXBT location.

TY Megi AXBT Data					
DATE:	**17-OCT-10**				
AXBT Time (hhmm)	**Latitude (degrees)**	**Longitude (degrees)**	**AXBT OHC (KJ/cm^2)**	**EASNFS OHC (KJ/cm^2)**	**Difference (Model-Observed)**
1511	17.45	125.08	94.92	77.93	-16.99
1449	18.04	124.71	86.01	83.86	-2.15
1440	18.31	124.55	92.72	76.03	-16.69
1420	17.51	125.27	108.4	66.69	-41.71
1350	18.38	124.7	86.66	83.39	-3.27
1328	17.69	125.36	118.05	66.69	-51.36
1305	17.95	124.9	110.54	75.19	-35.35
1254	18.49	124.98	86.9	78.07	-8.83

TY Megi AXBT Data					
DATE:			**17-OCT-10**		
AXBT Time (hhmm)	**Latitude (degrees)**	**Longitude (degrees)**	**AXBT OHC (KJ/cm^2)**	**EASNFS OHC (KJ/cm^2)**	**Difference (Model-Observed)**
1247	18.84	125	82.09	78.27	-3.82
1233	18.71	124.52	95.2	88.09	-7.11
1223	18.5	124.21	103.92	92.39	-11.53
1214	18.28	124.63	83.7	83.39	-0.31
1205	18	125.1	85.14	69.75	-15.39
1151	17.21	125.13	133.91	80.81	-53.1
1144	17.36	124.73	87.77	76.03	-11.74
1138	17.36	124.73	55.17	76.03	20.86
1137	17.62	124.38	104.38	80	-24.38
1115	18.1	125.2	100.21	67.83	-32.38
1048	19.14	126.44	98.24	70.6	-27.64
1040	19.39	126.91	69.52	61.67	-7.85
1032	19.64	127.37	67.41	48.96	-18.45
				RMSE	**24.80797769**
				BIAS	**-17.58047619**

Table 8. The AXBT data deployed in TY Megi on 17 October comparison with NRL EASNFS model analyzed OHC interpolated to the AXBT location.

B. TY MALAKAS

TY Malakas AXBT Data					
DATE:			**21-SEP-10**		
AXBT Time (hhmm)	**Latitude (degrees)**	**Longitude (degrees)**	**AXBT OHC (KJ/cm^2)**	**EASNFS OHC (KJ/cm^2)**	**Difference (Model-Observed)**
0352	17.59	142.33	62.84	78.87	16.03
0345	18.09	142.17	53.58	73.83	20.25
0339	18.61	142.17	81.47	77.23	-4.24
0327	19.59	142.17	73.15	92.33	19.18
0315	20.58	142.16	49.63	79.34	29.71
0305	20.21	142.71	61.74	97.54	35.8
0257	19.81	143.17	81.49	86.6	5.11
0250	19.44	143.6	70.94	80.24	9.3
0227	19.1	142.75	76.09	79.18	3.09

TY Malakas AXBT Data					
DATE:	**21-SEP-10**				
AXBT Time (hhmm)	**Latitude (degrees)**	**Longitude (degrees)**	**AXBT OHC (KJ/cm^2)**	**EASNFS OHC (KJ/cm^2)**	**Difference (Model-Observed)**
0203	19.2	141	61.2	93.73	32.53
0150	19.2	140	105.84	106.41	0.57
0137	19.2	139	107.46	114.55	7.09
				RMSE	**19.25301189**
				BIAS	**14.535**

Table 9. The AXBT data deployed in TY Malakas on 21 September comparison with NRL EASNFS model analyzed OHC interpolated to the AXBT location.

TY Malakas AXBT Data					
DATE:	**22-SEP-10**				
AXBT Time (hhmm)	**Latitude (degrees)**	**Longitude (degrees)**	**AXBT OHC (KJ/cm^2)**	**EASNFS OHC (KJ/cm^2)**	**Difference (Model-Observed)**
2351	19.9	141.23	62.58	67.41	4.83
2344	20.15	140.94	47.09	72.89	25.8
2331	20.98	140.86	40.5	45.44	4.94
2315	21.66	140.84	39.03	42.43	3.4
2305	21.24	141.84	57.42	47.5	-9.92
2246	20.7	143.1	71.05	78.56	7.51
2221	20.02	141.92	58.99	75.58	16.59
2205	19.55	140.99	55.1	82.3	27.2
2153	19.17	140.41	96.92	87.74	-9.18
2133	19.41	139.83	104.82	101.79	-3.03
2124	20.05	139.86	99.51	94.4	-5.11
2113	20.72	139.89	59.97	77.35	17.38
2103	20.41	140.47	57.81	71.83	14.02
2041	19.7	141.73	56.29	82.68	26.39
2004	18.33	143.31	71.29	59.35	-11.94
0232	17.39	142.16	84.14	70.53	-13.61
0220	17.84	142.43	59.77	65.79	6.02
0200	18.55	142.85	42.43	51.98	9.55
0146	19.04	143.15	51.09	56.31	5.22
0127	19.71	143.56	67.96	64.9	-3.06
0054	19.64	142.28	40.58	76.12	35.54

TY Malakas AXBT Data					
DATE:	**22-SEP-10**				
AXBT Time (hhmm)	**Latitude (degrees)**	**Longitude (degrees)**	**AXBT OHC (KJ/cm^2)**	**EASNFS OHC (KJ/cm^2)**	**Difference (Model-Observed)**
0045	19.06	141.93	53.63	77.39	23.76
0035	18.48	141.57	65.76	80.48	14.72
0024	17.9	141.22	80.93	77.14	-3.79
0013	18.57	141.22	77.83	84.41	6.58
0002	19.25	141.22	49.08	82.68	33.6
				RMSE	**16.32860645**
				BIAS	**8.549166667**

Table 10. The AXBT data deployed in TY Malakas on 22 September comparison with NRL EASNFS model analyzed OHC interpolated to the AXBT location

TY Malakas AXBT Data					
DATE:	**23-SEP-10**				
AXBT Time (hhmm)	**Latitude (degrees)**	**Longitude (degrees)**	**AXBT OHC (KJ/cm^2)**	**EASNFS OHC (KJ/cm^2)**	**Difference (Model-Observed)**
2243	22.56	140.64	31.96	38.05	6.09
2234	23.06	140.64	29.26	41.64	12.38
2205	24.74	140.5	47.17	47.8	0.63
2157	25.21	140.5	51.3	42.76	-8.54
2148	25.69	140.5	31.65	45.81	14.16
2137	25.39	141.29	38.61	41.83	3.22
2127	25.05	142.03	31.57	50.23	18.66
2109	24.29	141.35	26.9	45.07	18.17
2036	22.97	139.86	72.7	41.29	-31.41
2027	22.61	139.47	76.24	54.36	-21.88
2020	22.29	139.14	95.42	72	-23.42
2011	22.8	138.79	72.56	70.77	-1.79
2003	23.26	138.54	58.42	55.87	-2.55
1953	23.36	139.04	73.24	49.34	-23.9
1905	23.24	141.98	35	39.1	4.1
1858	23.24	142.3	32.86	35.9	3.04
1842	22.39	142.36	24.08	23.35	-0.73
1831	21.57	142.28	26.9	31.15	4.25
1820	21.86	141.87	7.85	15.96	8.11

TY Malakas AXBT Data					
DATE:			**23-SEP-10**		
AXBT Time (hhmm)	**Latitude (degrees)**	**Longitude (degrees)**	**AXBT OHC (KJ/cm^2)**	**EASNFS OHC (KJ/cm^2)**	**Difference (Model-Observed)**
1737	23.5	139.91	55.37	43.32	-12.05
1728	23.8	139.52	55.5	47.7	-7.8
1719	24.17	139.17	46.03	45.24	-0.79
1707	24.42	140	46.49	46.18	-0.31
1648	24.11	140.75	44.34	41.7	-2.64
1640	23.62	140.74	39.65	40.92	1.27
1601	21.3	141.17	14.55	26	11.45
1553	20.78	141.2	18.93	40.16	21.23
1545	20.29	141.2	24.09	55.32	31.23
				RMSE	**13.69979027**
				BIAS	**0.720714286**

Table 11. The AXBT data deployed in TY Malakas on 23 September comparison with NRL EASNFS model analyzed OHC interpolated to the AXBT location.

THIS PAGE INTENTIONALLY LEFT BLANK

APPENDIX D. OHC MODEL ERROR CORRELATION PLOTS

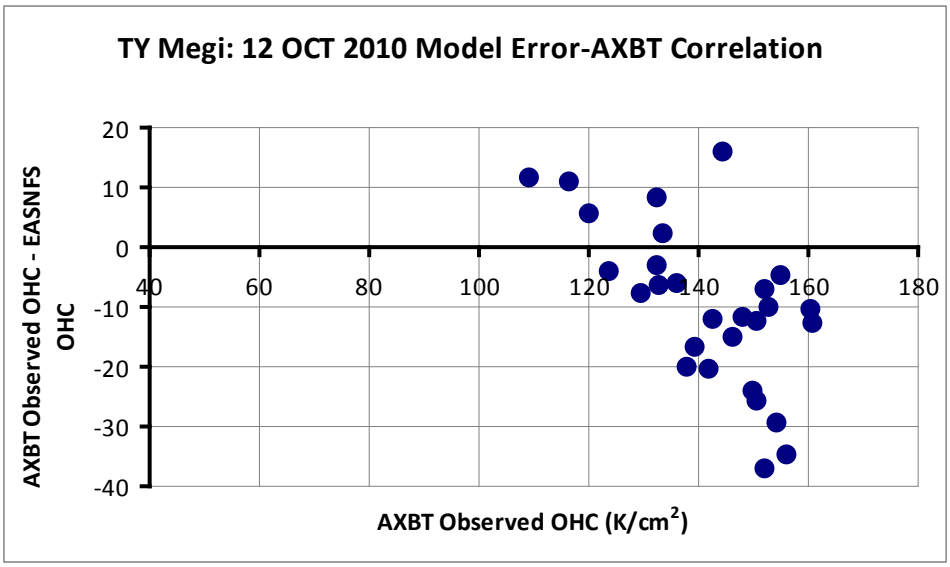

Figure 41. TY Megi 12 October 2010 observed AXBT OHC-NRL model OHC error distributions.

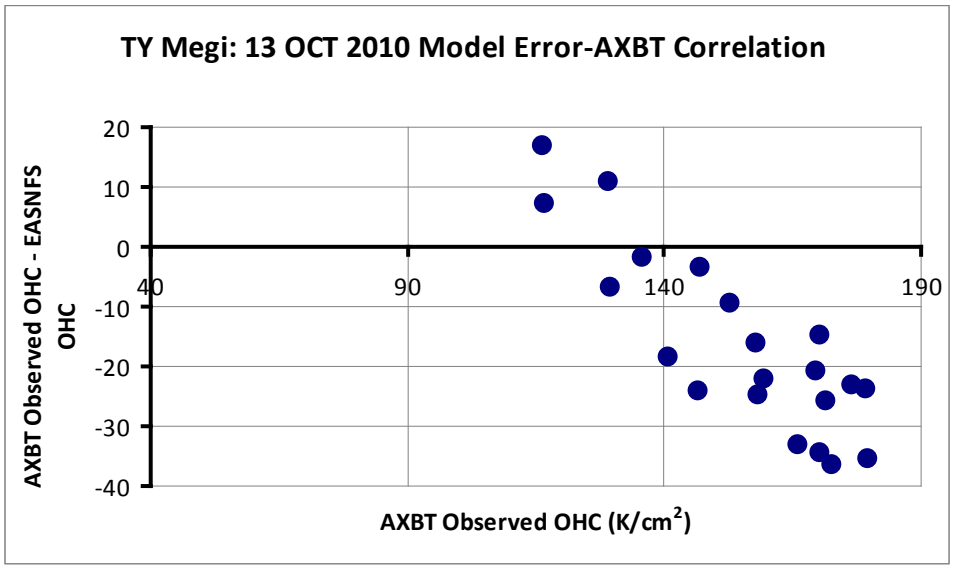

Figure 42. TY Megi 13 October 2010 observed AXBT OHC-NRL model OHC error distributions.

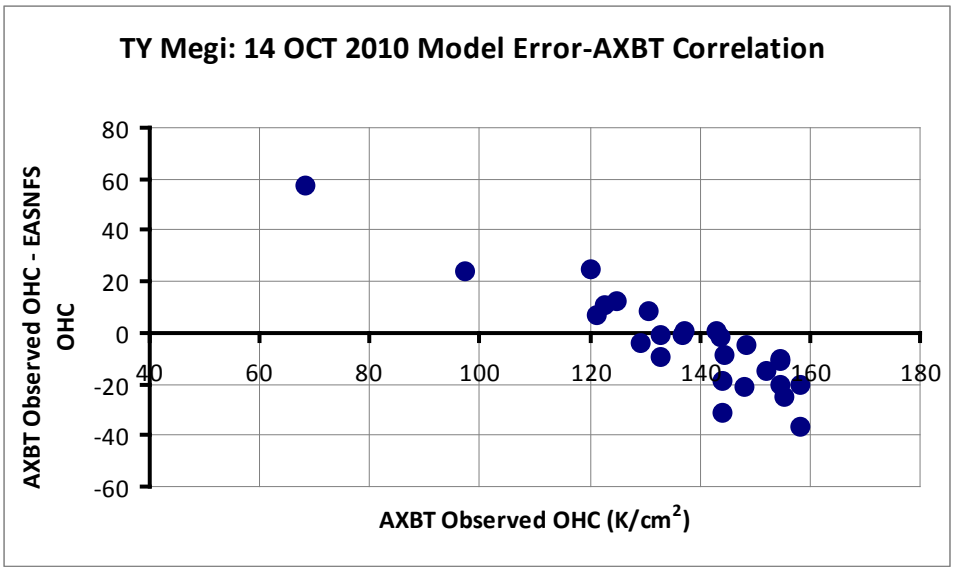

Figure 43. TY Megi 14 October 2010 observed AXBT OHC-NRL model OHC error distributions.

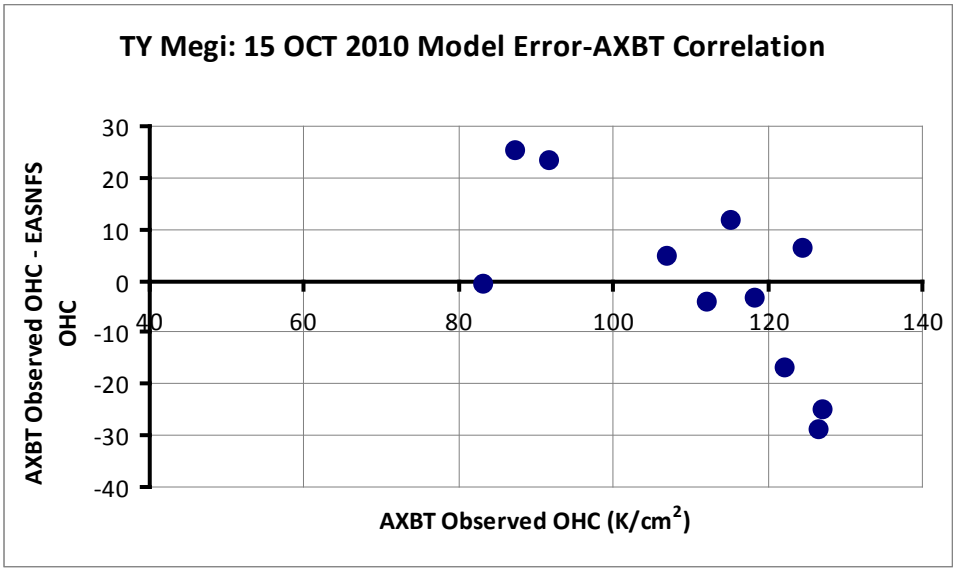

Figure 44. TY Megi 15 October 2010 observed AXBT OHC-NRL model OHC error distributions.

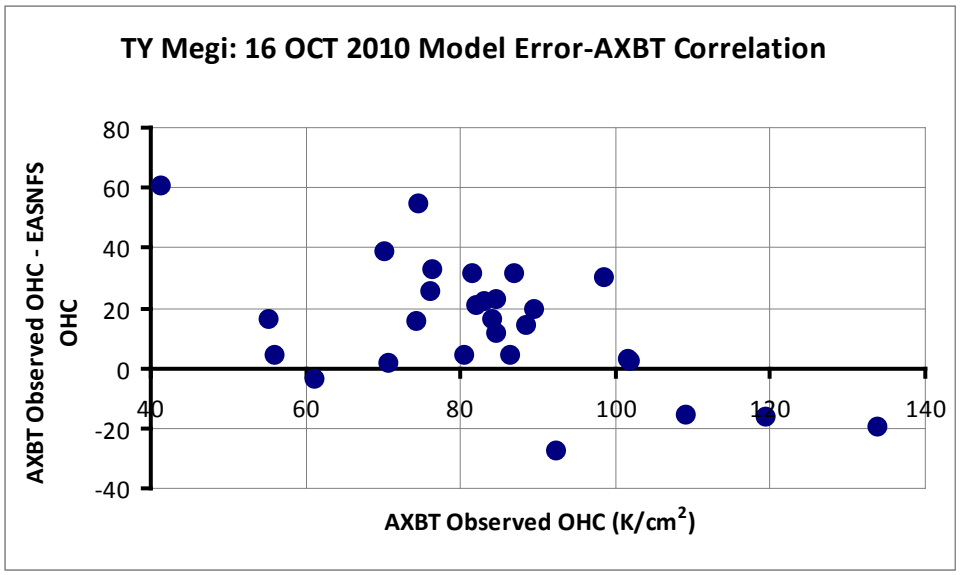

Figure 45. TY Megi 16 October 2010 observed AXBT OHC-NRL model OHC error distributions.

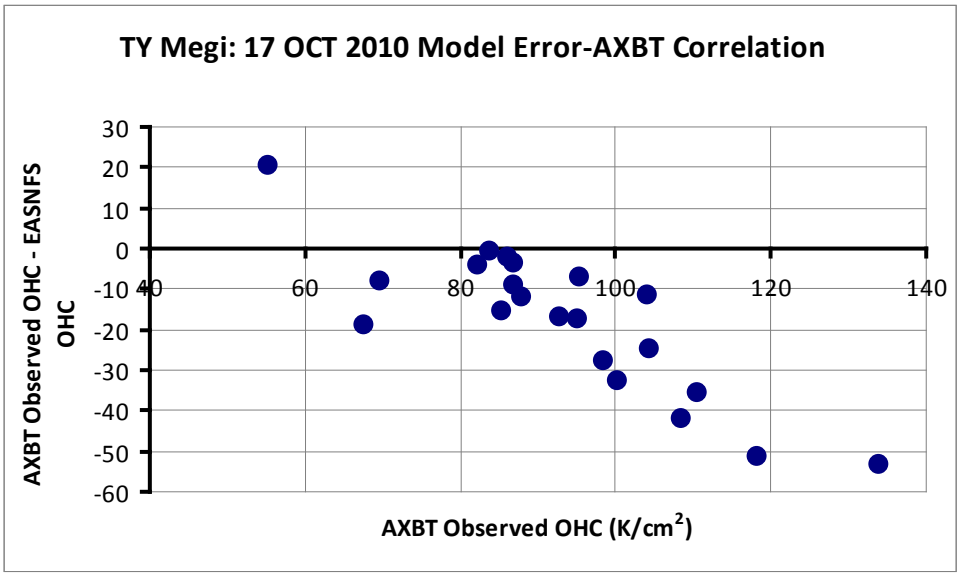

Figure 46. TY Megi 17 October 2010 observed AXBT OHC-NRL model OHC error distributions.

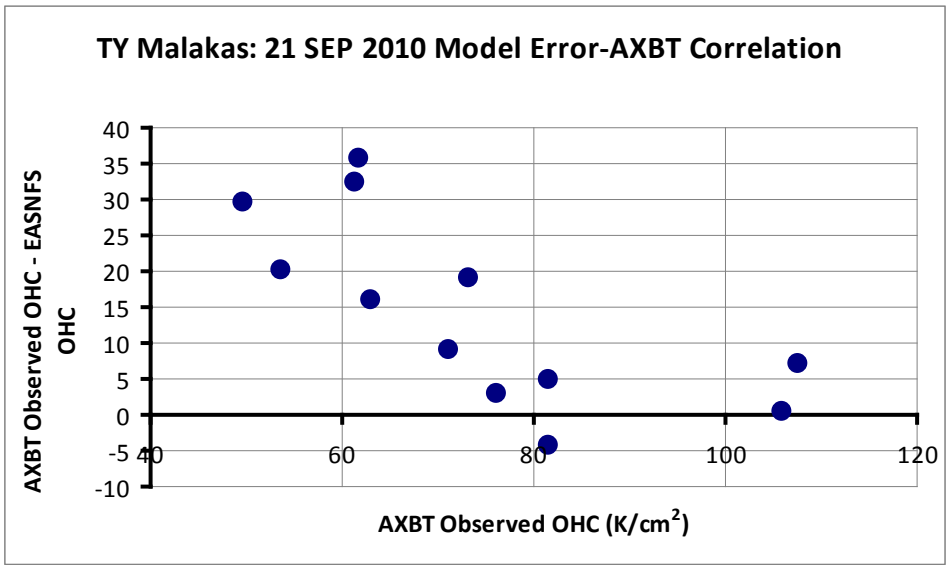

Figure 47. TY Malakas 21 September 2010 observed AXBT OHC-NRL model OHC error distributions.

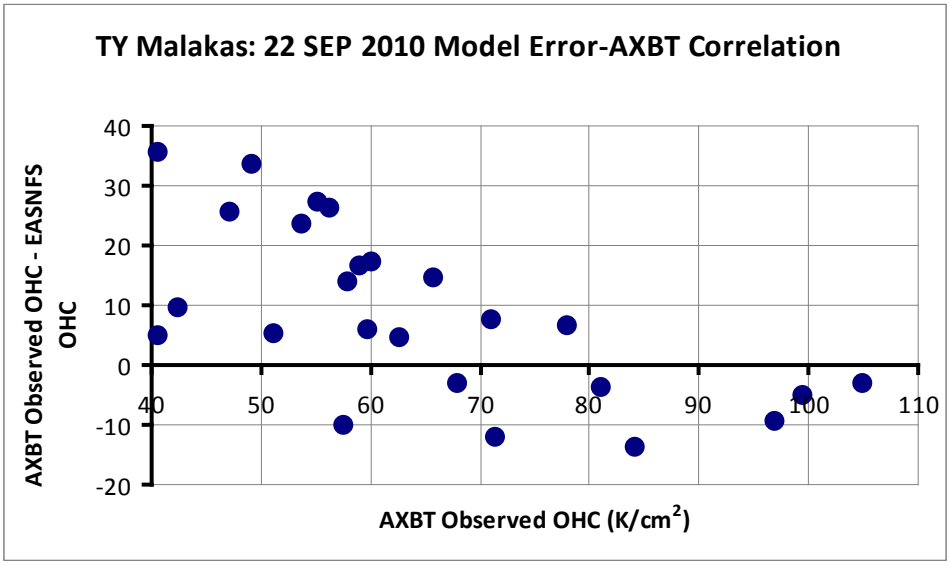

Figure 48. TY Malakas 22 September 2010 observed AXBT OHC-NRL model OHC error distributions.

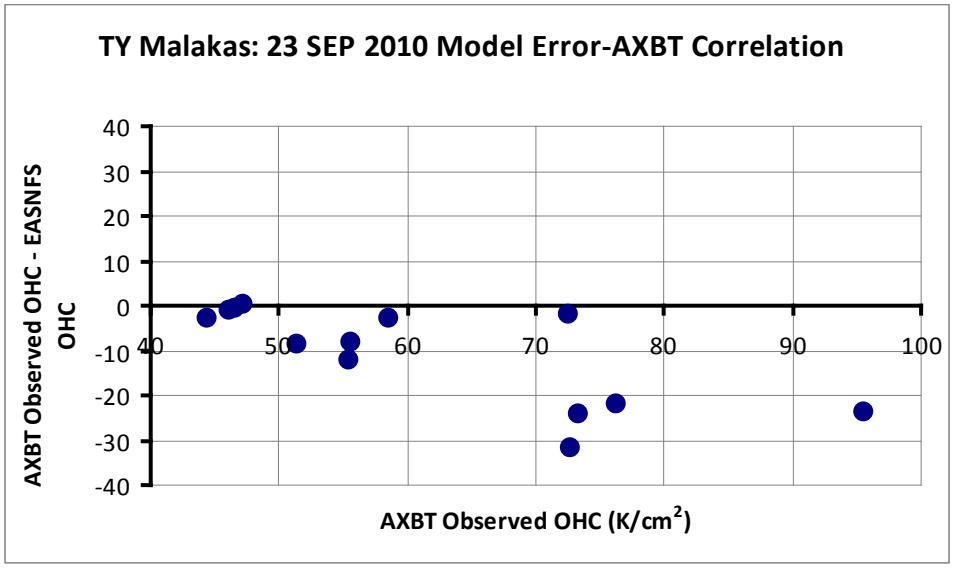

Figure 49. TY Malakas 23 September 2010 observed AXBT OHC-NRL model OHC error distributions.

THIS PAGE INTENTIONALLY LEFT BLANK

APPENDIX E. OBSERVED AXBT OHC VALUES COMPARED TO NRL OHC VALUE PLOTS

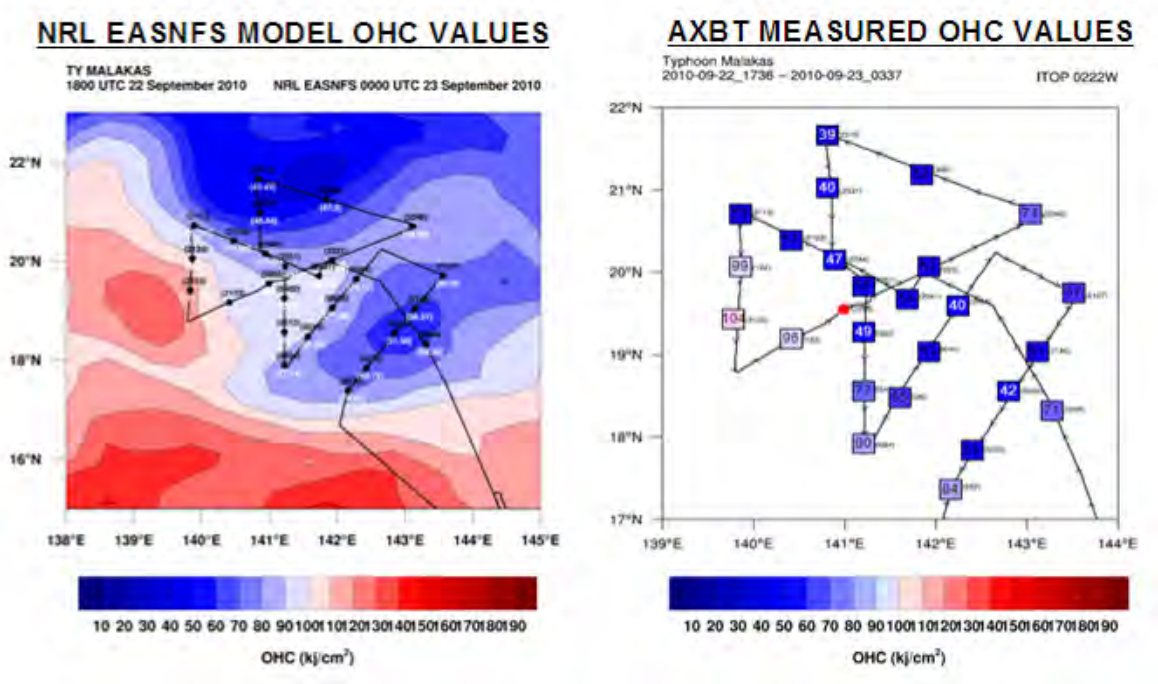

Figure 50. OHC at 0000 UTC 23 September from the NRL EASNFS (left) with the WC-130J flight path defined by the black line. Black circles identify the locations of AXBT deployments. (right) Flight track of the WC-130J with shaded squares at the locations of the AXBT deployments. The number in each square represents the observed OHC value that is also shaded according to the color bar below the figures.

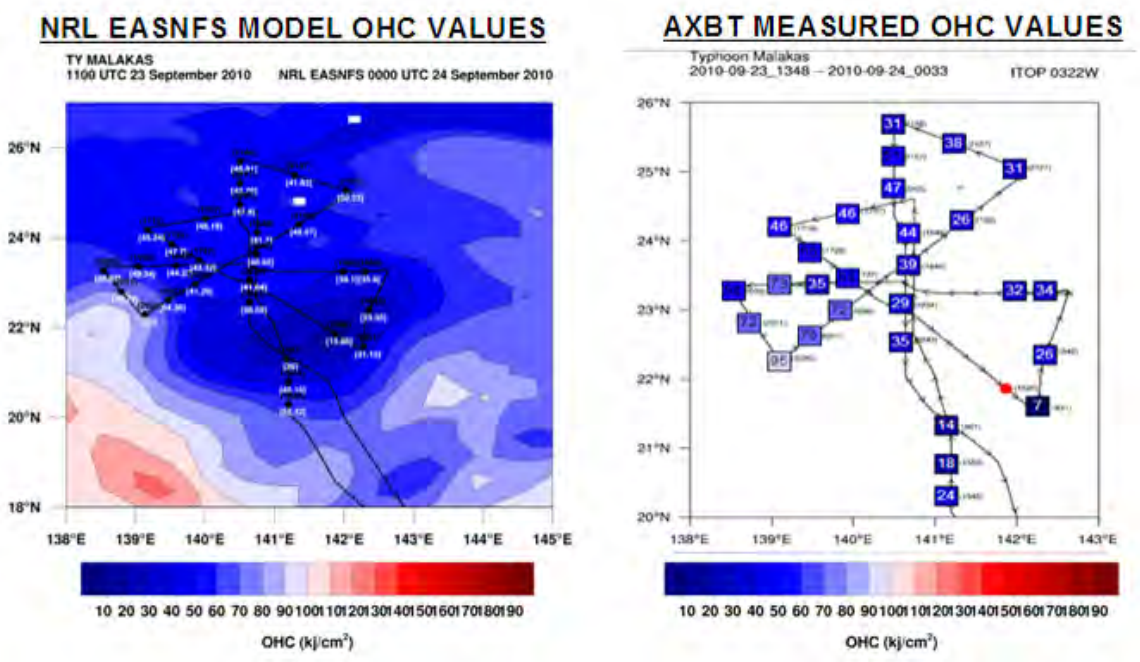

Figure 51. OHC at 1100 UTC 23 September from the NRL EASNFS (left) with the WC-130J flight path defined by the black line. Black circles identify the locations of AXBT deployments. (right) Flight track of the WC-130J with shaded squares at the locations of the AXBT deployments. The number in each square represents the observed OHC value that is also shaded according to the color bar below the figures.

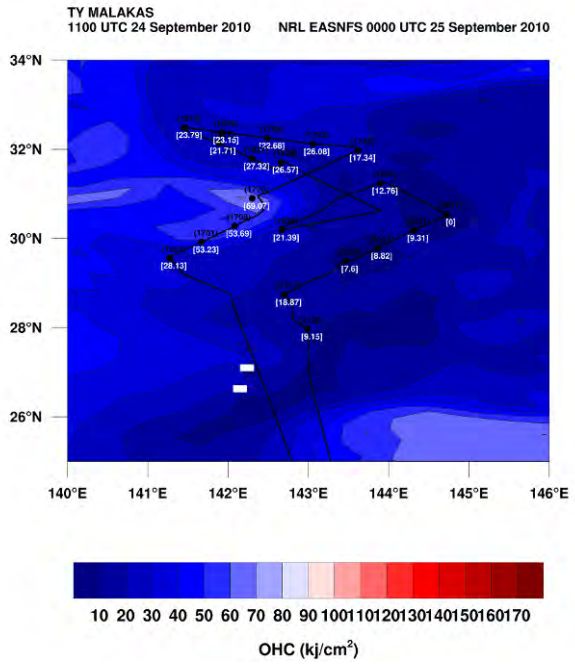

Figure 52. OHC at 1100 UTC 24 September from the NRL EASNFS (left) with the WC-130J flight path defined by the black line. Black circles identify the locations of AXBT deployments. The number in white represents the observed OHC value that is also shaded according to the color bar below the figures.

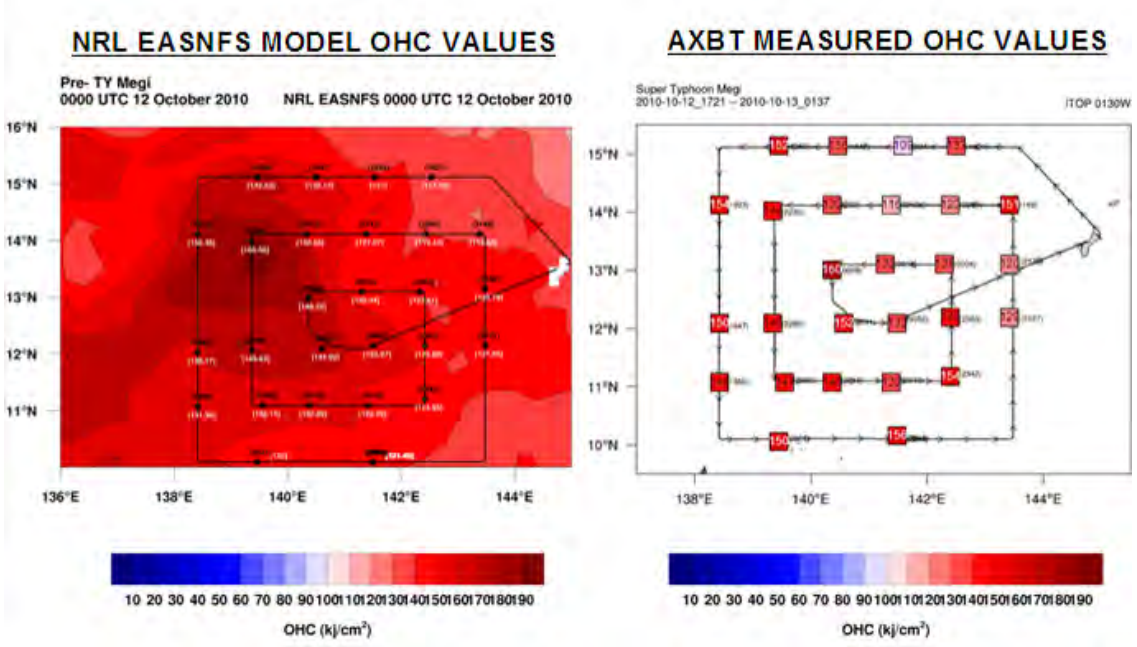

Figure 53. OHC at 0000 UTC 12 October from the NRL EASNFS (left) with the WC-130J flight path defined by the black line. Black circles identify the locations of AXBT deployments. (right) Flight track of the WC-130J with shaded squares at the locations of the AXBT deployments. The number in each square represents the observed OHC value that is also shaded according to the color bar below the figures.

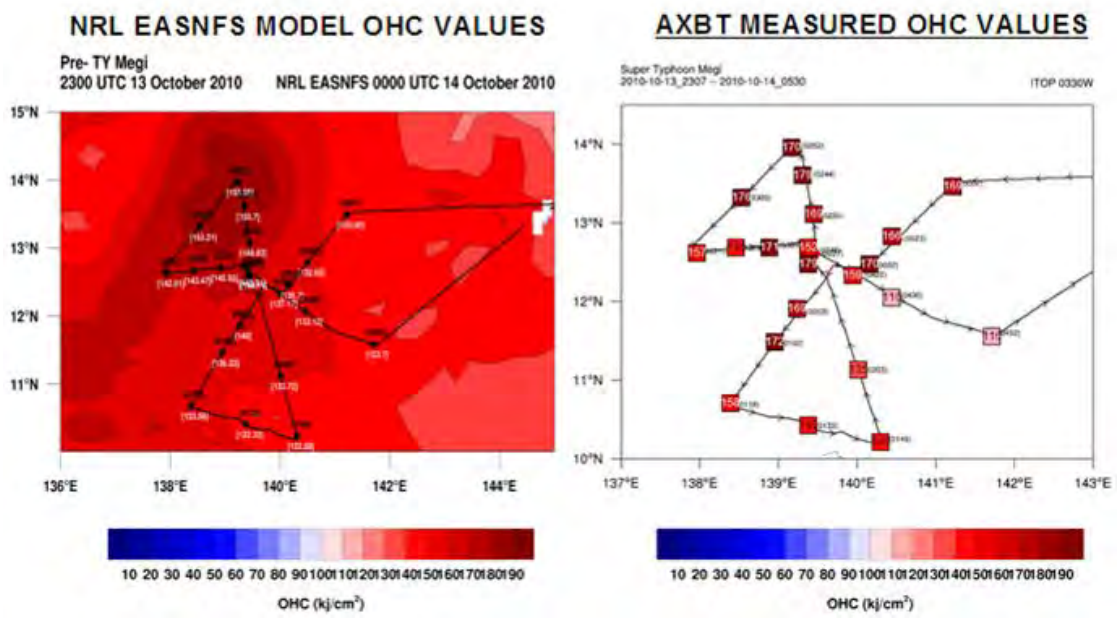

Figure 54. OHC at 2300 UTC 13 October from the NRL EASNFS (left) with the WC-130J flight path defined by the black line. Black circles identify the locations of AXBT deployments. (right) Flight track of the WC-130J with shaded squares at the locations of the AXBT deployments. The number in each square represents the observed OHC value that is also shaded according to the color bar below the figures.

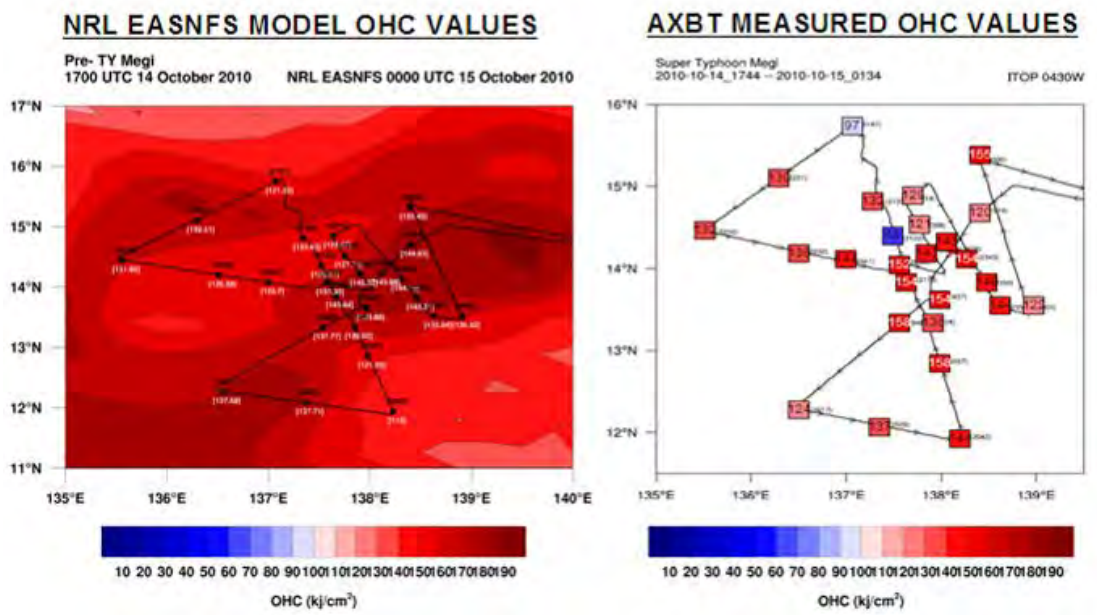

Figure 55. OHC at 1700 UTC 14 October from the NRL EASNFS (left) with the WC-130J flight path defined by the black line. Black circles identify the locations of AXBT deployments. (right) Flight track of the WC-130J with shaded squares at the locations of the AXBT deployments. The number in each square represents the observed OHC value that is also shaded according to the color bar below the figures.

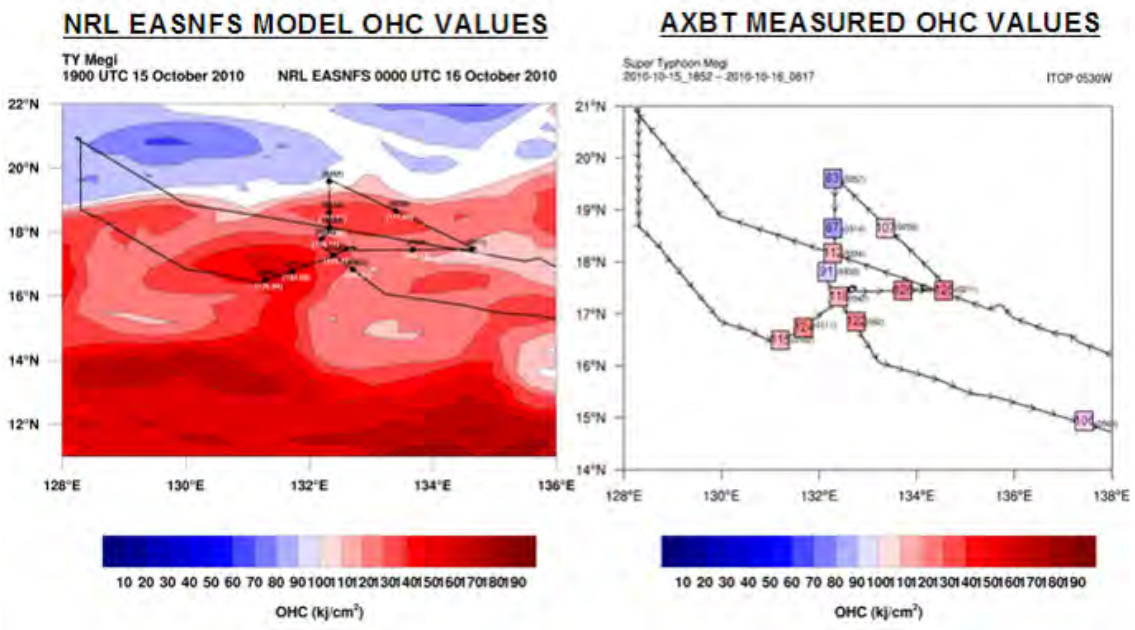

Figure 56. OHC at 1900 UTC 15 October from the NRL EASNFS (left) with the WC-130J flight path defined by the black line. Black circles identify the locations of AXBT deployments. (right) Flight track of the WC-130J with shaded squares at the locations of the AXBT deployments. The number in each square represents the observed OHC value that is also shaded according to the color bar below the figures.

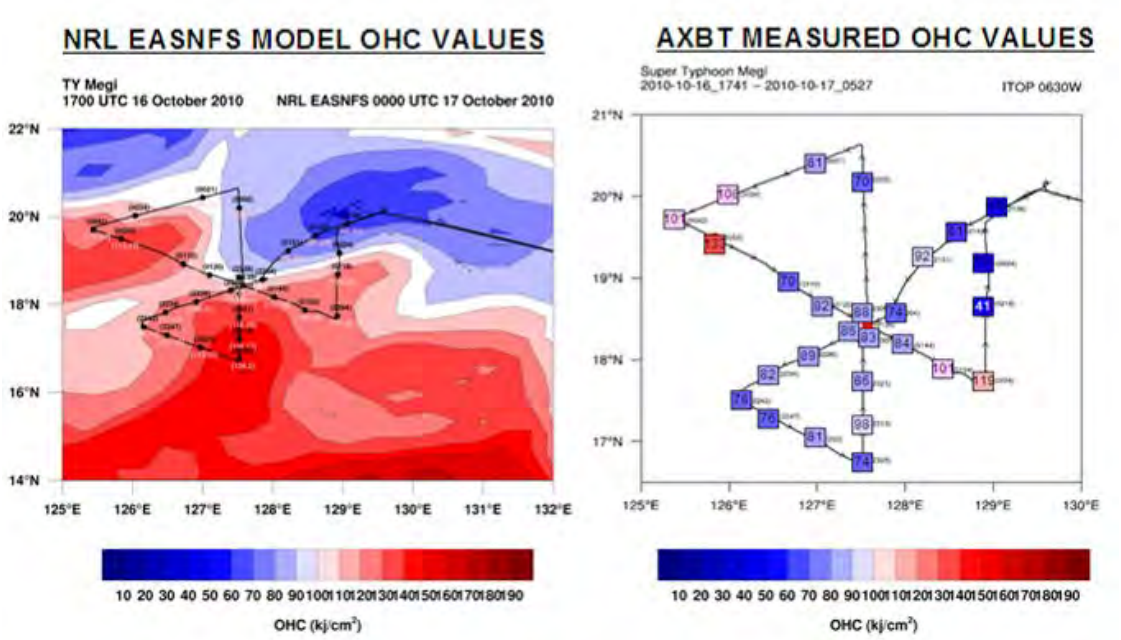

Figure 57. OHC at 1700 UTC 16 October from the NRL EASNFS (left) with the WC-130J flight path defined by the black line. Black circles identify the locations of AXBT deployments. (right) Flight track of the WC-130J with shaded squares at the locations of the AXBT deployments. The number in each square represents the observed OHC value that is also shaded according to the color bar below the figures.

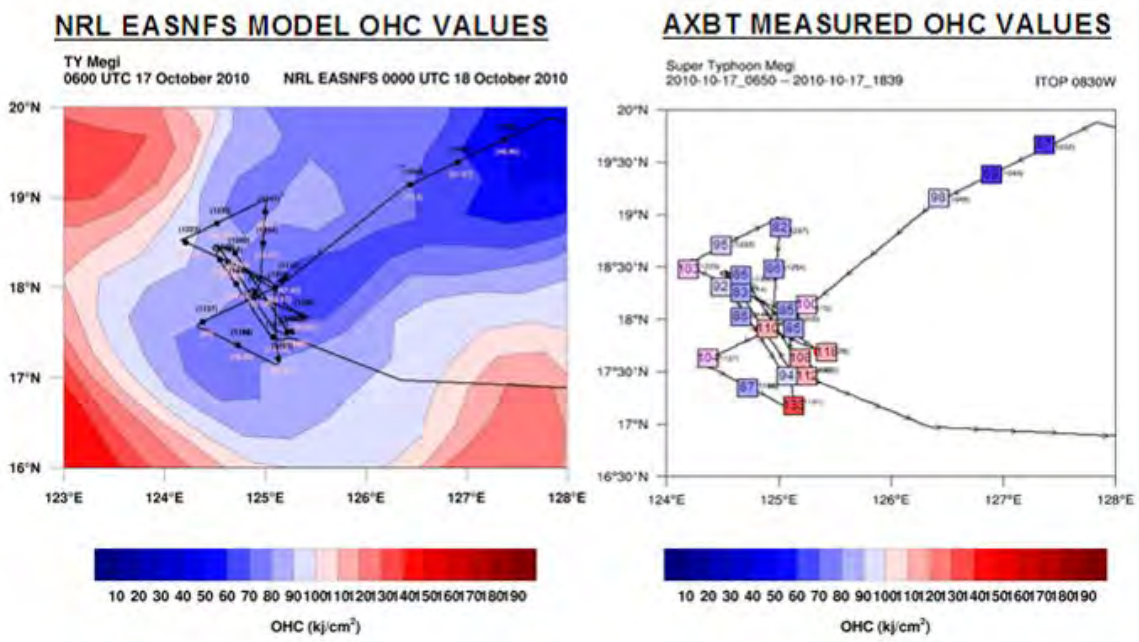

Figure 58. OHC at 0600 UTC 17 October from the NRL EASNFS (left) with the WC-130J flight path defined by the black line. Black circles identify the locations of AXBT deployments. (right) Flight track of the WC-130J with shaded squares at the locations of the AXBT deployments. The number in each square represents the observed OHC value that is also shaded according to the color bar below the figures.

THIS PAGE INTENTIONALLY LEFT BLANK

APPENDIX F. SATELLITE REMOTELY SENSED DATA

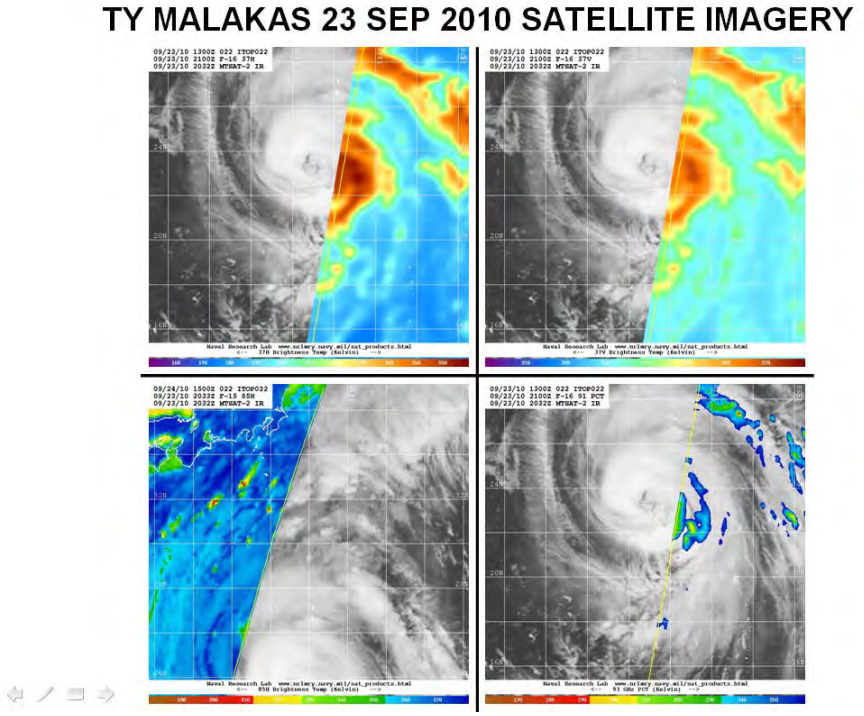

Figure 59. The 37GHz V, 37GHz H, 85GHz and 91GHz TY Malakas IR satellite imagery from 23 September 2010.

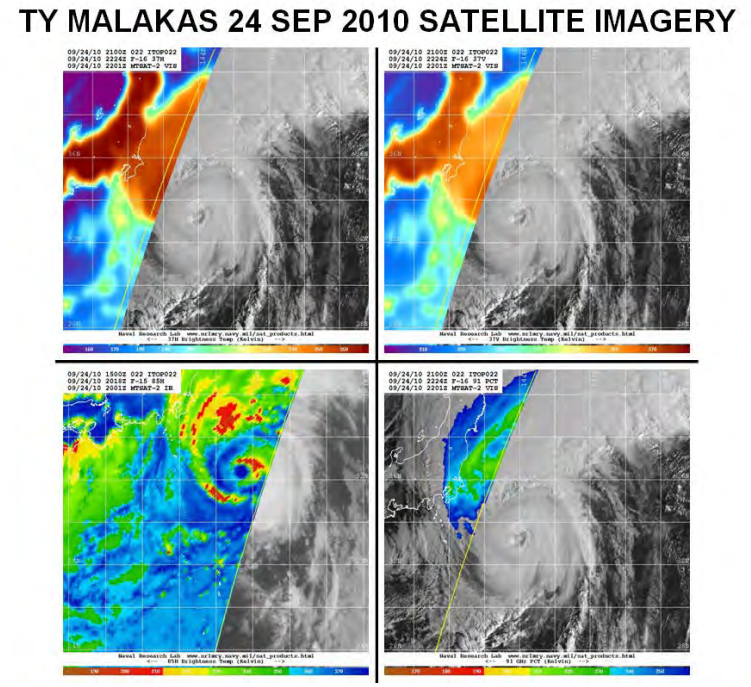

Figure 60. The 37GHz V, 37GHz H, 85GHz and 91GHz TY Malakas IR satellite imagery from 24 September 2010.

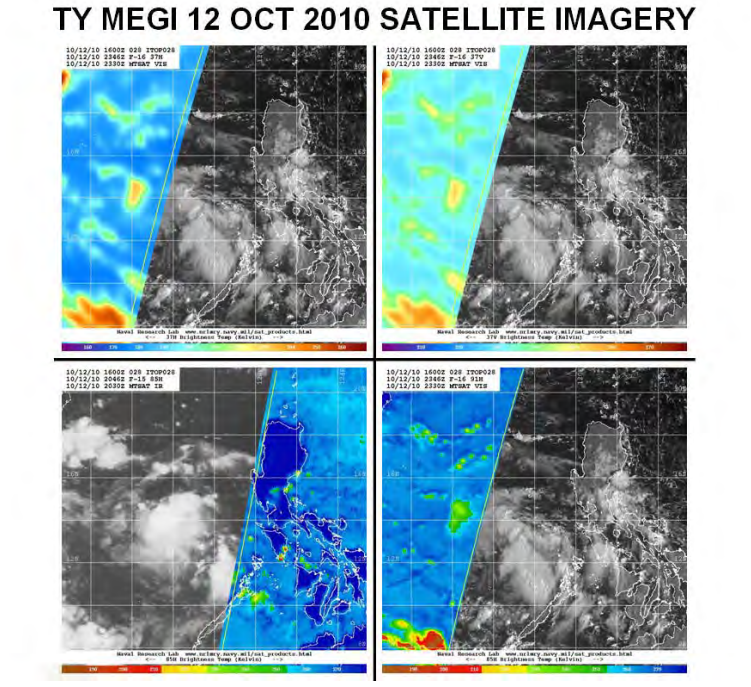

Figure 61. The 37GHz V, 37GHz H, 85GHz and 91GHz TY Megi IR satellite imagery from 12 October 2010.

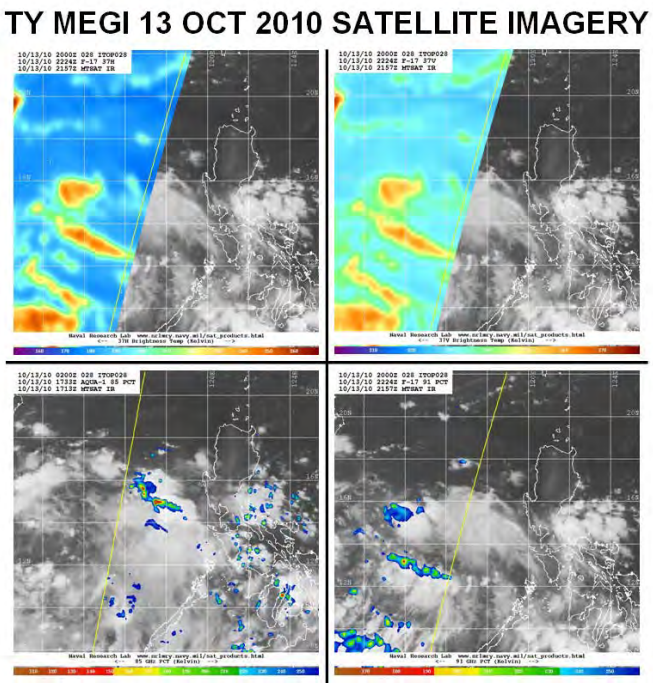

Figure 62. The 37GHz V, 37GHz H, 85GHz and 91GHz TY Megi IR satellite imagery from 13 October 2010.

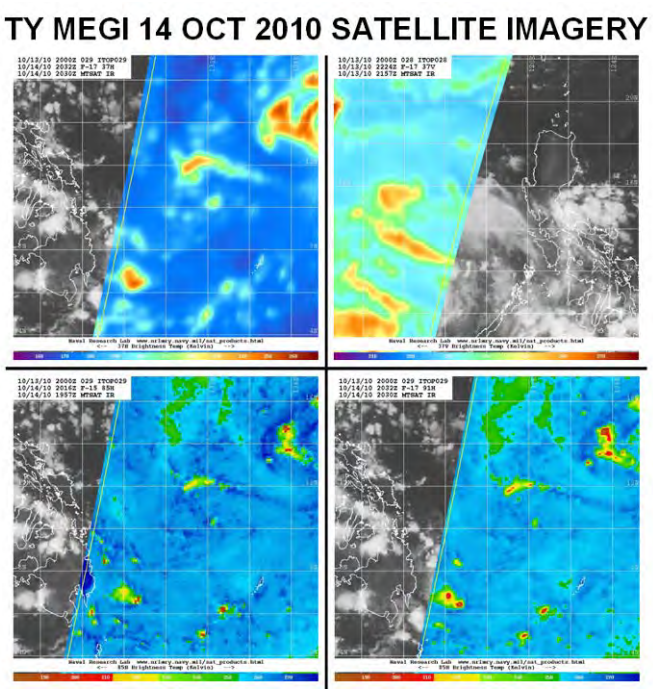

Figure 63. The 37GHz V, 37GHz H, 85GHz and 91GHz TY Megi IR satellite imagery from 14 October 2010.

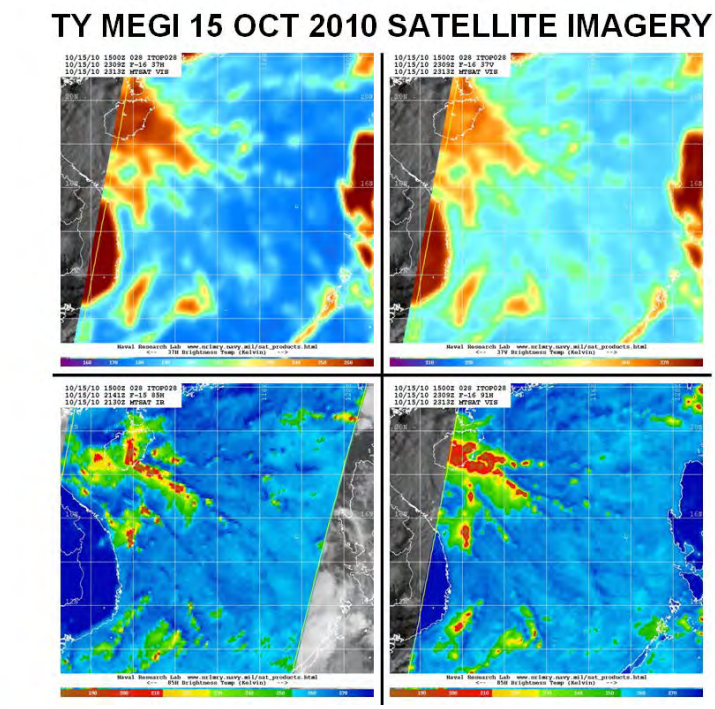

Figure 64. The 37GHz V, 37GHz H, 85GHz and 91GHz TY Megi IR satellite imagery from 15 October 2010.

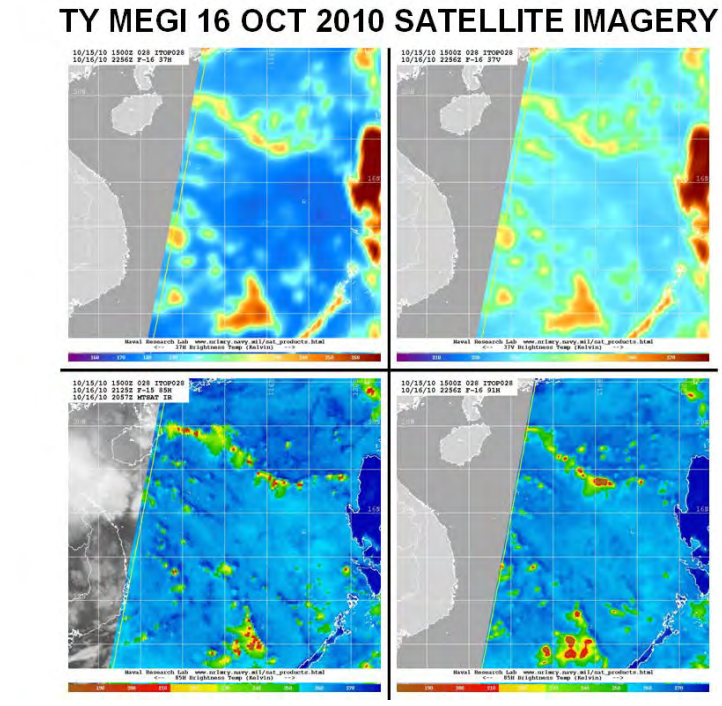

Figure 65. The 37GHz V, 37GHz H, 85GHz and 91GHz TY Megi IR satellite imagery from 16 October 2010.

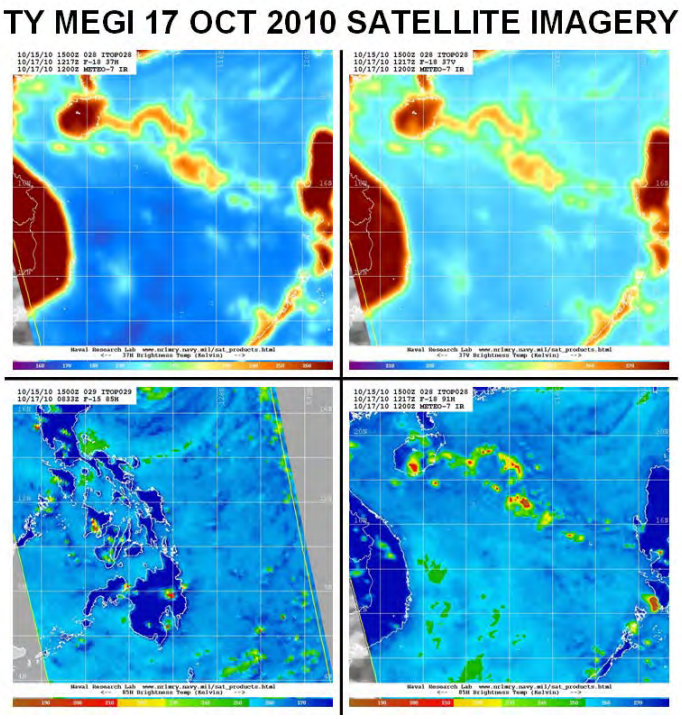

Figure 66. The 37GHz V, 37GHz H, 85GHz and 91GHz TY Megi IR satellite imagery from 17 October 2010.

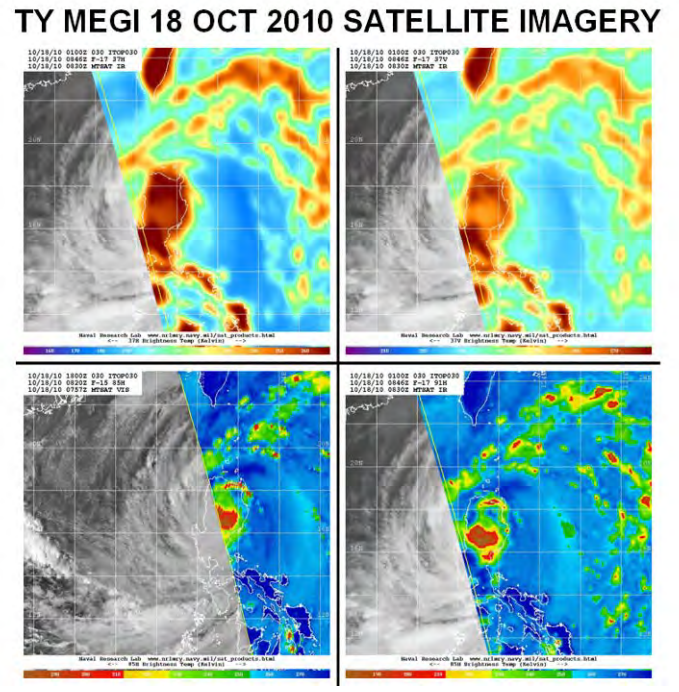

Figure 67. The 37GHz V, 37GHz H, 85GHz and 91GHz TY Megi IR satellite imagery from 18 October 2010.

THIS PAGE INTENTIONALLY LEFT BLANK

LIST OF REFERENCES

Bloomberg, cite 2010: Tropical Storm Malakas Churns Toward Japanese Islands, May Become Typhoon. [Available online at http://www.bloomberg.com/news/2010-09-22/tropical-storm-malakas-churns-over-western-pacific-toward-japanese-islands.html.}

Bowditch, N., 2002: *American Practical Navigator.* National Imagery and Mapping Agency, 879 pp.

Cione, J. J., and E. W. Uhlhorn, 2003: Sea Surface Temperature variability in Hurricanes: Implications with respect to intensity change. *Mon. Wea. Rev*., **131**, 1783–1796.

CNN, cited 2010: China braces for Typhoon Megi. [Available online at http://articles.cnn.com/2010-10-18/world/philippines.typhoon_1_philippines-strongest-storm-typhoon-megi?_s=PM:WORLD.]

DePalma, C, March 2011. Intensity changes in Typhoon Sinlaku and Ty[hoon Jangmi in response to varying ocean and atmospheric conditions. M.S. thesis, Naval Postgraduate School, 107 pp.

Elsberry, R. L., and P. A. Harr, 2008: Tropical Cyclone Structure (TCS08) field experiment: Science basis, observational platforms, and strategy. *Asian Pacific J. Atmos. Sci.*, **44**, 209–231.

Kepert, J. D., 2001: The dynamics of boundary layer jets within the tropical cyclone core. Part I: Linear theory. *J. Atmos. Sci*., **58**, 2469–2484.

KITAMOTO Asanobu, National Institute of Informatics (NII), Digital typhoon: Typhoon images and information, cited 2011: [Available online at http://agora.ex.nii.ac.jp/digital-typhoon/index.html.en.]

Leipper, D., and D. Volgenau, 1972: Upper ocean heat content of the Gulf of Mexico. *J. Physical Oceanography*, **2**, 218–224.

Lin, I-I, and C. C. Wu, 2005: The interaction of Typhoon Maemi (2003) with a warm ocean eddy. *Mon. Wea. Rev*., **133**, 2635–2649.

Mainelli, M., et al., 2008: Application of oceanic heat content estimation to operational forecasting of recent category 5 Atlantic hurricanes. *Weather and Forecasting*, **23**, 3–16.

Melton, B. F. Jr., 2007: *Sea Cobra, Admiral Halsey's Task Force and the Great Pacific Typhoon*, Lyons Press, 247–274.

NASA, cited 2010a: Hurricane Season 2010: Tropical Storm Malakas (Northwest Pacific Ocean. NASA's CloudSat satellite sees a Powerful Heat Engine in Typhoon Malakas. [Available online at http://www.nasa.gov/mission_pages/hurricanes/archives/2010/h2010_Malakas.html.]

NASA, cited 2010b: Hurricane Season 2010: Typhoon Megi (Northwest Pacific Ocean), NASA Map Tracks Heavy Rainfall from Typhoon Megi. [Available online at http://www.nasa.gov/mission_pages/hurricanes/archives/2010/h2010_Megi.html.]

NOAA, National Weather Service, Climate Predication Center, cited 2011: Cold and Warm Episodes by Season. [Available online at http://www.cpc.ncep.noaa.gov/products/analysis_monitoring/ensostuff/ensoyears.shtml

Pascquero, C., and K. Emanuel, 2008: Tropical Cyclones and Transient Upper Ocean warming. *J. Climate,* **21**, 149–162.

Pearl Harbor, Hawaii, cited 2010: Annual Tropical Cyclone Report, 2010. [Available online at http://www.usno.navy.mil/NOOC/nmfc-ph/RSS/jtwc/atcr/2010atcr.pdf.]

Price, J. F., 2009: Metrics of hurricane-ocean interaction: Vertically-integrated or vertically averaged ocean temperature? *Ocean Sciences*, **5**, 351–368.

Sadhuram, Y., K. Maneesha, and T. V. Ramana Murity, 2010: Importance of upper ocean heat content in the intensification and translation speed of cyclones over the Bay of Bengal. *Current Science* **99**, no. 9, 1191–1194.

Shay, L. K., 1999: Effects of a warm ocean feature on Hurricane Opal. *Mon. Wea. Rev.*, **128**, 1366–1383.

Shay, L. K., and J. K. Brewster 2010: Oceanic heat content variability in the Eastern Pacific Ocean for hurricane intensity forecasting. *Mon. Wea. Rev.*, **138**, 2110–2132.

U.S. Naval Maritime Forecast Center/ Joint Typhoon, Warning Center, cited 2010: 2010 Annual Tropical Cyclone Report. [Available online at http://www.usno.navy.mil/JTWC/annual-tropical-cyclone-reports]

Wang, B., and J. C. L. Chan, 2002: How strong ENSO events affect tropical storm activity over the western North Pacific. *J. Climate*, **15**, 1643–1658.

The Washington Post, cited 2010: Typhoon Megi likely to track east of Hong Kong. [Available online at http://voices.washingtonpost.com/capitalweathergang/2010/10/typhoon_megi_may_miss_hong_kon.html.]

Wu, C.-C., C.-Y. Lee, and I.-I. Lin, 2007: The Effect of the Ocean Eddy on Tropical Cyclone Intensity. *J. Atmos. Sci*., **64**, 3562–3578.

Yablonsky, R. M. and I. Ginis, 2007: Improving the Ocean Initialization of Coupled Hurricane-Ocean Models Using Feature Based Data Assimilation. *Mon. Wea. Rev*., **136**, 2592–2607.

THIS PAGE INTENTIONALLY LEFT BLANK

INITIAL DISTRIBUTION LIST

1. Defense Technical Information Center
   Ft. Belvoir, Virginia

2. Dudley Knox Library
   Naval Postgraduate School
   Monterey, California

3. Professor Patrick Harr
   Naval Postgraduate School
   Monterey, California

4. CDR J. Dumas
   Naval Postgraduate School
   Monterey, California